Master of Science Thesis

Analysis of optimum flight path for a general aviation hybrid electric airplane

T.E.F.J. Dumoulin B.Eng.

September 28, 2018

Faculty of Aerospace Engineering · Delft University of Technology

Analysis of optimum flight path for a general aviation hybrid electric airplane

Master of Science Thesis

For obtaining the degree of Master of Science in Aerospace Engineering at Delft University of Technology

T.E.F.J. Dumoulin B.Eng.

September 28, 2018

Faculty of Aerospace Engineering · Delft University of Technology

Delft University Of Technology
Department Of
Flight Performance and Propulsion

The undersigned hereby certify that they have read and recommend to the Faculty of Aerospace Engineering for acceptance a thesis entitled **"Analysis of optimum flight path for a general aviation hybrid electric airplane"** by **T.E.F.J. Dumoulin B.Eng.** in partial fulfillment of the requirements for the degree of **Master of Science**.

Dated: September 28, 2018

Head of department: _____
Prof.dr.ir. L.L.M Veldhuis

Supervisor: _____
Dr. F. Oliviero

Reader: _____
Dr.ir. G. La Rocca

Reader: _____
Dr. M.A. Mitici

Summary

Ever since the dawn of aviation the aircraft has been developed to a large extend in terms of aerodynamics, materials, structures and propulsion systems. Consequently, flying has become more accessible for larger amounts of the population leading to a substantial growth in aviation. In the beginning flying was only for the brave, thereafter only for the rich and nowadays largely accessible for average income people. With the current economic rise of large developing countries, it is expected the aviation industry will continue to grow quite significantly. Despite the development of the airframe and jet engines which leads to more efficient operation, the amount of environmentally harmful gases produced by aviation is predicted to continue the growth.

One of the promising solution to counter this growth, is the implementation of Hybrid Electric Propulsion Systems (HEPS). Using different energy sources and different energy conversion devices allow for better overall system efficiency and thereby reduce fuel consumption and emissions. The Internal Combustion Engine (ICE) which runs on fossil fuel has a low achievable peak efficiency. However, this is still rectified by the fuel having a substantially higher energy density compared to the recent electrical energy storage. Contrary, the Electro Motor (EM) has a relatively high efficiency and high specific power. In addition, the EM allows for different kind of propulsive system integration into the airframe due to its small scaling effects. For the implementation of HEPS into aircraft, there is a lot of research on how the airframe can change to give better propulsive and aerodynamic efficiency. However, most recently HEPS are only being integrated in existing airframes of general aviation aircraft. The effect that this new technology has on the optimum mission has not been sufficiently investigated yet, leading to the research question for this paper: *What is the effectiveness of flight path optimization for a general aviation aircraft with a series HEPS?*

The answer this question a reference aircraft is used which is the Pipistrel Panthera. This aircraft is currently in high technical readiness levels in implementing a HEPS into a conventional propulsion system aircraft. Therefore, a lot of empirical data is available for to propulsion system components and the aircraft and Pipistrel provided this research with that. This empirical data is combined with known relations to create a model for most parts of the propulsion system and the aerodynamics of the aircraft. With these models

the performance of the HEPS aircraft is determined. To optimize the flight path of the HEPS aircraft different objectives where used; minimum fuel, minimum total energy and minimum time. In addition, variables are introduced for the optimization with included flight conditions and the propulsion system conditions. The climb phase and cruise phase have the most significant influence of the overall mission performance for these objectives so these are first optimized separately and then connected together. As a fixed input to each optimization the taxi and take-off phase are included.

To determine the flight path performance of the HEPS a method is developed that discretizes the flight path and determined the performance for each flight path section. With increasing number of sections in the flight path the precision of the solution increases along with the computational time for the optimization. For the optimization the Matlab function *fmincon* is used. The optimum mission for the conventional propulsion system aircraft is compared with the optimum mission for the HEPS aircraft, and is proven to be considerably distinctive. The most limiting factors are the battery capacity and the power output of the HEPS ICE. For the reference mission cruise altitude of 8000 ft the battery is not able to supply enough energy to keep flying at the maximum rate of climb. Therefore, in terms of minimum fuel consumption the HEPS aircraft perform better, yet in terms of minimum time it performs worse. For the cruise different strategies are investigated and for each the cruise is optimized. Switching between battery recharge and battery discharge during cruise yields to no better performance due to more energy loss in the additional conversions, though only recharging the battery once and performing the rest of the cruise with only the ICE yields to less fuel being used for this mission phase. For all the investigated strategies the optimum time to cruise is less for the HEPS aircraft due to the battery being drained during the climb phase. Coupling the climb and cruise phase together yielded into different results, mainly for the minimum fuel objective. The most influential parameter on the optimum conditions is the battery capacity. Different capacities are investigated and yield into notable different optimum conditions. In addition, the cruise altitude has a similar effect.

The flight path discretization method works sufficiently for larger amount of segments and for the optimization of fuel and total energy. However, for the time optimization an influence of the initial point is observed due to the time being directly related to the discretization. Since *fmincon* uses gradient based methods it becomes more difficult to assure adequate convergence if there are discontinuities in the objective function. In addition, the bottle neck in terms of optimization time is the battery model which uses exponential functions and requires small time steps to assure acceptable modeling of the inherent battery parameters. Therefore, a simplified model is used for comparison and yields into different results. Therefore, modeling the battery more accurately is proven to be advantageous. Overall, it is concluded that the implementation of HEPS into an exiting airframe varies the optimum mission substantially and should always be investigated thoroughly to assure more appealing mission performance.

Acknowledgements

At first and mostly I wish to thank my thesis supervisor Fabrizio Oliviero for his extensive coaching and advise during this research. I wish to express my gratitude for his time and effort in answering my questions and providing essential feedback. In addition, I wish to thank the members of my committee for taking their time to read and judge this work. Likewise, I wish to thank Maurice Hoogreef for his comprehensive feedback on the green light paper. Moreover, I wish to thank Pipistrel for providing the data that made this thesis possible.

Furthermore, I want to thanks the guys at the 1.05 office with whom I shared the office for their support and being a good source of energy. There was always room to discuss each others work and subjects. Lastly, I wish to thank my girlfriend and family for their support.

Delft, The Netherlands
September 28, 2018

T.E.F.J. Dumoulin B.Eng.

Contents

List of Figures

List of Tables

Nomenclature

Latin Symbols

A	Exponential zone amplitude	V
B	Exponential zone time constant	Ah^{-1}
C_D	Drag coefficient	-
C_L	Lift coefficient	-
$C_{L_{max}}$	Lift coefficient	-
C_P	Pressure coefficient	-
C_T	Thrust coefficient	-
D	Drag force	N
D_f	Derating factor	N
D_g	Ground drag force	N
d	Diameter	m
E_0	Battery constant voltage	V
g	Gravitational acceleration	m/s^2
h	Altitude	m
i	Battery current	A
$i*$	Filtered current	A
it	Actual battery charge	Ah
J	Advance ratio	-
k	Polarisation resistance	Ω
L	Lift force	N
m	Mass	kg

N	Normal force	–
P_a	Power available	$Watt$
P_{br}	Shaft brake power	$Watt$
P_r	Power required	$Watt$
Q	Battery capacity	Wh
R	Internal resistance	Ω
S	Wing reference area	m^2
T	Thrust force	N
U	Voltage	V
u	Energy density	J/kg
V	Velocity	m/s
V_c	Maximum structural cruise speed	m/s
V_{fuel}	Voluma of fuel tank	m^3
V_{stall}	Stall speed	m/s
V_{ne}	Never exceed speed	m/s
V_R	Rotation Speed	m/s
W	Weight	kg
x	Horizontal distance	m

Greek Symbols

α	Angle of attack	deg
γ	Flight path angle	deg
δ_f	flap deflection	$^\circ$
η	Efficiency	%
θ	Pitch angle	deg
μ	Friction coefficient	–
ρ	Air density	kg/m^3
ρ_0	Air density at sea level	kg/m^3

Abbreviations

AC	Alternating current
ADT	Actuator Disc Theory
ASK	Available Seat Kilometer
BEM	Blade Element Method
BHP	Brake Horse Power

BSFC	Brake Specific Fuel Consumption
CS-23	Certification Specifications number 23
DC	Direct Current
EASA	European Aviation Safety Agency
EAS	Equavalent Air Speed
EM	Electro Motor
FBD	Free Body Diagram
HEPS	Hybrid Electric Propulsion Systems
HMI	Human Machine Interface
IAS	Indicated Air Speed
ICE	Internal Combustion Engine
MTOW	Maximum Take Off Weight
OEI	One Engine Inoperative
RPM	Rounds Per Minute
SQP	Sequential Quadratic Programming
TAS	True Air Speed
UAV	Unmanned Areal Vehicle

Chapter 1

Introduction

More than 100 years ago the first powered flight took off from the fields near Kitty Hawk, North Carolina. The Wright Flyer, built and designed by the two brothers Orville and Wilbur Wright, provided a kick start to powered flight across the world. Since then, the aviation industry has experienced massive growth. Nowadays, aviation is a large part of modern society. It is predicted that the aviation industry will grow, accompanied by an increasing energy demand of about 10% in the next two decades. [22] [16]. Currently, 85% of the primary world's energy production is based on fossil fuels and the aviation industry is exclusively dependent on fossil fuels [23]. During the last decades, the aircraft along with its engines, have been developed significantly. The amount of fuel consumption per seat kilometer for aircraft with jet engines has decreased significantly by almost 70% (40% due to efficiency of the engines and 30% due to aerodynamic and structural improvements), as illustrated in figure 1.1. Alongside, the energy consumption per Available Seat Kilometer (ASK) has decreased as well over the years, as shown by the trends in figure 1.2. The development in jet engines resulted in a large decrease in energy consumption in the first few years and has stagnated slightly during the 1980's. The predicted future development for jet engines is extrapolated in this graph as well. It still shows a decrease in energy consumption of jet engines for the upcoming two decades but it is slowly stagnating.

Contradictory to the decrease in fuel consumption, the amount of passengers and freight being transported by aircraft has increased to a greater extend [22]. The resulting consequence of this greater increase is that the total amount of harmful emissions from aircraft has not decreased over time alongside the fuel consumption, but actually increased. From the carbon dioxide emissions perspective, this is shown in figure 1.3. The graph shows that the amount of carbon dioxide being emitted into the Earth's atmosphere by the aviation industry, is growing. Although the aviation industry is only a small fraction of the total amount of anthropogenic carbon dioxide emissions ($\approx 2.5\%$), it is still worth considering. Mainly, because the relative portion of anthropogenic carbon dioxide emissions by the aviation industry is growing. In addition, relative to the total transportation sector impact, the aviation industry is guilty of 12% of the carbon dioxide emissions [25]. If the

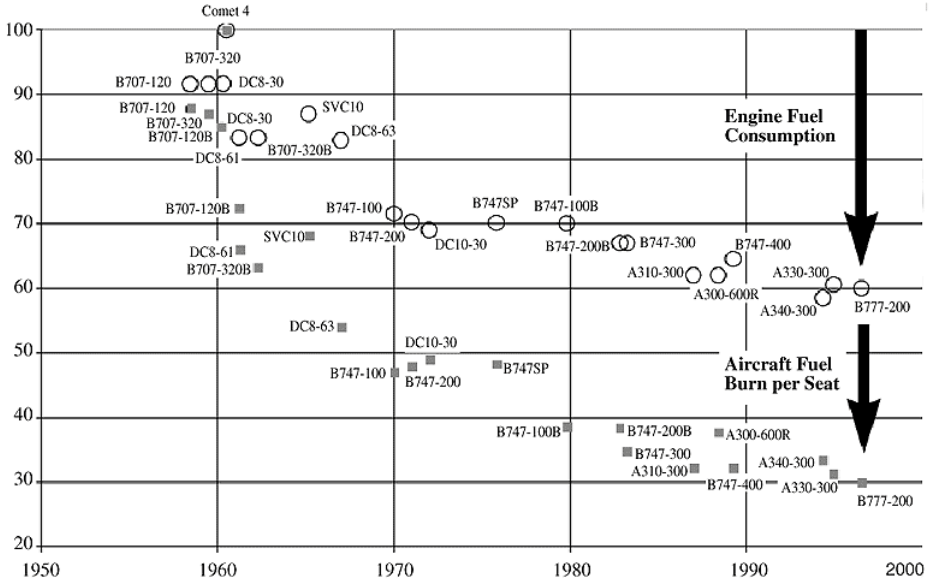

Figure 1.1: Fuel consumption of aircraft, as a percentage of the base aircraft Comet 4 versus the years of development. The circles represent the percentage of engine fuel consumption and the squares represent the percentage of aircraft fuel consumption per seat [33]

growth of carbon dioxide emissions accompanied by other green house gases by aviation would continue in a likely manner, the amount in the Earth's atmosphere will continue to grow resulting in an increase of the average temperature on Earth and a deterioration of air quality. Alternative means of propulsion might be an advantageous solution to reduce the growth in aircraft emissions.

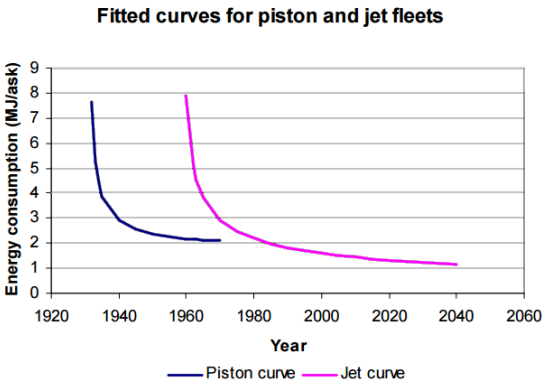

Figure 1.2: Energy consumption of aircraft over the years of development [33]

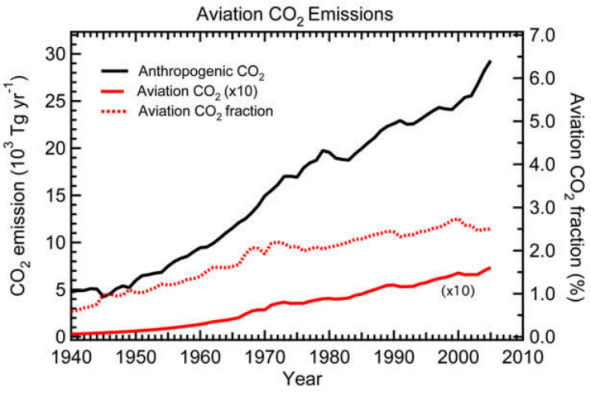

Figure 1.3: Carbon dioxide emissions over the years of development [13]

New ideas and innovations are therefore vital for the conservation of our own planet and quality of life. One of these is electric propulsion. Already in use for quite a while now for railroads, electric propulsion is now making there way into the automotive industry and slowly into some small demonstrator aircraft, with the Hybrid Electric Propulsion System

(HEPS) as a transition technology. The main advantage of a HEPS in automobiles is that the performance of the vehicle becomes better in a wider operating regime. The relatively high efficiency of the Electric Motor (EM) and (for some configurations) the possibility to operate the Internal Combustion Engine (ICE) at its most efficient conditions, makes this possible. In addition, the EM can be used as a generator to convert some of the kinetic energy of the vehicle back into electrical energy to be stored in the battery, by means of regenerative braking which is already applied in many electric and hybrid automobiles.

Nowadays, one of the most promising alternatives as means of propulsion for aircraft, are Hybrid Electric Propulsion Systems. These propulsion systems make use of electrical propulsion combined with one or more other power sources and therefore combine the advantages of each power source. As a matter of fact, the only outweighing advantage an ICE has relative to the EM is the specific energy of the energy source. This becomes a larger problem when applied to an aircraft which has to create a lift force, counteracting the additional weight. Contrary, there are some significant advantages for applying a HEPS to an aircraft. For instance, a hybrid electric aircraft can use electric power only for taxiing when not a lot of power is required, while using both systems for take-off when high power is required. This reduces the amount of fuel consumption due to the higher efficiencies of the system, and thereby reduces the amount of emissions in the form of harmful gases or noise around airports. In addition, the position of the components of a HEPS is more flexible which can result in better aerodynamic shaping of the aircraft. The EM is extremely compact compared to an ICE with the same maximum power output and can even be fitted into the spinner of a propeller [27]. Furthermore, because EM's are relatively scale independent, distributed propulsion by means of more yet smaller EM's is possible.

Due to the large influence of weight on the performance of the vehicle, fully electric aircraft are not yet practical for large scale aircraft and long range missions. The next large step in the development of aircraft might be the hybridization of the aviation industry to sustain the range performance of the aircraft. Currently, some minor development for the implementation of HEPS in small aircraft is carried out. In the last years, the Technology Readiness Level achieved high values of about seven or eight, and some light demonstrator aircraft have already flown with HEPS. The next step is to implement HEPS into slightly larger aircraft, which is currently being accomplished for the General Aviation category aircraft: Pipistrel Panthera. It is considered, that the successful implementation of HEPS into small general aviation aircraft will trigger further development to implement the system into larger aircraft, as a break through technology. For now, the operating performance of HEPS have been assessed quite thoroughly by means of simulations and experiments [42]. However, the impact of this technology on the flight performance has not been fully investigated yet. With the use of two different power sources, the optimum flight path together with the utilization of the battery power can vary significantly for the aircraft's mission.

Chapter 2

Literature review

In order to set up the research proposal the author carries out a literature review. In this literature review information is gathered on the main subject and associating data that can be used during the research. One of the most important aspects of the literature review is the HEPS. Therefore, at first information is obtained on previously completed research and existing application of HEPS as of current state. Since the HEPS needs to be modeled in order to obtain sufficient results, the components of the HEPS and how to model these components is investigated as well. Finally, the aircraft performance needs to be modeled as well together with the mission of the aircraft. Furthermore, the control of the power flow is investigated, the constraint that regulations have on the mission is stated and some existing model are found for HEPS aircraft.

2.1 Hybrid Electric Propulsion Systems

HEPS are defined as systems that provide propulsive power to a vehicle by means of two or more energy sources, where at least one of the energy sources delivers electrical energy. The main idea is to use the different energy sources separately or in combination to adapt the power system for different mission segments. With this aspect, the fuel consumption or energy usage can be minimized and the safety can be increased. So overall the performance of the system improves. Currently, HEPS are used in many automotive applications, ranging from small compact cars such as the Toyota Yaris (figure 2.1) to bigger SUV hybrid cars such as the Mitsubishi Outlander plugin hybrid (figure 2.2) and ranging from super cars such as McLaren P1 (figure 2.3) to commune buses such as the Optare Versa (figure 2.4).

Previously, the ICE has always been preferred for transportation against an EM due to its relative advantages. A list of the advantages and drawbacks of both propulsive systems are given below indicated by a + and − sign respectively, where the ICE type refers to a four stroke cylinder engine. The main reason that ICE's are used instead of EM's for propulsive vehicles is due to the high specific energy of fossil fuels compared

Figure 2.1: Toyota Yaris, small sized hybrid electric car

Figure 2.2: Mitsubishi Outlander, SUV sized plug-in hybrid electric car

Figure 2.3: McLaren P1, super car hybrid electric

Figure 2.4: Optare Versa, hybrid electric commune bus

to batteries. However, this gap is slowly closing by the development of batteries with a higher specific energy. And since the efficiency of an EM is much higher than the ICE, combining both the engine and motor with its energy source and considering the entire drive train, makes this gap even smaller. In addition, the efficiency of an ICE can decrease to about 15% when operating beyond the design point of the engine, whereas the EM has high efficiency over a broader performance range. However, a fully electric propulsive system either decreases the range or endurance or increases the weight of a vehicle significantly due to its relatively low energy density. Therefore, the idea behind the HEPS is to combine both the ICE with the EM accompanied with two different energy sources (battery and fuel tank) to apprehend the advantages of each sub system: the energy density of the ICE and the efficiency of the EM. Thereby conserving the range of the mission but minimizing fuel and energy consumption.

ICE:

+ The specific energy of the energy source (fossil fuel) is high
– Low specific power
– Low peak efficiency
– Most efficient at narrow range of Rounds Per Minute (RPM) and torque
– More noise production and harmful emissions
– Requires more maintenance due to more moving parts

EM:

+ High specific power
+ High power density
+ High peak efficiency
+ Most efficient over wide range of RPM and torque
+ Less noise and harmful emissions
+ Requires less maintenance due to less moving parts
− The specific energy of the energy source is relatively low

In the automotive industry the HEPS mainly consist out of an EM and an ICE together with a fuel cell and a battery as energy source. In between this components, additional parts might be added such as an inverter/converter which control the amount and type of electricity transferring between components or a mechanical clutch that can disconnect mechanical linkage between components. In addition, some systems use a transmission when a different rotational velocity is required and some use an additional EM which functions as a generator or only as a generator. The components used most widely in the automotive industry are also used in the few aircraft that implement HEPS to this day. There are some UAV that use different components, mainly due to the different power sources they use (i.e. hydrogen) [41], however for civil aviation the type of HEPS components are similar to the automotive industry [11]. The manner in which these components are connected can differ resulting in different lay outs.

2.1.1 HEPS Lay outs

In this section the different lay outs of HEPS are discussed. There are different means possible to connect the components for HEPS and most are classified in the categories of parallel, series or combined systems [10]. In the parallel lay out the power flows from the ICE and the EM are added together mechanically as shown schematically in figure 2.5. In the series lay out the EM is supplied with electrical power by the battery and the generator that is connected to the ICE as shown schematically in figure 2.6. The combined uses both of these power flows.

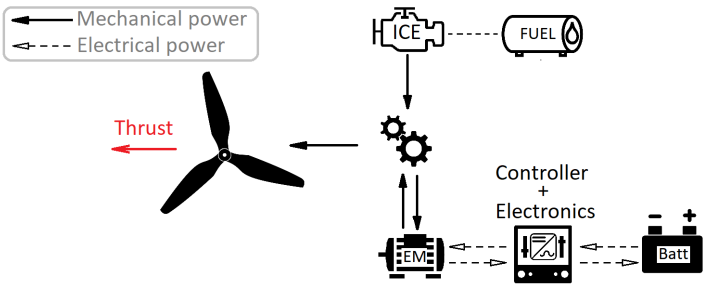

Figure 2.5: A schematic representation of a HEPS in parallel configuration

The series HEPS are the most straight forward configurations of the power train. Because the EM drives the propeller it is connected to the controller of the system by means of electrical wiring. The controller will supply the amount of current and voltage to the EM and thereby control the RPM and torque of the propeller. Therefore, the controller acts

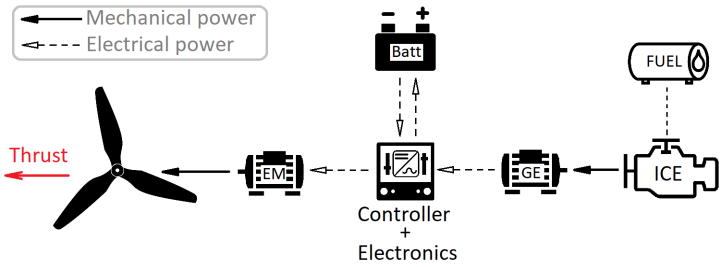

Figure 2.6: A schematic representation of a HEPS in series configuration

as a converter/inverter by transforming the current, voltage and type of electricity from Direct Current (DC) to Alternating Current (AC) because the EM requires AC and the batteries supply DC. The greatest advantage of the series configuration is that the ICE is decoupled from the main drive shaft enabling the ICE engine to run at its peak efficiency for all operating modes and mission segments, autonomously from the required RPM or torque for the drive shaft. Running the ICE at its maximum efficiency results in the minimum amount of fuel consumption and emissions regardless of the mission requirement. This is the main reason the reference aircraft uses this type of lay out. Moreover, decoupling the ICE from the main drive shaft makes the position of the components of the series HEPS quite flexible, which is considerable for aerodynamically shaped bodies. Another relative advantage of the series configuration is that zero emission operation is possible by EM-only mode, which also decreases noise production. Contrary, the essential disadvantage of series HEPS is that it requires an additional generator, which increases the weight of the system. Furthermore, the series HEPS has more energy conversions compared to the parallel configuration resulting in more losses [23]. In addition, the EM must be sized to meet maximum power requirements making this component larger and heavier. Overall the power flow for the series lay out is relatively more flexible. The charging of the battery can be done more independently and even allowing recharging by extracting energy for the vehicles motion (i.e. regenerative braking for automotive vehicles or extracting power from the propeller for aircraft in descent). The advantages and disadvantages of the series HEPS are summarized below.

Series lay out:

+ More efficient off design point operation
+ Position of components more flexible
+ Zero emission operation possible without additional required components
+ Possibility to manage more power flows
– Larger EM for sizing to maximum power output
– More energy conversion so more losses
– Larger size EM

For the parallel HEPS, the ICE and the EM are connected mechanically by a transmission. This implies that the RPM of the ICE and the EM have a fixed ratio depending on the type of transmission that is used. The battery is connected to a converter which converts the electrical delivered power. The EM is connected mechanically to the transmission to which the ICE is also connected mechanically. Because, for the parallel HEPS the EM can function as a generator as well, no additional generator is required resulting

in the advantage that the parallel HEPS has less propulsive components which tend to add to most weight and volume [10]. If the weight of the vehicle is considered, any implementation of additional clutches is not beneficial. This results in no possibility of EM-only mode because of the low efficiency related to turning the ICE against its compression. In addition, the EM adds a mechanical drag to the system once the batteries are fully charged, due to the absence of the clutch. Compared to the series HEPS, this is a significant disadvantage since the system performs only efficiently during hybrid operating mode (both ICE and EM running) and during recharging mode (ICE running and EM acts as a generator). In addition, when operating at off design point the RPM of the ICE is not at its most efficient RPM due to the mechanical connection to the EM. This results in less off design point operating efficiency. Furthermore, there is less flexibility in controlling the power flow, where the battery cannot be charged by using the vehicles motion when deceleration is required. The advantages and disadvantages of the parallel HEPS are summarized below.

Parallel lay out:

+ Potentially less weight (depending on type of EM and transmission)
+ Propulsion redundancy, since both the ICE and the EM drive the power train
– Zero emission operation possible only with additional components
– Increased control complexity
– Complex mechanical couplings
– Lower off design point operating efficiency
– Less flexibility in position of components
– Less flexibility in controlling the power flows

Lastly, there is the combination of both systems, the combined (or series-parallel) HEPS. These systems combine both the advantages of the series and parallel HEPS and therefore perform at better efficiencies for the different operating modes. During off design point operation, a series HEPS would perform more efficiently but during on design point operation the parallel HEPS would perform more efficiently. The decoupling of the power supplied by the ICE from the power demanded by the drive train or control system allows for lighter and more efficient ICE design, increasing the power density of the engine. The inherent disadvantage of the combined HEPS is that the system becomes more complex making it more expensive and more sensitive for maintenance. In addition, the more components add more weight to the system and these combined hybrid systems are currently in their early stages of development and are therefore not feasible to implement in prototype aircraft [10] [29]. The advantages and disadvantages of the combined HEPS lay out are given below.

Combined lay out:

+ Combines advantages of series and parallel
– More complex control strategy
– More weight

2.1.2 HEPS definitions

HEPS are usually defined by two different definitions to define the relative amount of the additional means of propulsion that are added, compared to the conventional system

[11]. This definitions vary for the different lay outs HEPS. The definitions presented in this subsection are for a series HEPS layout, similar to the reference aircraft for this study. The Hybridization Factor (HF) defined by the ratio between the maximum useful electrical power and the sum of the maximum useful power output of each individual power source, as shown in equation 2.1. This means that for a conventional propulsion system $HF = 0$ and for a fully electric propulsion system $HF = 1.0$. Additionally, the definition of Electrification Factor (EF) is used which states the ratio between the total useful energy that is primarily produced electrical to the total amount of useful energy available from all individual sources, given by equation 2.2 for a series lay out HEPS with two power sources. A third definition is added by the author for HEPS which is called the power split factor and which is not based on the design but on the operating condition. It is defined by the same ratio between the electrical power out of the battery and the sum of the power out of each individual power source when it is in operation. The ratio is similar to the HF however it can differ during operation of the HEPS. Due to the fact that the reference aircraft implements a series lay out HEPS, there are two decoupled mechanical drive trains. To distinguish between these two drive train one is called the main drive train, which consists of the propeller that is coupled directly to the EM. The secondary drive train is where the ICE is coupled directly to the generator. Therefore, when the rotational velocity is mentioned it must always be accompanied by the specific drive train.

$$HF = \frac{P_{EM} - P_{ICE+GE}}{P_{EM}} = \frac{P_{batt}}{P_{batt} + P_{ICE+GE}} \tag{2.1}$$

$$EF = \frac{E_{in_{EM}} - E_{out_{ICE+GE}}}{E_{in_{EM}}} = \frac{E_{out_{batt}}}{E_{out_{batt}} + E_{out_{ICE+GE}}} \tag{2.2}$$

$$f_{P_{split}} = \frac{P_{out_{batt}}}{P_{out_{GE}} + P_{out_{batt}}} \tag{2.3}$$

2.1.3 HEPS in Aircraft

Nowadays, HEPS are not yet implemented into large aircraft but are making there way into small general aviation aircraft. The use of HEPS in the aviation industry has been somewhat mediocre. So far, only a hand full HEPS have been successfully retrofitted into small demonstrator aircraft, like the ECO-eagle shown in figure 2.7. Currently, a HEPS is on its way to being implemented into the slightly larger Pipistrel Panthera (the reference aircraft of this study) shown in figure 2.8. The promising advantages of a HEPS used in small aircraft involve less emissions of environmental harmful gases, less production of noise, less fuel consumption affecting directly the operating costs, improved short term performance, reduced heat signature, smaller engine size and long operating life [11] [23]. The essential drawbacks of HEPS in aircraft is that the propulsion system tends to have more weight for the same maximum power due to the additional components as well as the fact that the weight of the batteries does not change during flight because it is independent on the SOC. This increases the aircraft empty weight and therefore decreases the payload capabilities. For the general use of HEPS in aircraft most advantages were

previously mentioned in the beginning of section 2.1. In addition, to those advantages some others are discussed in this section. Depending on the configuration, different advantages and disadvantages of HEPS in aircraft are discussed below.

Figure 2.7: Eco Eagle

Figure 2.8: Pipistrel Panthera

For the series configuration of HEPS in aircraft one of the most significant advantage is that the position of the propulsion components is very flexible. This can be quite substantial for aerodynamically shaped bodies. Furthermore, in the series HEPS the EM is the only propulsion component that directly drives the propeller and EM's are relatively scale independent because their power to weight ratio and efficiency are essentially the same for different sizes. Therefore, the ability to integrate the propulsion system anywhere, or distribute the propulsion system over the airframe comes penalty free. This allows different kind of propulsion system integration design which influence the aircraft design as well. Moreover, since the EM is the only component that drives the propeller, it is more easily possible to use the propeller as a windmill during descent to recharge the batteries, where the EM functions as a generator. The essential disadvantage of series HEPS in aircraft is the size of the EM. Because the EM is the only component that drives the propeller, it must be sized for maximum thrust that is required for take off and climb. This results in a larger EM with more weight than is required during cruise. Together with the additional generator for the ICE this results in a heavier propulsion system relative to the parallel HEPS. The essential advantages and disadvantages of series HEPS in aircraft are summarized below.

Series lay out HEPS in aircraft:

+ Propulsion system components position flexible for aerodynamically shaped bodies
+ EM is relatively scale independent so distributed propulsion is possible
+ More easily possible for using propeller as windmill to recharge the batteries during descent
– EM is sized relatively larger due to higher power requirement on EM
– Relatively heavier system

The parallel HEPS in aircraft can be considered to have less weight relative to the series HEPS due to the fact that it does not have an additional generator and the EM can be sized smaller since both the EM and ICE can drive the drive train directly for maximum power requirements. It is commonly known that the weight of an aircraft significantly influences the performance of an aircraft so the advantage can be decisive. In addition,

because both the EM and ICE are connected directly to the transmission which is connected to the drive train, the aircraft will have engine redundancy. Meaning that if one of the two propulsion components would fail during flight, the other can take over. This is called One Engine Inoperative (OEI). This results in the advantage that the parallel HEPS in aircraft can presumed to be slightly safer. The essential disadvantage of HEPS in aircraft is that the efficiency during off design point operation is relatively less, due to the mechanical link between the drive train and the ICE. It is possible to increase this efficiency by adding variable pitch control to the propeller, however this results in a weight penalty. Furthermore, no emission operation is only possible by adding a clutch to the system resulting is a weight penalty as well, so it can be considered that EM only mode is not favorable for parallel HEPS in aircraft. This takes away some of the general advantages for HEPS in aircraft such as no emissions and less noise during taxiing about the airport. The advantages and disadvantages of parallel HEPS in aircraft are summarized below.

Parallel lay out HEPS in aircraft:

+ Less weight of system
+ Redundancy in propulsion components
− Less efficient during off design point operation
− More noise and emissions during taxi

2.1.4 Existing HEPS in aircraft

Pursuing the proven benefits of HEPS in the automotive industry, some demonstrator HEPS aircraft were designed and produced. However, these demonstrator aircraft all make use of an existing airframe to which the HEPS is implemented. This means that the aircraft design is optimized for conventional propulsion systems. The first documented hybrid electric aircraft called the Hybrid Alatus, designed by the Cambridge University in association with Flylight Airsports, had its maiden flight in 2010. The airframe used for this ultra light weight aircraft is the Alatus-M with a Maximum Take Off Weight (MTOW) of only 235 kg. Followed by this, the larger weight hybrid electric aircraft of the ECO-eagle project had its maiden flight in 2011. The airframe used for this project is the Stemme S10 with a MTOW of 980 kg. After that the maiden flight of the E-Star and E-star 2 were in 2011 and 2013 respectively, which both have a slightly less MTOW of 770 kg. It can be concluded that HEPS are making there way into larger aircraft as their development improves. Therefore, the MAHEPA project is currently on its way to implement a HEPS into a Pipistrel Panthera aircraft with a MTOW of 1315 kg and can house up to four people on board. An overview of the six hybrid electric aircraft is given in table A.1 in Appendix A.

Out of the six aircraft which currently implement HEPS, three use parallel configurations and three use series configurations. It is therefore not certain yet what would be the best configuration to implement in aircraft, although design choices for both systems are carefully assessed. For instance, the Embry-riddle ECO-eagle used a parallel HEPS configuration with a power plant consisting out of a 75 kW Rotax 912 for the ICE and a 30 kW EM powered by lithium-polymer batteries. An overrunning clutch system was

installed to allow the aircraft to take-off with power from the ICE only and perform cruise flight with the EM only. And the DA36 E-star uses a series configuration for the HEPS with a EM of 75 kW and a 30 kW Wankel ICE, which is the opposite of the ECO-eagle. The battery system is therefore able to provide the power for take off and climb and is recharged during the cruise phase. This concept is intended to be used in large scale aircraft and promises to reduce emissions and fuel consumption by 25% relative to current most efficient aircraft propulsion systems [28]. In addition, it has been predicted that the combination of HEPS development accompanied by structural, material and aerodynamic advancements have a fuel saving potential of about 70% [10].

2.2 Propulsion system components

In order to calculate performance characteristics of the aircraft with a HEPS, models are used for the propulsion system components. Accordingly, the propulsion system components are discussed in this section in order to obtain more information and knowledge about how each component is modeled, and what limitation the models might have. For instance, a model of a battery might not have the self discharging characteristics implemented meaning that in reality the battery has slightly less capacity after not being used for some time. Or the influence of temperature on battery performance is not implemented in the model resulting in a less accurate representation. A HEPS consists of a battery, an EM/generator, an ICE, a converter/inverter and a propeller, which are described below.

2.2.1 Battery

Historically, the word 'battery' refers to a device made of multiple cells. Nowadays, the word battery is most likely used as a reference for the storage of chemical energy which can be released to produce electrical power, even if it consists of only one cell. Each cell has its own capacity (Q), nominal voltage (U_{nom}), internal resistance (R) and charge/discharge current (i). A battery usually consists of multiple cells, and the total quantity of the previously mentioned parameter depends on how the cells are connected, with the exception of the total capacity which is always the sum of all individual cell capacities given by equation 2.4. If the battery cells are connected in parallel, shown in figure 2.9, the total nominal voltage, internal resistance and charge/discharge current are given by equation 2.5, 2.6 and 2.7, respectively. Contrary, if the battery cells are connected in series the total nominal voltage, internal resistance and charge/discharge current are given by equation 2.8, 2.9 and 2.10, respectively.

$$Q_{tot} = Q_1 + Q_2 + ... + Q_n \tag{2.4}$$

$$U_{tot} = U_1 = U_2 = U_n \tag{2.5}$$

$$R_{tot} = \left(\frac{1}{R_1} + \frac{1}{R_2} + ... + \frac{1}{R_n}\right)^{-1} \tag{2.6}$$

$$i_{tot} = i_1 + i_2 + ... + i_n \tag{2.7}$$

$$U_{tot} = U_1 + U_2 + ... + U_n \tag{2.8}$$

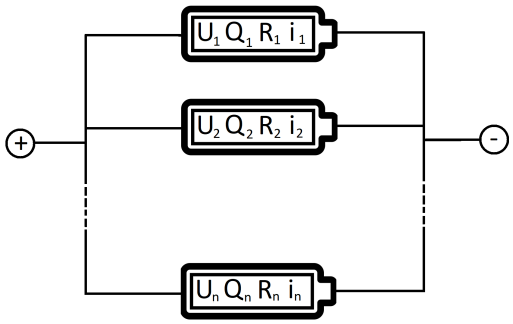

Figure 2.9: Schematic representation of battery cells connected in parallel

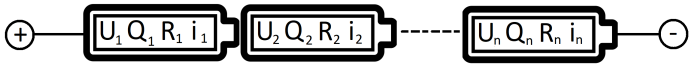

Figure 2.10: Schematic representation of battery cells connected in series

$$R_{tot} = R_1 + R_2 + ... + R_n \tag{2.9}$$

$$i_{tot} = i_1 = i_2 = i_n \tag{2.10}$$

A variety of chemical elements is used in batteries. The choice of chemical element usually depends on the application of the battery. Table 2.1 shows the different chemical elements used in practical batteries accompanied by two different fuels for combustion. Because the battery itself has to be carried as well, it will require more energy for a fixed weight battery with lower specific energy. From table 2.1 it is observed that lithium ion batteries have the most practical specific energy and would be the best option. However, if we compare that with fuel cells, batteries are still not the most efficient means of power storage in weight, especially considering the use of hydrogen combined with ambient air which outperforms the lithium ion battery by more than 200 times. Furthermore, the practical values given in this table have been obtained with batteries discharged at moderate current so that the energy output is optimized. Other conditions may decrease these values. In addition to the high energy in the battery, vehicles acquire high power as well. For lithium based batteries the range is quite extensive, as is observed in figure 2.11. Therefore, in selecting a battery type a trade off between specific power and specific energy is made.

Battery type	**Specific Energy (Wh/kg)**
Lead-acid	35
Nickel-cadmium	35
Nickel-zinc	60
Nickel-hydrogen	55
Nickel-metal hybrid	75
Lithium-ion	150
Lithium-manganese dioxide	120
Hydrogen-ambient air	32702
Methanol-ambient air	6225

Table 2.1: Chemical elements used in practical batteries accompanied by two different fuels for combustion with the specific energy [35]

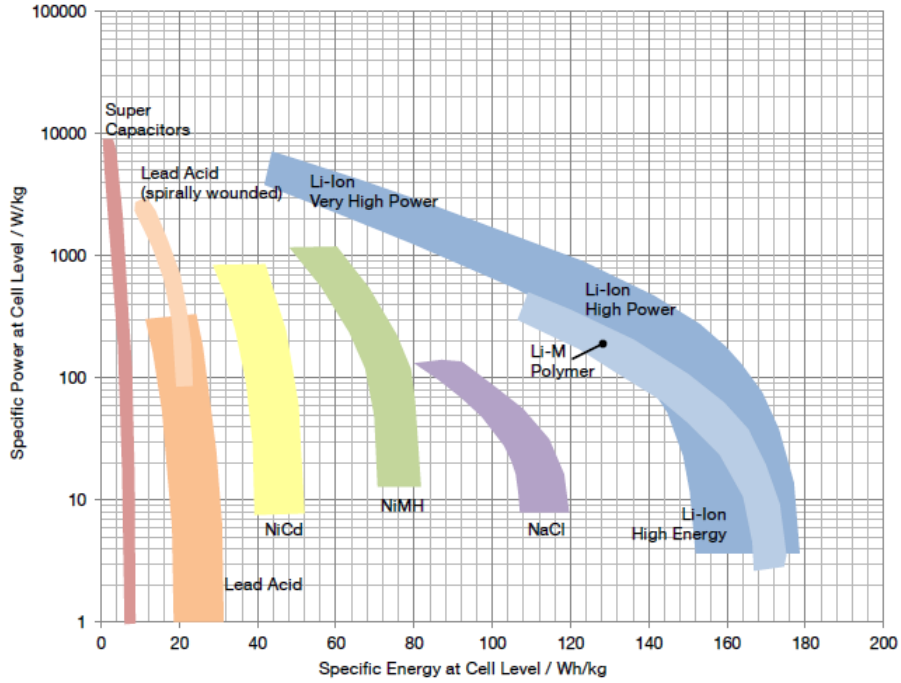

Figure 2.11: Specific Power versus Power Energy for different battery types [39]

The most important aspect of the battery is the charge/discharge performance. The charge/discharge rate of a battery is often expressed in C-rate to normalize against battery capacity which describes the amount of energy the battery is able to contain. Therefore, a C-rate is a measure of the rate at which a battery is charged/discharged respective to the maximum capacity of the battery. A 1C rate means that the current will charge/discharge the complete battery capacity in 1 hour. Therefore, a battery which is charged/discharged at a 2C rate discharges in 30 minutes and vice versa, at a 0.5C rate in two hours. The rate of charge/discharge for a battery also influences the output voltage, capacity and hence efficiency of the battery. Figure 2.12 and 2.13 illustrate the voltage versus the capacity and time of a Kokam Superior Lithium Polymer Battery used during operation, for multiple C-rates. Clearly, the capacity of the battery decreases with increasing C-rate. Furthermore, since the voltage profile becomes lower, less power is gained from the battery cell for higher C-rates. For safety reasons, each type of battery cell specifies a maximum continues charge and discharge C-rate. In addition, the behavior of the battery's charge/discharge cycle is observed to be highly non-linear meaning it is harder to model, with all parameters in mind.

Energy is never ideally obtained from an energy source, meaning there are always losses in some form and magnitude. Relatively, for a battery these losses are not large but still considerable. In the process three types of losses occur called; activation losses, concentration losses and resistive losses. The Sankey diagram for this energy conversion is shown in figure 2.14. The resistive losses are the largest of these three losses and are caused by the battery's internal resistance. These losses determine the efficiency of the energy conversion of the battery and are depended on the type of battery used. Table 2.2 shows the efficiency range for the currently three mostly used battery types.

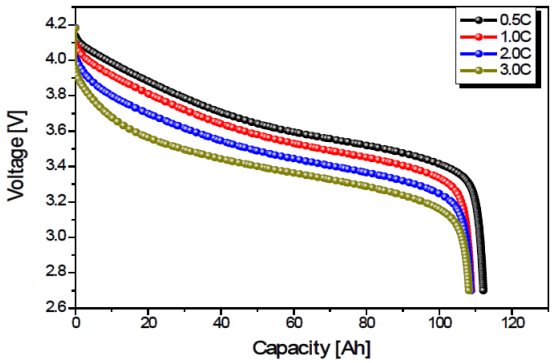

Figure 2.12: Discharge curves for a Kokam Superior Lithium Polymer Battery with a capacity of 110 Ah [1]

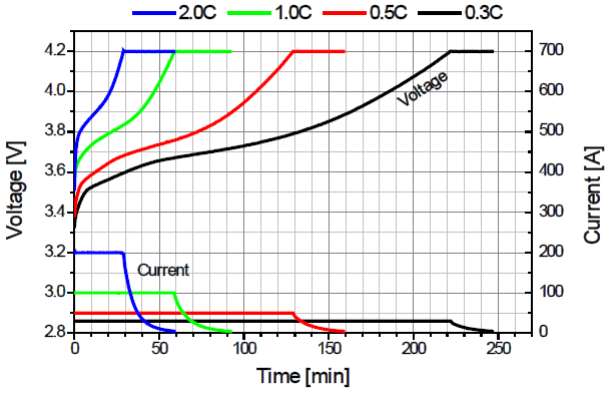

Figure 2.13: Charge curves for a Kokam Superior Lithium Polymer Battery with a capacity of 110 Ah [1]

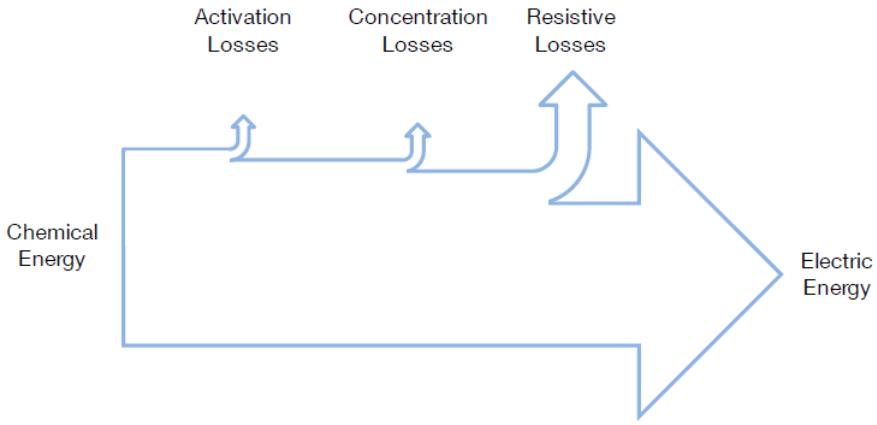

Figure 2.14: The Sankey diagram for battery efficiency [39]

Battery type	Efficiency range [%]	Source
Lithium-ion	80-99%	[24]
Lead-acid	50-95%	[3]
Nickel-method	66%	[26]

Table 2.2: Efficiency range for different battery types

Currently, the most widely used batteries in newly designed aircraft are Lithium-Polymer batteries due to the high energy density. For batteries used in aircraft there are slightly different requirements than for land based vehicles. The two most important requirements are safety and low weight. Other requirements are reliability, safety, operating efficiently over wider range and require minimum maintenance. Although the safety has been somewhat overlooked as there was an incident in 2013 where a lithium-polymer battery overheated and caused a smoky fire in a new Boeing 787 Dreamliner [38]. Besides overheating and causing fire, battery leakage can cause corrosion of surrounding materials. So safety is quite a significant concern when implementing batteries in aircraft. In

addition to the enhanced safety, lithium based batteries are of low maintenance. Nowadays, these type of batteries are also known for the high specific density, sound reliability and a good safety record. These trends also helped introduce the lithium based batteries into the aviation industry.

2.2.2 Electro motor/Generator

The EM is a machine which converts electrical energy to mechanical energy. The motor does this by running currents through windings which create a magnetic field which than produces a force to rotate the motor. The main reason the EM is not yet largely used in propulsive vehicles as part of the main drive train is that the electrical energy source cannot yet be efficiently stored in terms of weight, relative to fossil fuels. But as battery technology grows, the implementation of the EM in propulsive vehicles becomes more attractive. In addition, the power to weight ratio of an EM is much higher than that of an ICE. The component is also able to perform an opposite energy conversion, where mechanical energy is converted into electrical energy. During this operation the EM is called a Generator. The efficiency of an EM is given by the output mechanical energy divided by the input electrical energy, and opposite for a generator. The losses of an EM this are illustrated by the Sankey diagram given in figure 2.15. The friction losses are caused by the friction that occurs between the Rotor and the Stator, usually in the bearings and by the surrounding air of the Rotor, but also for brushed motors by the brushes. The resistive losses occur due to the ohmic resistance in the electrical wires used by the EM. The other losses are called iron losses which consists of hysteresis losses and Eddy Current losses. Hysteresis losses are caused by the energy losses that occur in the alternating magnetization of the iron core and Eddy Current losses are caused by the changing magnetic field as well.

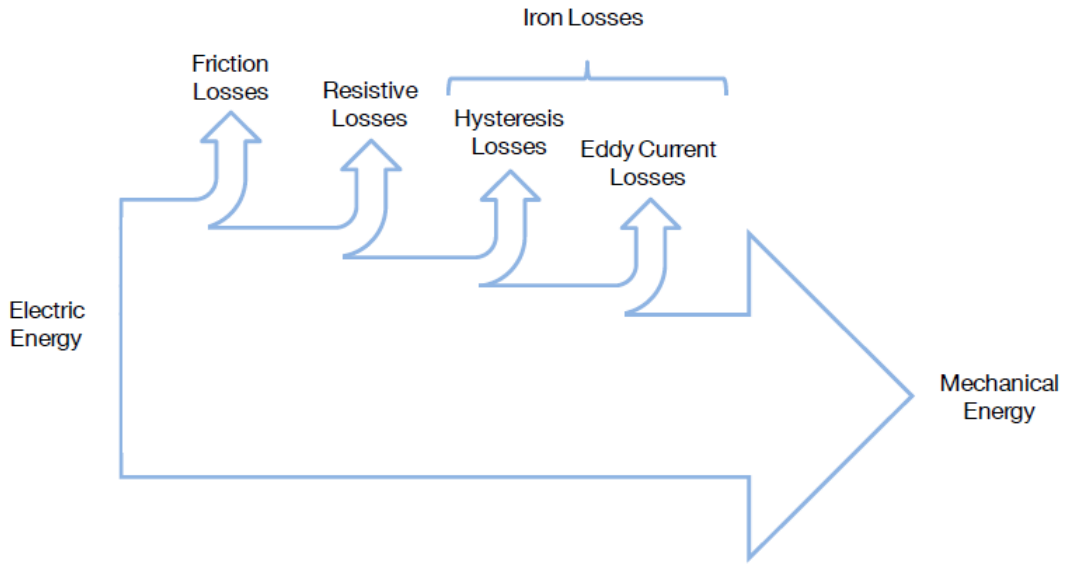

Figure 2.15: Sankey diagram for losses in an EM [39]

For every type of EM, efficiency depends on several factors like specific torque and ro-

tational speed. For a given rotational velocity, the efficiency of an EM increases with a higher torque and for a given torque, the efficiency increases with higher rotational velocity [19]. Efficiency increases with the size of the EM only substantially at very small scale. The range is quite extensive where wrist watches can have EM with efficiencies of $\approx 1\%$ and very large EM can have efficiencies up to $\approx 95\%$. The reason for this is that the resistive losses become dominant for a smaller EM. In addition, the power output of a brushless EM rises with increasing rotational speed while electrical losses that occur stay almost constant. In this manner, the efficiency of an EM increases with increasing rotational velocity. For a brushed EM this is quite the contrary, where the friction forces increase with increasing rotational velocity due to the friction produced by the brushes. The typical maximum achievable efficiencies of the different type of EM's are given in table 2.3.

EM type	**Efficiency [%]**	**Source**
Brushed DC motor	$\approx 80\%$	[17]
Induction motor	$\approx 90\%$	[21]
Permanent Magnet AC motor	$\approx 95\%$	[14]

Table 2.3: Efficiency for different EM types

Whether altitude has an effect on the performance on an EM is rather debatable. Multiple sources state that the EM is essentially insensitive to changes in atmospheric conditions due to altitude. However, operating manuals for the Siemens NEMA motor state otherwise [5]. It states that due to less denser air the heat dissipation rate will be less, resulting in a decrease in the EM's performance. In addition, the ambient temperature also influences the performance of an EM, because lower ambient temperatures result in higher heat dissipation rates. Because the ambient temperature decreases with increasing altitude this effect works vice versa. However, according to this source the decrease in air density influences the heat dissipation rate more than the decreasing ambient temperature. Therefore, a derating factor is specified for these EM's which is depending on the operating altitude as well as the operating ambient temperature. This derating factor must be multiplied with the nominal power output at sea level to gain the power output at altitude. The combination of altitude and ambient temperature for the derating factor of a Siemens NEMA motor is shown in figure 2.16. The Siemans NEMA motors are designed for operating at ambient temperature of $40°C$ and at 1000 meters altitude. Therefore, the derating factor is 1 at that point. The data is obtained by Siemens from experiments and the derating factor is determined by measuring the Brake Horse Power (BHP) at different altitudes and ambient temperatures and dividing that by the calculated input power.

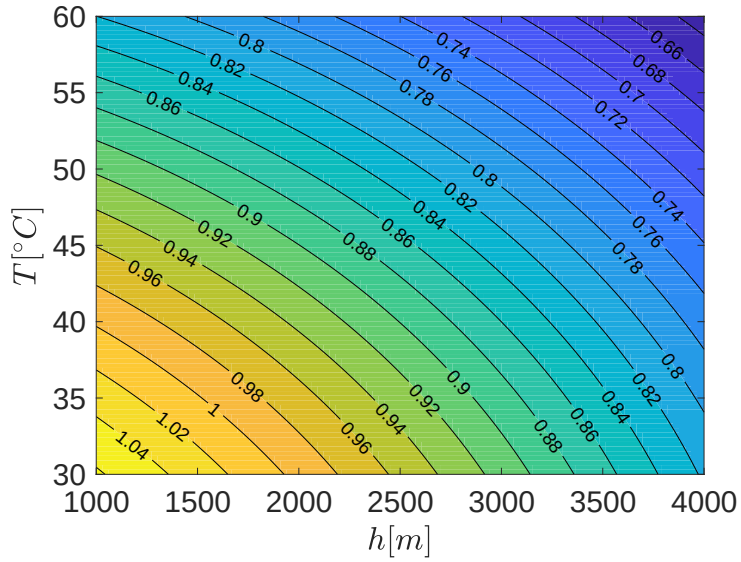

Figure 2.16: Derating factor versus the ambient temperature and altitude, interpolated data from source [6]

2.2.3 Internal Combustion Engine

The ICE is a machine which converts chemical energy in a fuel into mechanical power by means of combustion. ICE's are widely used in propulsive vehicles. The main advantage of the ICE is that it uses fossil fuel which has a relatively high specific energy. The main disadvantage of the ICE is that it has relatively low efficiency and requires more maintenance. The ICE mentioned in this section is a piston engine that uses combustion of a fuel together with an oxidizer to produce the mechanical energy. This takes place inside a cylindrical combustion chamber with a piston. Generally, there are two types of ICE's; 2-stroke engines and 4-stroke engines. 4-stroke engines are most efficient and are therefore most widely used in propulsive vehicles. Due to the low efficiency of ICE's only a small amount is converted into mechanical energy. The rest is lost due to heat transfer, incomplete combustion, leakage and friction. These loses are shown in the Sankey diagram for ICE's given by figure 2.17. Fuel conversion losses tend to be the largest of the losses that occur in an ICE. Fuel conversion losses include thermal conversion losses and combustion losses. The thermal conversion losses are the part of the total amount of energy that is released that is not converted into work, such as the heat dissipation. The combustion losses describe the energy that is not released from the fuel during the combustion process due to incomplete combustion. The friction and volumetric losses occur due to imperfections in the mechanics of the engine.

The influence of altitude on the performance of an ICE is quite important when the engine is mounted in an aircraft. The most significant effect is the decrease in atmospheric pressure, because the inlet air pressure has a significant effect on the performance of an ICE. Less inlet air pressure results in less mass of oxidizer available for combustion. This results in a decrease in engine output power and efficiency. With increasing altitude temperature decreases as well. The effect of temperature is less significant on the power and efficiency of an ICE than pressure but does have an adverse effect. With decreasing

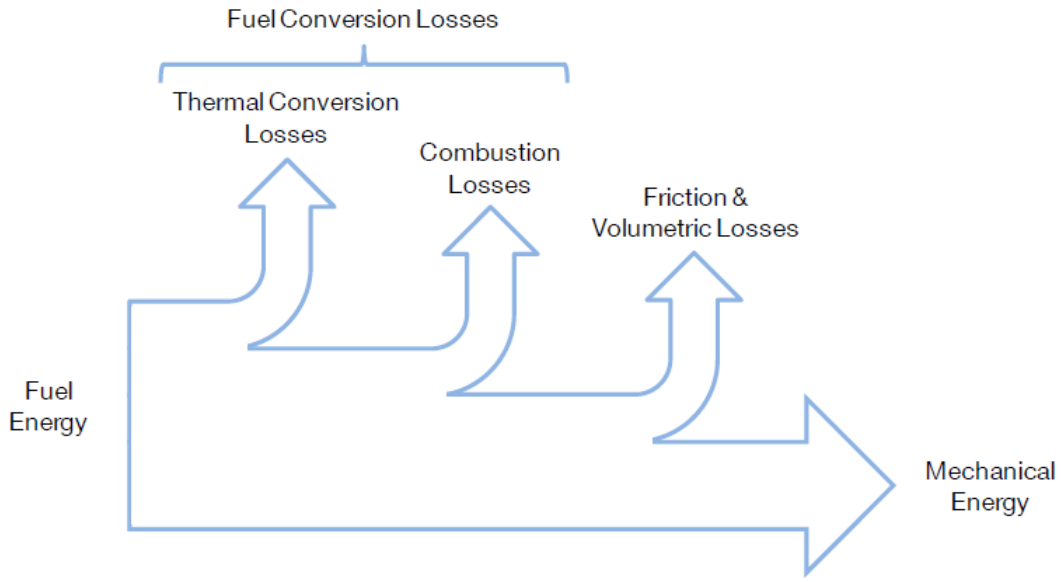

Figure 2.17: Sankey diagram for losses in an Internal Combustion Engine [39]

temperature an ICE operates more efficiently. Overall, it can be concluded that the performance of an ICE decreases with increasing altitude like shown in figure 2.18.

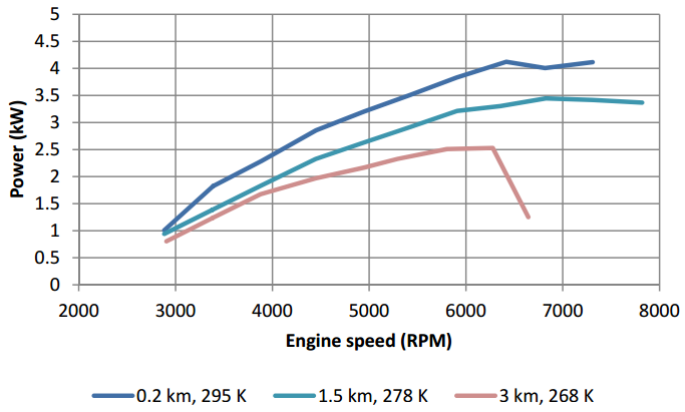

Figure 2.18: The output power of an ICE versus the rotational speed for different altitude [20]

2.2.4 Power management module

The power management module or controller of the HEPS is an electronic unit that controls the entire system. The component receives inputs from the operator as well as from a control computer. One of the important task for the power management module is to control the amount of torque and rotational velocity of the EM and monitor the status. Another task is to invert the DC supplied by the battery to AC required by the EM and vice versa for the generator. This is called the inverter which is shown graphically

in figure 2.19. The main components of the inverter are diode rectifiers and switching components, which are connected in parallel or series [32].

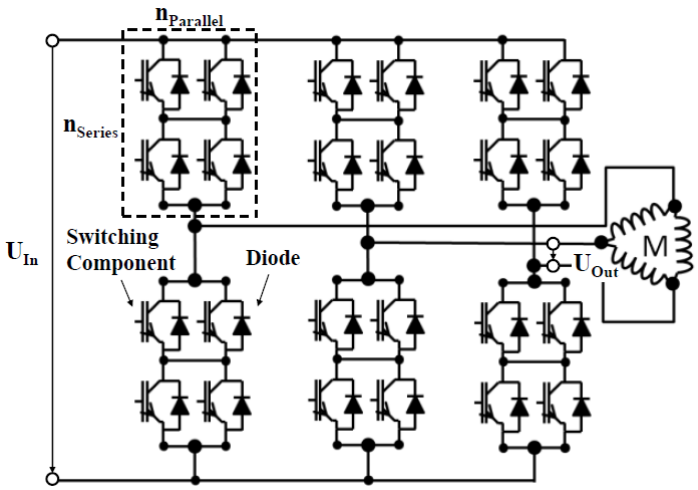

Figure 2.19: Graphically representation of an inverter for an EM [32]

For the inverter, the efficiency can be modeled by using data from existing switching components and using scaling dependencies for the estimation. The efficiency is estimated by equation 2.11, where the power of the losses is equal to the sum of all individual losses. These losses include conduction and switching losses from the transistor as well as the diode, and therefore the sum is multiplied by the number of switches in parallel and series, shown in equation 2.12. In practice these losses are usually quite low resulting in high inverter efficiencies ($\approx 99.5\%$) [32].

$$\eta_{inverter} = \frac{P_{out}}{P_{in}} = \frac{P_{out}}{P_{out} + P_{losses}} \tag{2.11}$$

$$P_{losses} = (P_{IGBT,switch} + P_{IGBT,cond} + P_{diode,switch} + P_{diode,cond}) \cdot n_{paralell} \cdot n_{series} \tag{2.12}$$

2.2.5 Propeller

The propeller is also a component that is part of the drive train of a HEPS in a small general aviation aircraft. The propeller is the component that transfers the mechanical energy produced by the propulsion system, into a propulsive force. It achieves this by spinning the component and thereby creating an aerodynamic pressure difference resulting in a suction force. To model the propeller, the efficiency is one of the most important aspects. The efficiency depends largely on the advance ratio, which is the ratio between the forward flight speed and the tip speed of the propeller. For generic propellers the efficiency curve is shown in figure 2.20. For this case the efficiency has a maximum value of about 87% [36]. The propeller can be modeled in many different ways but the most common models are the Actuator Disk Theory (ADT) and the Blade Element Method (BEM). For these models the dimensions of the propeller are required.

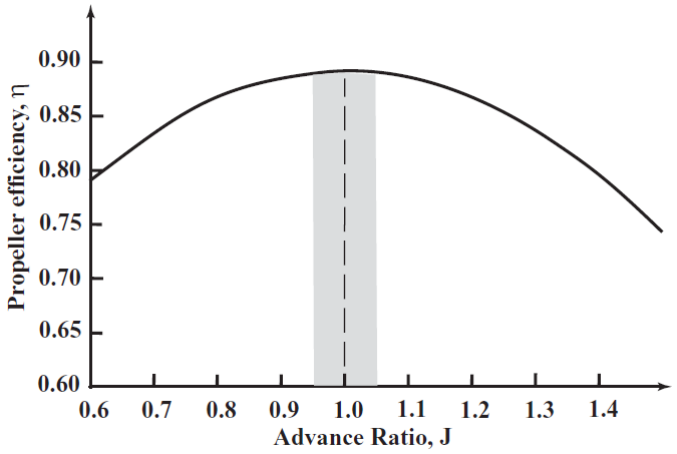

Figure 2.20: Propeller efficiency versus advance ratio [36]

The most important aspect of the propeller model is the power that is available, which equals the thrust force that is created multiplied with the forward speed. This power is also the jet propulsive efficiency multiplied with the shaft brake power, shown in equation 2.13. Therefore, the power available depends on the jet propulsive efficiency which depends on the advance ratio. So for a fixed RPM the power available depends largely on the forward flight speed. Basically, there are two different propellers for piston engines. There is the constant speed propeller that has a fixed RPM and can change the pitch angle of the blade along with the inlet manifold pressure of the ICE, to change the amount of thrust. The other propeller is a fixed pitch propeller for which the pilot can change the RPM of the propeller to change thrust. The difference between the two in terms of performance can be seen in figure 2.21 and 2.22. From these graphs it is observed that the constant speed propeller has more power available at a wide range of flight velocity. Only at the highest velocity both propeller powers are equal. Furthermore, the efficiency of the constant speed propeller is also better than the fixed pitch propeller for a wider range of advance ratio. Overall it can be concluded that the constant speed propeller has better performance. However, it should always be considered whether the additional weight and complexity of a constant speed propeller is worth the increase in performance during the initial design phase of an aircraft propulsion system.

$$P_a = \eta_j P_{br} \tag{2.13}$$

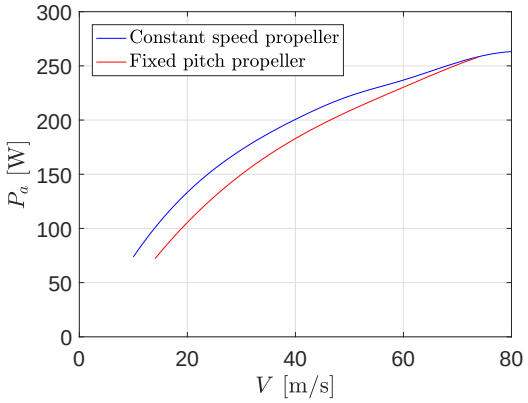

Figure 2.21: Power available versus flight speed for constant speed propeller and fixed pitch propeller [37]

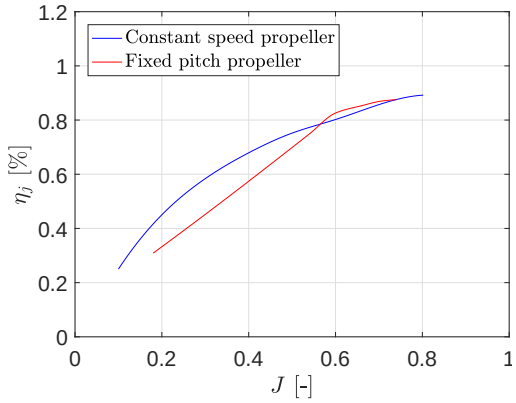

Figure 2.22: Propulsive efficiency versus advance ratio for constant speed propeller and fixed pitch propeller [37]

2.3 Modeling of Performance

In this section the modeling of the performance of the aircraft and its HEPS are discussed. At first the two driven parameters in aircraft performance are discussed. Thereafter, the mission analysis is discussed for a conventional case for comparison with the obtained results for this thesis. In addition, an existing method is discussed for the mission analysis for a HEPS aircraft. This information is used as an input on the methodology for analyzing the mission for this study. Furthermore, the methods to control the power flow are presented with there capabilities and limitations. Because optimization theory is used to solve the problem statements for this study, some basic information of this subject is presented as well. For this optimization problem constraints and bounds exist and some of them are enforced by regulations. Therefore, the constraints on the flight path that are applicable are presented as well. Lastly, some existing models for HEPS aircraft are discussed and presented.

2.3.1 Power available and Power required

The two most important parameters to determine the performance of an aircraft are the power available (P_a) and power required (P_r). The power available is the useful power that the aircraft has during flight and is therefore the product of the thrust (T) the propeller induces and the airspeed (V). The power required is the power that the aircraft must have to perform a specific part of the flight and therefore differs in each segment. The most general equation for power required is the summation of the product of the drag (D) and the airspeed, which represents the power the aircraft needs for steady symmetric flight, and with the change in kinetic and potential energy with time it needs for a certain part of the flight. This is given by equation 2.14 and can be rewritten as equation 2.15.

$$P_r = DV + \frac{d}{dt}\left(E_k + E_p\right) \tag{2.14}$$

$$P_r = DV + \frac{d}{dt}\left(\frac{WV^2}{2g} + Wh\right) \tag{2.15}$$

For steady and level flight, where there are no accelerations and the altitude remains constant, the change of kinetic and potential energy with respect to time becomes zero. In that case the difference between the power available and power required can be plotted in a graph, which is shown in figure 2.23 for a propeller aircraft with the important points. The first point is the lowest flight speed point on the power required curve. This point represents the minimum speed at which the aircraft is able to perform steady symmetric level flight. This is also called the stall speed (V_{min}) which occurs at the highest achievable value of the lift coefficient ($C_{L_{max}}$). The maximum endurance is the point where the power required has the lowest value. The next point on the graph is the maximum range point. This point is important for the performance of an aircraft because range is usually more important than the endurance in terms of performance. The last point is where both curves intersect. Beyond this point the aircraft does not have enough thrust to overcome the drag of the aircraft and can not have steady level flight. Hence, the velocity of this point represents the maximum flight speed of the aircraft.

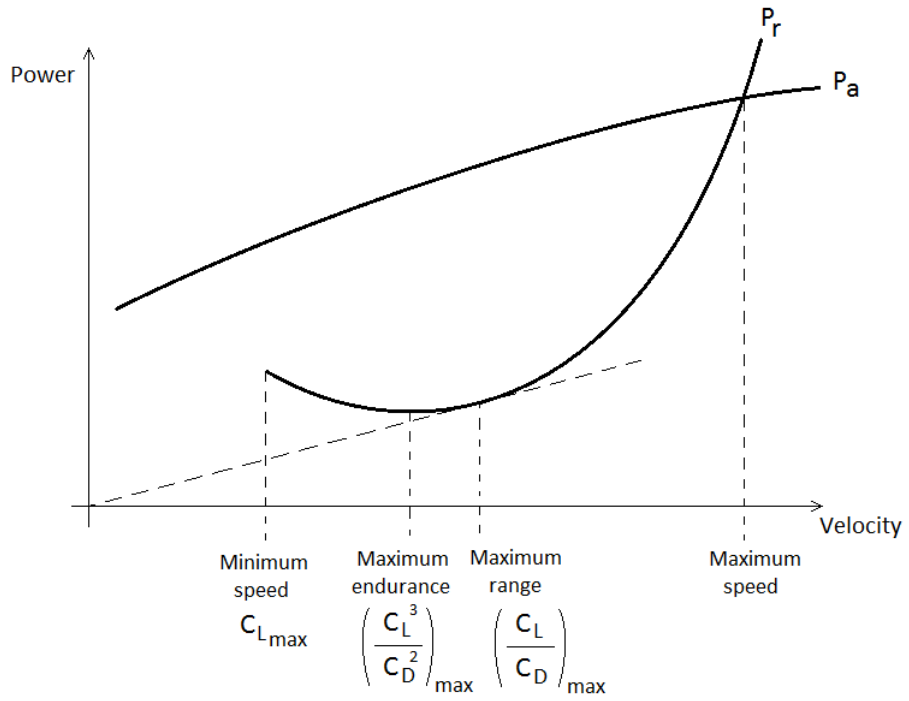

Figure 2.23: A performance diagram of a typical small propeller aircraft with piston engines

2.3.2 Mission analysis for conventional aircraft

In this section the mission of a conventional aircraft is analyzed. The mission of a conventional aircraft usually consists out of segments that are described below and shown in figure 2.24. The total mission profile also includes a part where the aircraft is able to

climb out, loiter and descent again in case of emergency or a failed landing attempt. This means that there must be certain amount of reserve energy available at the end of the main mission segment. For a flight the take-off and landing segments are required and are restricted by the regulations as well as the dimensions of the airfield. The airborne phase of the aircraft is usually split into three segments called the climb, cruise and descent. For normal aircraft mission profiles the cruise is by far the longest segment of the flight and it is therefore of economic interest to get to cruise altitude as quickly as possible because higher altitudes result in less overall drag, which saves fuel. After the cruise the aircraft start to descent towards the airfield. Below the main sections of flight which are optimized for this study are discussed with the appropriate Free Body Diagram (FBD) and equations of motion.

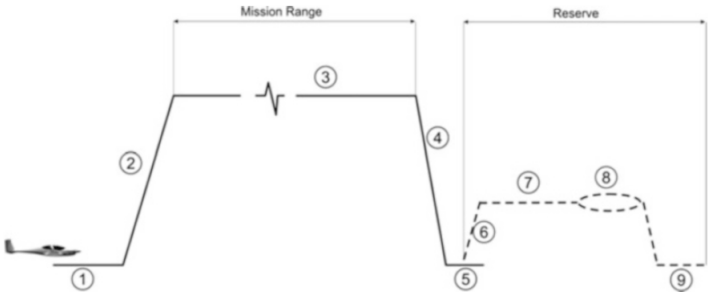

Figure 2.24: Mission profile Pipistrel Panthera [42]

The take-off is defined as the section of flight where the aircraft begins at stand still position and then accelerates along a runway to a rotation speed (V_R) at which the pilot is able to command the aircraft to increase its angle of attack to increase lift. The aircraft then lifts off and begins climbing until it reaches a height of 15 m above the take-off surface. The take-off maneuver can therefore be split into two segments, the ground phase and the airborne phase. During the ground phase the FBD shown in figure 2.25 with the equations of motion given by equation 2.16 to 2.18 determine the performance. For the airborne phase a different FBD is given by figure 2.26 resulting in the equations of motion given by equation 2.19 to 2.22.

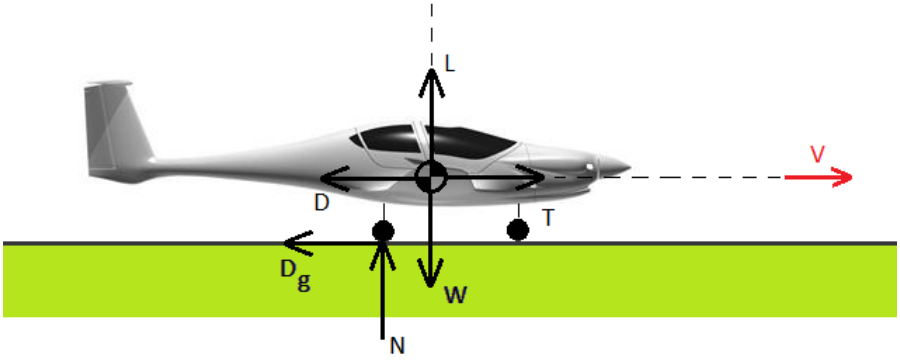

Figure 2.25: Free Body Diagram ground run

$$\dot{v} = \frac{T - D - D_g}{m} \tag{2.16}$$

$$0 = N + L - W \tag{2.17}$$

$$D_g = \mu N \tag{2.18}$$

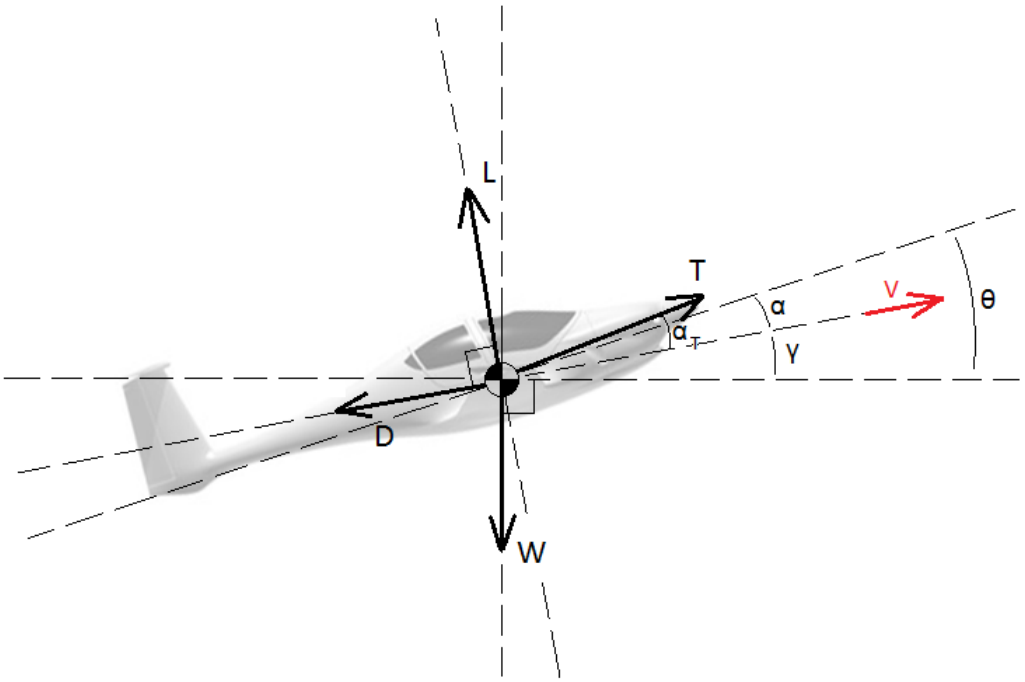

Figure 2.26: Free Body Diagram airborne phase

$$\dot{x} = v\cos(\gamma) \tag{2.19}$$

$$\dot{h} = v\sin(\gamma) \tag{2.20}$$

$$\dot{v} = \frac{T\cos(\alpha) - D}{m} - g\sin(\gamma) \tag{2.21}$$

$$\dot{\gamma} = \frac{T\sin(\alpha) + L}{vm} - \frac{g}{v}\cos(\gamma) \tag{2.22}$$

The climb segment of an aircraft mission is the segment after take off where the aircraft gains altitude. The climb is usually performed to gain altitude for the cruise segment since drag is less at higher altitude. For climb the same FBD applies as in figure 2.26 and hence the equations of motion are also given by equation 2.19 to 2.22. A pilot usually performs a climb by keeping the air speed on the cockpit instrument, called Indicated Air Speed (IAS), constant. With increasing altitude the density decreases meaning that the dynamic pressure also decreases resulting in an increasing difference in IAS relative to the True Air Speed (TAS). Therefore, when a pilot performs such a climb, the aircraft accelerates during this maneuver and the flight path angle slowly decreases. This means

that the climb is unsteady. However, most of the time the change in flight path angle is significantly small and the flight path can be considered quasi-rectilinear. For the minimum time to climb for a propeller driven aircraft the result is quite simple. The aircraft needs to fly at its maximum rate of climb. Therefore, the aircraft must fly at the airspeed where the maximum excess power occurs. For the minimum amount of fuel consumption this is somewhat different where the ratio between the steady rate of climb to fuel flow must be maximized.

Generally, the cruise segment of the mission profile is the largest segment of the flight. Hence, the performance during cruise is of most importance for the design of aircraft. Aircraft are usually optimally designed for performance during cruise and for other segments additional devices are added to increase the performance of flight such as flaps or variable pitch propellers. The most important requirements for cruise flight are usually endurance and range. Endurance is of significant performance for flights where the amount of time in the air is important, e.g. observation flights. Whereas range is of importance when the mission of the flight is to transport payload from point to point. For the mission profile of the aircraft considered the range is of most importance. Because cruise is the largest segment of the mission the most amount of fuel is used. This results in larger differences in initial and final weight of the aircraft during cruise flight and therefore the flight path is generally not at constant altitude or rectilinear. The FBD for cruise is given by figure 2.26 as well and the same equation of motion apply as for the climb segment, however, some parameters might by significantly smaller such as flight path angle γ and angle of attack α.

2.3.3 Existing method for mission analysis HEPS aircraft

T. Nam et al. [40] proposes a method to divide the mission into small legs, which allows to assume that several parameters, such as the aerodynamic coefficients and the overall efficiencies of the power paths, are constant during each leg. This simplifies the associated equations significantly, compromising the analysis accuracy as little as possible. For each of these legs, the amount of consumable energy is determined and the summation of these determine the total amount of energy that is required for the mission. For the power available they state that it is the summation of n individual power path, as shown by equation 2.23. This expression can be modified by introducing a fraction factor (τ_i) resulting in equation 2.24. In addition, the power from each source (P_{i_0}) is converted through multiple energy conversions with individual efficiencies (η_i) resulting in equation 2.25 for each individual power path. For the fact that the flight conditions vary, a power lapse factor (α_i) is used so that the source power can be written in terms of sea level conditions, shown in equation 2.26. Combining the equations results in one equation for the source power at sea level condition given by equation 2.27. This equation combined with Newton's second law to describe an aircraft motion given by equation 2.28, results in this so called master equation, given by equation 2.29. Here, R represents the additional drag due to changes of the configuration, β represents the weight fraction, K_1 is the drag polar coefficient for the 2nd order term and K_2 is the drag polar coefficient for the 1st order term. This master equation applies for each flight segment, but has different conditions for each flight segment.

$$P_a = \sum_{i=1}^{n} p_i \tag{2.23}$$

$$P_i = \tau_i P_a \tag{2.24}$$

$$P_i = \Pi_{\eta_i} P_{i_0} \tag{2.25}$$

$$P_{i_0} = P_{i_0 SL} \alpha_i \tag{2.26}$$

$$P_{i_0 SL} = \frac{\tau_i P_a}{\Pi_{\eta_i} \alpha_i} \tag{2.27}$$

$$(T - (D + R))V = W \frac{dh}{dt} + \frac{W}{g_0} \frac{d}{dt} \left(\frac{V^2}{2} \right) \tag{2.28}$$

$$\frac{P_{i_0 SL}}{W_{TO}} = \frac{\tau_i \beta}{\Pi_{\eta_i} \alpha_i} \left\{ \frac{qS}{W_{TO}} \left[K_1 \left(\frac{n\beta}{q} \frac{W_{TO}}{S} \right)^2 + K_2 \left(\frac{n\beta}{q} \frac{W_{TO}}{S} \right) + C_{D_0} + \frac{R}{qS} \right] + \frac{1}{V} \frac{d}{dt} \left(h + \frac{V^2}{2g_0} \right) \right\} V \tag{2.29}$$

2.3.4 Optimization of mission profile and flight conditions

For the optimization of the mission profile and flight conditions, first some general theory about optimization is discussed. Optimization is always about finding maximums or minimums. So that means finding the values for the n-length vector $\vec{x}$, given by equation 2.30, for which an objective function $J = f(\vec{x})$ has either a minimum of maximum. The necessary conditions for a minimum or maximum (extremum) to occur is that the partial derivatives of the function to each variable x_i either vanish simultaneously or at which one or more of these derivatives are discontinuous [30]. The points at which these occur are called the stationary points of J and represent local extrema. In practical optimization problems, the variables x_i are defined in a region R. That means that the variables x_i may be bound between certain values, as well as the solution J may be constraint by equality and inequality constraints. Therefore, the values of J along the boundary of region R have to be checked and compared with the found local extrema, which means that the global minimum or maximum will be defined in this region or on the boundary of this region. The variables x_i that are subject to m equality constraints in the form of relations given by equation 2.31.

$$\vec{x} = (x_1, x_2, ..., x_n) \tag{2.30}$$

$$\begin{aligned} &g_1(x_1, x_2, ..., x_n) = 0 \\ &g_2(x_1, x_2, ..., x_n) = 0 \\ &... \\ &g_m(x_1, x_2, ..., x_n) = 0 \end{aligned} \tag{2.31}$$

In general, literature states that the problem of determining the optimum flight path of an aircraft is very complex problem. Overall, it cannot be solved without using numerical computation based on models of the aircraft, atmosphere and propulsion system [30]. At first it is recommend to investigate the segment of flight separately and later combine them. For instance, combining the segments may results in an excessive energy use in one segment which is gained in the other segment.

2.3.5 Constraints on flight path by regulations

In this section the constraints on the flight path by regulations are reported. Every aircraft must comply to regulations set by the European Aviation Safety Agency (EASA) in order to certify. Some of these regulations concern the flight path of an aircraft. For this thesis assignment the flight path is optimized for the Pipistrel Panthera aircraft and therefore the regulations for Normal, Utility, Aerobatic, and Commuter Category Aeroplanes are used. These are given by the Certification Specifications number 23 (CS-23). Table 2.4 gives the number of the requirements that are applicable to the flight path to a certain extent, with a short explanation of how they influence the flight path of an aircraft.

Requirement	Influence on flight path
CS 23.49 Stalling speed	Determines the minimum speed at which the aircraft may or is able to fly
CS 23.51 Take-off speeds	Determines the speed and flight path angle at which the climb segment starts
CS 23.65 Climb: all engines operating	Determines the minimum climb gradient
CS 23.69 En-route climb/descent	Determines the minimum climb speed
CS 23.73 Reference landing approach speed	Determines minimal speed in approaching the runway for landing
CS 23.75 Landing distance	Determines the maximum descent gradient before landing

Table 2.4: The CS-23 constraints per number and influence on flight path [15]

2.3.6 Existing models

The modeling of a HEPS aircraft is challenging and requires some different kind of tools and disciplines. This is mainly due to the different kind of timescales involved in the dynamics of the systems. For the aircraft modeling the time step could be in the order of minutes while for the modeling of the engine and energy storage the time step would be in the order of seconds. One step further, modeling the electrical system requires time steps in the order of micro seconds. Models for aircraft might consist out of three different categories present in literature; detailed physics-based models, first-order analytical models, linearized models created from higher fidelity tools [12]. In this section some of the existing models for aircraft and hybrid propulsion system are discussed including the software packages that might be used for these models.

C. Friedrich et al. [16] make use of Matlab Simulink to model the HEPS and for the aircraft dynamics it is coupled and synchronized with X-plane (Plane-Maker) by Real-Time Windows Target. X-Plane provides the aerodynamic constants to predict the lift-drag polar of the aircraft by analytical and empirical calculations. For the modeling of the HEPS components, data is used that the author's gathered by bench testing some of the components. For the ICE an engine map is used modeled by ADVISOR automotive simulator. The propeller is modeled by making use of JavaProp and using that data in

look up tables for Matlab Simulink. For the EM they tested the motor in a bench test as well and created a model with the data for the copper and iron losses. This data is then extrapolated to higher power levels. The battery is modeled by the data the manufacturer of the battery supplies.

V. Cipolla and F. Oliviero [42] recently developed a simulation tool for the analysis of performance of hybrid aircraft called HyPSim. This tool is composed of three main software parts: a Flight Simulator which calculates the flight data, a Flight Planner which defines the mission of the aircraft and if the flight is performed manually or autonomously; a Performance Module in which the HEPS is modeled by analytical expressions and the flight data. The main flight parameters are displayed on a Human Machine Interface (HMI) for visualization. For the Flight Simulator X-Plane (Plane-Maker) is used since it provides reliable data on aircraft aerodynamics by use of a panel method, and it is easy to couple with other programs. Comparing the model with experimental data of the power required provided by the manufacturer of the reference aircraft, shows a good model accuracy, with a small deviance at low speeds, shown in figure 2.27. The aerodynamic forces and flight data is provided to the Performance Module which determines the power available and predicts the endurance of the aircraft. The Performance Module is developed in Matlab Simulink with two different blocks; one for the modeling of the HEPS and one for the endurance estimation. Within the Performance Module the HEPS is modeled, including the propeller, in Matlab Simulink shown in figure 2.28. In the ICE block the efficiency is determined depending on the altitude, by means of interpolating data provided by the manufacturer of the ICE used in this case. In the P block the propulsive efficiency is calculated for the propeller by means of the ADT. With the flight conditions as input, this block also calculates the power demand for the EM. The CON block simulates the control system for the HEPS by means of control laws and methods. The SOC block represents the SOC of the battery. This block uses the power request from the batteries as input and calculates the SOC by means of an energy balance which takes internal losses into account. The FUEL block represents the model for the fuel consumption by uses the power required by the ICE as input. For the electric components such as the EM, Generator and inverter/converter, the models are still in development and are currently represented by constant gains representing the efficiencies. For initialization of the model these values can be changed. Another part of the Performance Module is the Predictor which determines the remaining flight endurance at each time step. It is updated throughout the flight to account for external interferences such as wind. The last part called the Flight Planner is an in-house build software program which acts as an autopilot for the simulation.

T. H. Bradley et al. [41] make use of a simplified aircraft and propulsion system model which is based on experimental data. The simplification is necessary because the optimization of flight path problem they implement requires it to reach sufficient and generalizable conclusions. For the aircraft characteristics the same equations of motions are used as discussed in subsection 2.3.2. The propulsion system is based on a hybrid system with hydrogen as fuel so it is somewhat different as for this study. Therefore, the propulsion system is modeled as a static polarization curve that represents the performance of the fuel cell and balance of the systems. The efficiency and consumption of the fuel cell are

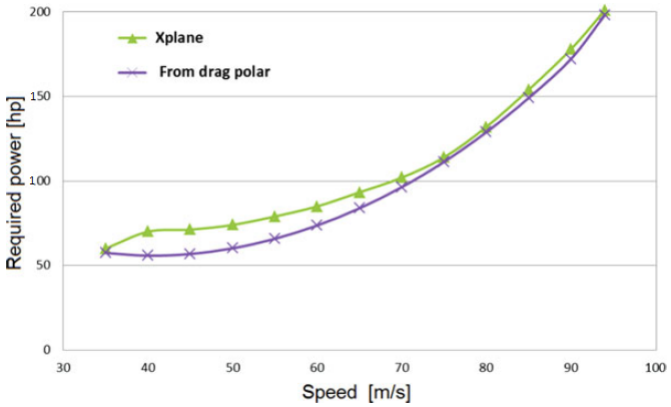

Figure 2.27: Power required versus velocity for the Pipistrel Panthera. Results from model in X-Plane and results from measurement of the drag polar [42]

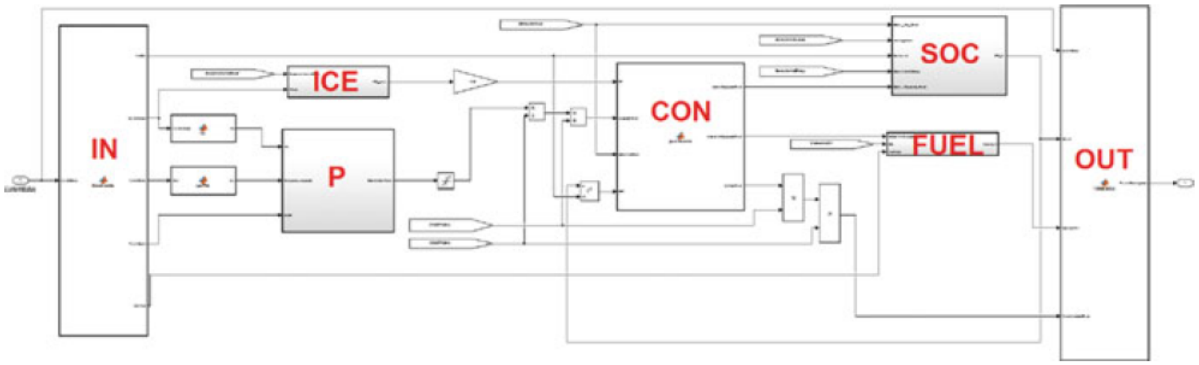

Figure 2.28: Matlab Simulink model of HEPS of HyPSim for Pipistrel Panthera aircraft [42]

modeled by interpolating experimental data. The aircraft EM is modeled using a three layer perceptron neural network surrogate model which is trained by experimental data. The efficiency of the EM and motor controller as a function of torque, rotational speed and input voltage are given by the neural network model. The propeller is modeled by use of standard equations and data derived from wind tunnel testing. In addition, the battery is modeled by experimental data as well. Contrary, the thermal state of the battery is not modeled in this investigation. Furthermore, the ICE is modeled by use of experimental data based on a existing commercial Unmanned Areal Vehicle (UAV) engine. The analysis assumes that the ICE can not run idle and can start up instantly.

A. T. Klesh and P. T. Kabamba [9] use a model for their solar powered aircraft, consisting out of three parts. The first is the aircraft model which is a kinematic model based on some simplified equations of motion. The second is an energy collection model for the solar power production and the third is an energy loss model. The energy loss model is also based on analytical equations which represent the energy loss of the system like for instance through drag.

Chapter 3

Research proposal

In this chapter the research proposal is stated by means of a research question with applicable sub questions, a hypotheses that the author states to predict the answers to each sub question and the methodology is stated that the author proposes to answer the research questions.

3.1 Research question

As of current state, there is not much to find in literature on flight path optimization of HEPS aircraft for a fixed airframe design, except for T. H. Bradley et al. [**?**]. Here, the flight path is optimized for a hydrogen fuel cell HEPS unmanned aircraft, which is mainly focused on optimizing endurance. The models used for these optimizations are based on experimental data and severely simplified. Results show that the flight path optimization does not yield in better endurance for the HEPS aircraft than for the fuel cell powered aircraft for a fixed airframe design. Therefore, with the gap in science found by the author and supervisor for the thesis subject, a research question with sub questions arise. The resulting main question for this research is:

What is the effectiveness of flight path optimization for a general aviation aircraft with a series HEPS?

In this question, the word 'effectiveness' applies to the difference the optimized flight path has on the overall performance of the aircraft relative to the conventional mission and the overall aircraft performance. To answer this main question, a reference aircraft is selected and used, which is the Hybrid Pipistrel Panthera. Pipistrel is very collaborative and supplies a lot of reference data of the aircraft and the HEPS components which are used for producing the required models. Furthermore, additional sub questions are proposed and given below to aid in answering the main research question.

- How does the degree of hybridization influence the optimum mission profile and flight conditions?
- What control strategies for the propulsion system is best applicable for the problem?
- How do you best utilize the battery?
- What are the most significant parameters that affect the optimum conditions and what are their impact on overall performance of the aircraft?

3.2 Methodology

To answer these questions optimizations are used. The optimizations in this research are performed by means of the Matlab function *fmincon*. The function uses a specified algorithm to search for a local minimum in a certain function which is constraint. The algorithm chosen for the optimizations in this study is the Sequential Quadratic Programming (SQP) algorithm. For the optimization different objectives are used such as to minimize fuel or to minimize time. For these optimizations an objective function is developed which calculates these objectives by means of changing selected variables. That means that in this function the flight conditions are coupled to the aircraft aerodynamics and the propulsion system. For this, sub functions are required which determine the aircraft aerodynamics and the performance of the propulsion system components which are connected together. Because for a lot of these models empirical data is available on certain performance parameters and the aircraft with the propulsion system design does not vary during the optimizations, models are created based on this empirical data. Therefore, the main steps the author proposes to methodically answer the research questions are listed below:

Obtaining model for HEPS and aircraft:

- Set up model for aircraft the aircraft using Matlab
- Set up model for the HEPS using Matlab
- Define limitations of models (assumptions, linearization, etc)

Optimization of flight path:

- Set up optimization problem for each segment of flight
- Define what to optimize (Minimum energy, minimum time, etc)
- Define limitations and assumptions used for flight path optimization
- Determine optimum solutions and compare results

Evaluation and conclusions:

- Evaluation of results and conclusions
- Evaluate impact of most significant parameters on the overall performance
- Recommendations for future and further research

Chapter 4

Reference Data

In this chapter the reference data that is used for this master thesis is presented and discussed. This reference data consists out of the data for the aircraft, the data for the conventional propulsion system and the data for the HEPS. The data that can not be obtained by open sources is given by the reference aircraft manufacturer Pipistrel. Some of this data is for non disclosure and will therefore be presented in graphs without the numbers on the axes.

4.1 Reference aircraft data

An aircraft manufacturer from Slovenia called Pipistrel has been involved in researching, developing and designing hybrid and electric aircraft. The company has been involved in the MAHEPA project where one of their existing airframes will be used to implement a HEPS. Currently, a general aviation aircraft from Pipistrel, called the Panthera shown in figure 4.1, is used to implement a series HEPS. Therefore, this aircraft has been chosen as a reference aircraft for this research.

Figure 4.1: General Aviation aircraft Pipistrel Panthera

The data that is used for this reference aircraft is given by the researchers working on the MAHEPA project and some is obtained from the Pipistrel website [2]. The basic aircraft data is given in table 4.1 which includes some basic performance data as well for the aircraft.

Parameter	Value	Unit
S	11.2	m^2
$MTOM$	1315	kg
$S_{takeoff_{max}}$	530	m
$S_{landing_{max}}$	570	m
$V_{stall_{flaps}}$	60	$KIAS$
V_{stall}	65	$KIAS$
V_c	175	$KIAS$
V_{ne}	220	$KIAS$
Range with reserve	> 1000	nm
Ceiling	20000	ft

Table 4.1: The basic parameters of the Pipistrel Panthera [2]

In addition to this data, the lift coefficient and drag coefficient versus the angle of attack, for different flap settings and gear retracted or down, is provided by Pipistrel. This data is used to produce the lift-drag polars of the aircraft shown in figure 4.2. The lift to drag ratio versus the angle of attack is shown in figure 4.3.

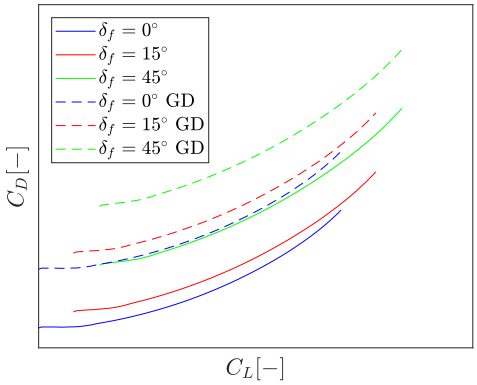

Figure 4.2: Lift-drag polar for the Pipistrel Panthera for different flap setting (df) and gear down (GD)

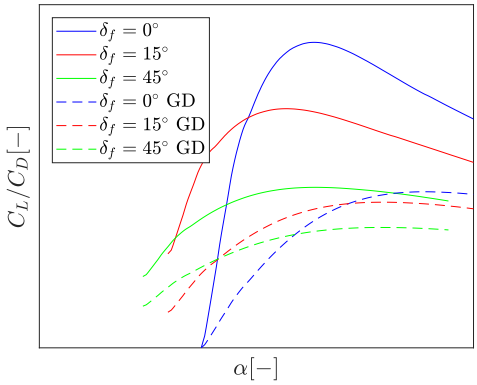

Figure 4.3: Lift to drag ratio versus the angle of attack for different flap setting (df) and gear down (GD)

4.2 Conventional propulsion system data

The conventional propulsion system of the Pipistrel Panthera uses a simple drive train of an ICE connected to a propeller as shown in figure 4.4. The drive ratio of the propeller for the ICE that is used in this case is 1:1 meaning that there is no transmission between the ICE and propeller. Therefore, the ICE of the conventional propulsion system and the propeller are the only component presented and discussed in this section.

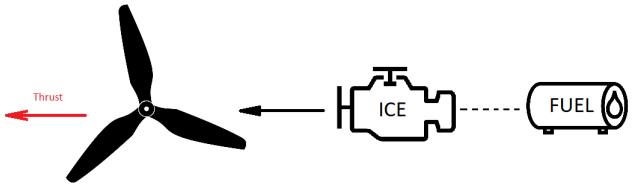

Figure 4.4: Schematic representation of conventional propulsion system

4.2.1 Propeller

The propeller is a three blade fixed pitch propeller with a diameter of 1.8 meters. The data of the propeller provided by Pipistrel consists out of data for the thrust coefficient, the blade angle and propeller efficiency versus the power coefficient and advance ratio. Figure 4.5 shows a contour plot of the data for the propeller's thrust coefficient versus the power coefficient and the advance ratio. In addition, the contour plot of the efficiency data versus the power coefficient and advance ratio is shown in figure 4.6.

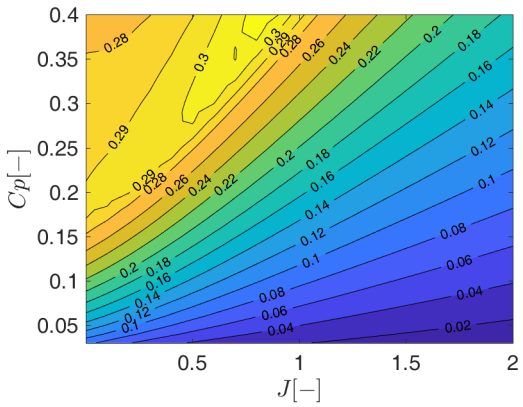

Figure 4.5: Thrust coefficient versus the power coefficient and the advance ratio of the propeller

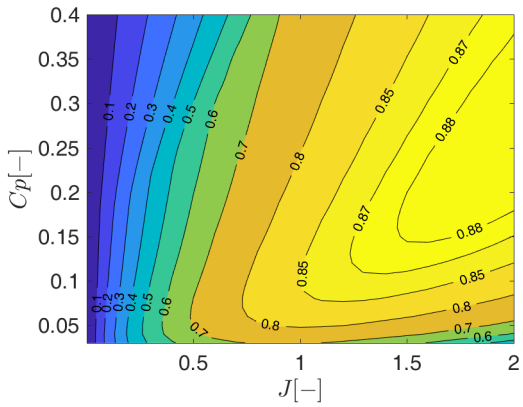

Figure 4.6: Efficiency versus the power coefficient and the advance ratio of the propeller

4.2.2 Conventional ICE

The ICE of the conventional propulsion system is a Lycoming O-540 series engine and the basic data for this engine is obtained by the Lycoming operators manual [8]. Some of this basic data is given in table 4.2. The fuel that the Lycoming ICE uses is 100LL AVGAS and the parameter for this fuel are also given in table 4.2 [7]. In addition, a graph is available for fuel consumption versus the actual brake power for different values of RPM. This graph is computationally read and because the data is in horsepower and gallons it is converted computationally to kilowatt and liters for comparison, shown in figure 4.7. The solid line represents the best power mixture setting and the dashed line represents the best economy mixture setting. In addition, a table is available that represents a correction percentage that needs to be applied to the full throttle power versus the altitude. This data is represented in figure 4.8.

Parameter	Value	Unit
P_{rated}	194	kW
$P_{75\%}$	145	kW
$P_{60\%}$	115	kW
RPM_{rated}	2700	rpm
$RPM_{75\%}$	2450	rpm
$RPM_{60\%}$	2350	rpm
$\dot{m}_{fuel_{75\%}}$	56.78	l/h
$\dot{m}_{fuel_{60\%}}$	45.43	l/h
ρ_{fuel}	0.718	kg/l
u_{fuel}	44	MJ/kg

Table 4.2: The basic parameters of Lycoming O-540 series ICE [8]

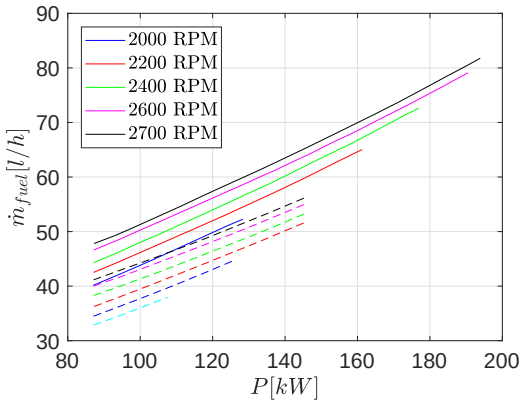

Figure 4.7: Fuel consumption versus actual brake power for different RPM and mixture settings

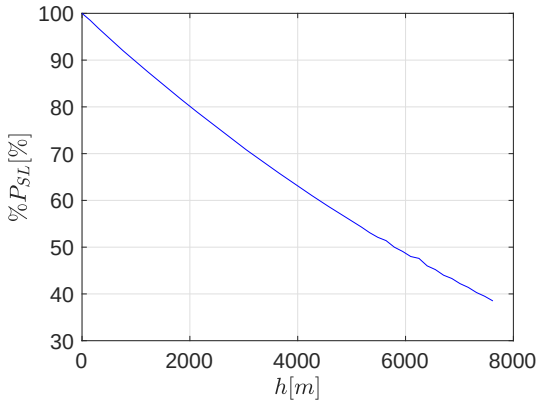

Figure 4.8: Power correction percentage to Sea Level condition versus altitude

4.3 HEPS data

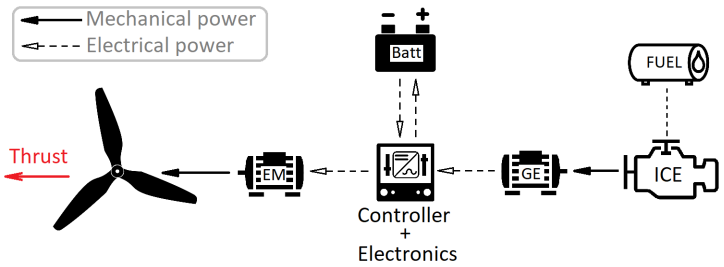

Figure 4.9: Schematic representation of HEPS

As mentioned previously, the HEPS that is implemented into the Pipistrel Panthera airframe has a series lay out as shown in figure 4.9. The propeller data for the HEPS is discussed in subsection 4.2.1, since the propeller of the HEPS is the same as the propeller for the conventional aircraft. The components discussed in this section are therefore the EM, inverter/converter, generator, battery and the ICE. Some basic parameters of the

HEPS are given in table 4.3.

Parameter	Value	Unit
V_{fuel}	200	L
Q_{batt}	14.9	kWh
W_{batt}	125	kg
$P_{out,EM_{max}}$	200	kW
$P_{out,ICE_{max}}$	80	kW
d_{prop}	1.8	m

Table 4.3: The basic parameters of the HEPS of the Pipistrel Panthera [2]

4.3.1 Electro motor

The EM used for the propulsion system of the hybrid Pipistrel Panthera is a 200 kW dual winding electro motor developed by Siemens. The motor is able to deliver a maximum power of 200kW to the propeller shaft. The specific power of this motor is very high ($\approx$ 4.6 kW/kg). The motor's rotational speed and torque influence the efficiency to a minor extent. Some coarse test data of the EM is provided by the MAHEPA project with the efficiency at different rotational velocities and torques. This data extends from a rotational velocity of 500 RPM to 2250 RPM in four steps, and extends from a torque of 100 Nm to 850 Nm in four steps as well. The efficiency is determined by equation 4.1, where the power that goes into the EM is determined by the sum of the outgoing power and the power that is lost, as shown in equation 4.2. The power that is lost in the energy conversion process is the sum of the copper losses and iron losses. The copper losses are determined by equation 4.3, where the values for resistance are measured for each torque and RPM setting. The iron losses are measured data as well for each torque and RPM setting. The power that comes out of the EM is determined by equation 4.4. A contour plot of the coarse data is shown in figure 4.10.

$$\eta_{EM} = \frac{P_{out_{EM}}}{P_{in_{EM}}} \tag{4.1}$$

$$P_{in_{EM}} = P_{out_{EM}} + P_{losses} \tag{4.2}$$

$$P_{loss_{copper}} = I^2 R \tag{4.3}$$

$$P_{out_{EM}} = \tau \cdot \omega = \frac{\tau \cdot \Omega \cdot 2\pi}{60} \tag{4.4}$$

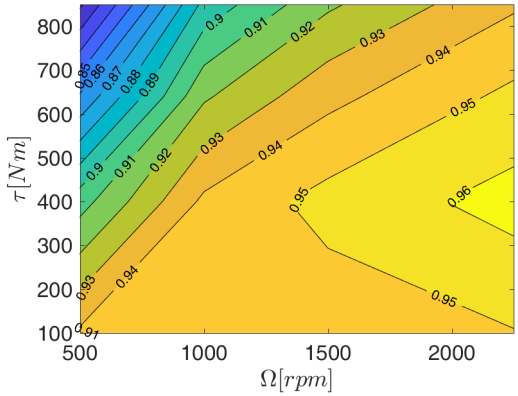

Figure 4.10: Efficiency versus Torque and rotational velocity

4.3.2 Battery

The type of battery cell that is used for the hybrid Pipistrel Panthera is the Kokam Superior Lithium Polymer Battery. It is not known which Kokam battery cell is used so a reference battery cell from Kokam is chosen. Contrary, some of the basic data of the total battery is known. The maximum continues power output of the battery is 120 kW, the total rated capacity is 14.9 kWh and the total battery pack weight is 125 kg. This means that the battery cells must meet with these requirements. Because the number of total cells is not known, but does have to correspond with the battery cell, that is investigated first. As mentioned previously in subsection 2.2.1, the total amount of power and capacity of the battery is the sum of the individual cells power and capacity, no matter how the battery cells are connected. This means that the total number of cells can be presented by equation 4.5 and 4.6. Since the total number of cells must be equal for both, a ratio is obtained between the maximum power and capacity of the battery cell. This ratio is the same as the maximum continues discharge rate the battery cells must have. Therefore, the table of different battery cells from Kokam is observed for battery cells with a maximum continues discharge rate of 8C. There are more than one different cells who fit this criteria so the one with the least specific energy and internal resistance is chosen, which is the SLPB125255255H Kokam battery cell. The chosen battery cell data is provided by Kokam and consists of some main battery parameter shown in table 4.4, together with charge/discharge graphs for several charge/discharge rates, shown in figure 4.11 and 4.12.

$$\#cells = \frac{P_{batt_{max}}}{P_{cell_{max}}} \tag{4.5}$$

$$\#cells = \frac{Q_{batt_{max}}}{Q_{cell_{max}}} \tag{4.6}$$

$$\frac{P_{cell_{max}}}{Q_{cell_{max}}} = \frac{P_{batt_{max}}}{Q_{batt_{max}}} = 8.05\left[h^{-1}\right] \tag{4.7}$$

Parameter	Value	Unit
Q_{cell}	75	Ah
W_{cell}	1.73	kg
R	0.55	$m\Omega$
U_{full}	4.15	V
U_{nom}	3.7	V
U_{cutoff}	2.7	V
$I_{disch_{max}}$	600	A
$I_{charge_{max}}$	225	A

Table 4.4: The basic parameters of Kokam 75Ah battery cell [1]

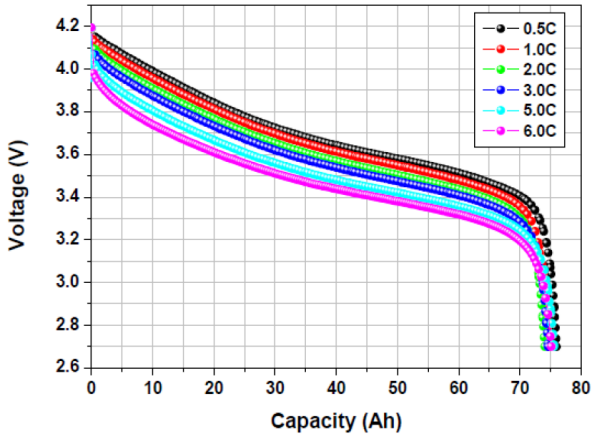

Figure 4.11: Voltage versus the capacity for different discharge rates of the Kokam 75 Ah battery [1]

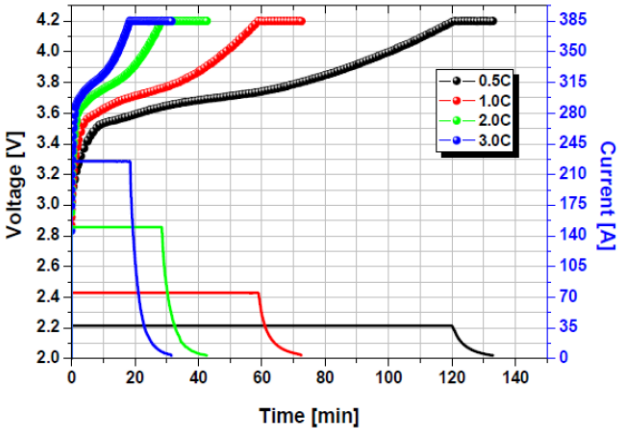

Figure 4.12: Voltage and current versus the capacity for different charge rates of the Kokam 75 Ah battery [1]

4.3.3 HEPS ICE

The ICE used by the hybrid Pipistrel Panthera is the Rotax 914 series engine. The basic data for this engine is given by Rotax in the operators manual [4]. This data includes some fixed constants shown in table 4.5. The fuel that the Rotax ICE uses is 100LL AVGAS and the energy density and volumetric density are also given in the table 4.5 [7]. In addition, the engine performance curve and fuel consumption curves are provided and the data is digitalized into the graphs shown in figure 4.13 and 4.14, respectively. Furthermore, the performance of the ICE at altitude is also given in the form of a table. This data is used to create a map of the power output with respect to altitude and temperature difference to the standard atmosphere. These maps are shown for maximum continuous and take-off setting in figure 4.15 and 4.16, respectively. From this data, a power lapse factor is obtained for each altitude and this factor is applied to the entire power curve. The results of this is shown in figure 4.17

Parameter	Value	Unit
$\dot{m}_{fuel_{TO}}$	33.0	l/h
$\dot{m}_{fuel_{maxcon}}$	27.2	l/h
$\dot{m}_{fuel_{75\%}}$	20.4	l/h
P_{TO}	84.5	kW
P_{maxcon}	73.5	kW
$P_{75\%}$	55.1	kW
ρ_{fuel}	0.718	kg/l
u_{fuel}	44	MJ/kg

Table 4.5: The basic parameters of Rotax 914 series ICE [4]

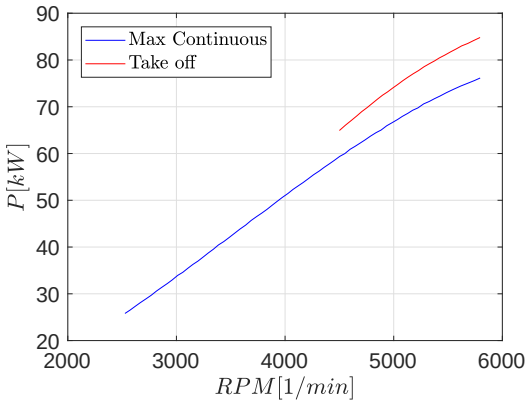

Figure 4.13: Power versus RPM for maximum continuous and take-off of the Rotax 914 series ICE [4]

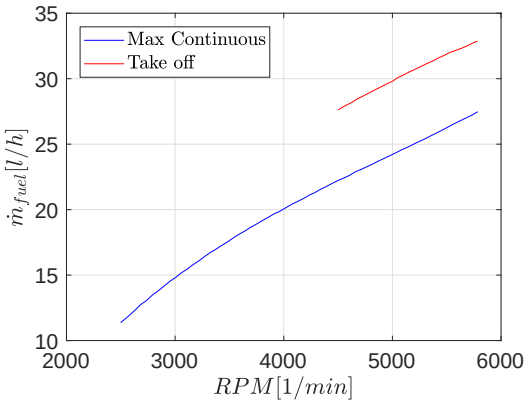

Figure 4.14: Fuel consumption versus RPM for maximum continuous and take-off of the Rotax 914 series ICE [4]

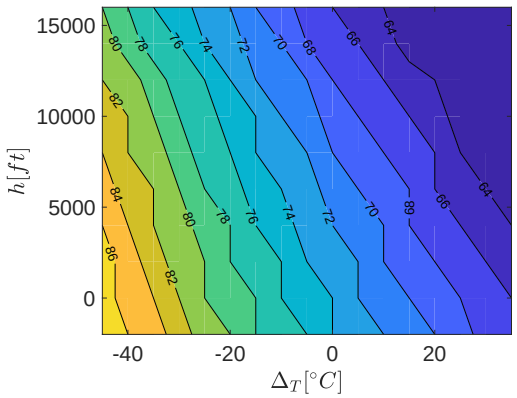

Figure 4.15: Shaft power versus altitude and temperature difference to standard atmosphere for the Rotax 914 ICE in maximum continuous setting [4]

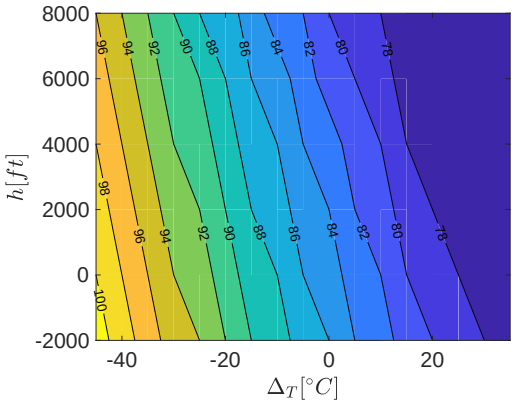

Figure 4.16: Shaft power versus altitude and temperature difference to standard atmosphere for the Rotax 914 ICE in take-off setting [4]

Because the power and fuel consumption versus the rotational velocity are known, the

Brake Specific Fuel Consumption (BSFC) can be determined. The BSFC is the ratio between the fuel mass and a certain amount of energy that the engine produces with that fuel mass. The BSFC versus the rotational velocity for different altitude is shown in figure 4.18. The minimum amount of BSFC means the least amount of fuel weight is required for 1 kWh of energy, which means the highest efficiency is obtained at this rotational velocity. The most efficient rotational velocity for take-off is obtained at the highest rotational velocity possible which is 5800 RPM. However, the most efficient rotational velocity for maximum continuous is not at the maximum RPM but rather at 5280 RPM. At this point the BSFC is also much lower, resulting in a larger efficiency.

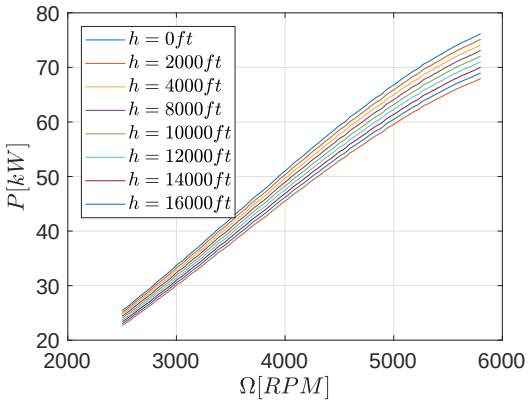

Figure 4.17: Power versus the rotational velocity for different altitudes for the Rotax ICE

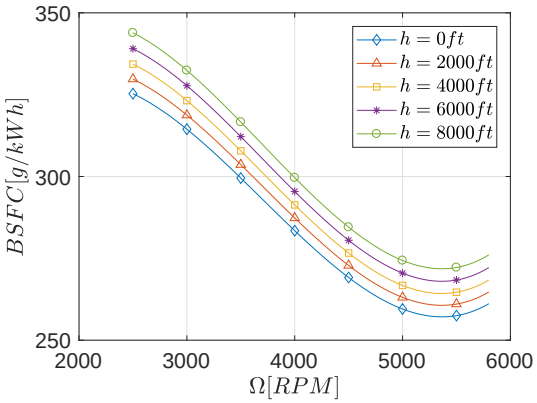

Figure 4.18: BSFC versus rotational velocity for different altitudes, for Rotax 914 series ICE

4.3.4 Generator

For the generator not much data is available. This because the generator is still under development as of current state. The generator used for the propulsion system of the hybrid Pipistrel Panthera is a 100kW bearing less generator currently in development by Siemens. The generator must be coupled directly to the ICE to save any additional weight of a transmission in between. A feasibility study for coupling the Rotax 914 series engine directly to the generator is therefore being conducted. The RPM and torque efficiency regions of both components must therefore overlap to successfully couple these components directly. The estimated performance of the generator is that it has an efficiency of approximately 95% at and rotational velocity of 5500 RPM and a torque of 250 Nm which indeed almost coincides with the most efficient RPM and torque of the ICE. The main parameters that are known at the moment for the design of the generator ar given in table 4.6.

Parameter	Value	Unit
P_{nom}	100	kW
τ_{nom}	250	Nm
Ω_{nom}	5500	RPM
η_{nom}	$> 95\%$	$-$
m_{GE}	≈ 20	kg

Table 4.6: The basic parameters of generator in development

4.3.5 Inverter/Converter

For the inverter/converter the same applies as for the generator, it is is still under development as of current state so not much data is available. Especially the data that is required for modeling the efficiency of the inverter/converter. However, the data that is available at the moment is presented in this subsection shortly. The inverter/converter will consist out of two parts, a 100kW converter for the EM and a 50 kW converter for the generator. Some basic intermediate data for the inverter/converter is given in table 4.7.

Parameter	Value	Unit
U_{nom}	533	V
U_{max}	605	kW
$m_{inv,conv}$	$10 - 15$	kg

Table 4.7: The basic parameters of inverter/converter in development

Chapter 5

Modeling

In this chapter the modeling of the performance of the aircraft with its conventional propulsion system and with its HEPS is discussed. The data that is provided and obtained mostly consists out of experimental and empirical data, meaning the data is not continuous. Gradient based optimization algorithms work effectively when the functions it uses to optimize are continuous and smooth. For the modeling it is therefore important to uses continuous functions if applicable. The mission analysis calculation procedure influences the input and output of the produced models. The procedure uses the flight conditions such as altitude, velocity, flight path angle and weight to calculate the power that is required by the propulsion system to perform a certain segment of flight. Therefore, the output power is requested for the most of the propulsion system components and the input power is calculated by means of the model. Furthermore, some models calculate additional parameters that are important to consider or required for further investigation. The modeling is divided into the modeling of the conventional aircraft and the HEPS aircraft. Most of these models use a fitted polynomial through the data to produce a simplified model. Depending on the amount of variables in the data these polynomials vary from single variable polynomials, given by equation 5.1 and dual variable polynomials given by equation 5.2. By increasing the order of the fitted polynomial the error between the data and the polynomial function decreases. This process is done until the error becomes reasonably small. Figure B.1 in appendix B shows all the models connected together with their corresponding inputs and outputs. The *Performance* module is the main control function of the entire model and includes the calculation of the aircraft aerodynamic forces.

$$P(x) = a_n x^n + a_{n-1} x^{n-1} + ... + a_1 x + a0 \tag{5.1}$$

$$P(x, y) = \sum_{m=0}^{n} a_{ij} x^i y^j \quad i + j \leq m \tag{5.2}$$

5.1 Conventional aircraft

5.1.1 Aircraft aerodynamic forces

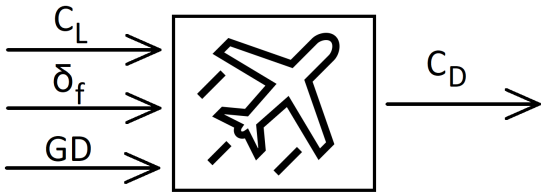

Figure 5.1: Schematic representation of aircraft aerodynamics model

The lift coefficient and drag coefficient versus the angle of attack data that is provided by Pipistrel is used to create a model for the drag coefficient as a function of the lift coefficient, flap setting and gear setting. That means that the model gets a lift coefficient, flap setting and gear setting as an input and than calculates the drag coefficient to give to output of the function, as shown in figure 5.1. Together with the flight conditions, the basic aerodynamic forces can then be determined. Because Mach number and Reynold's number effects are limited on the lift drag polar for this case, the effects are not included.

5.1.2 Propeller

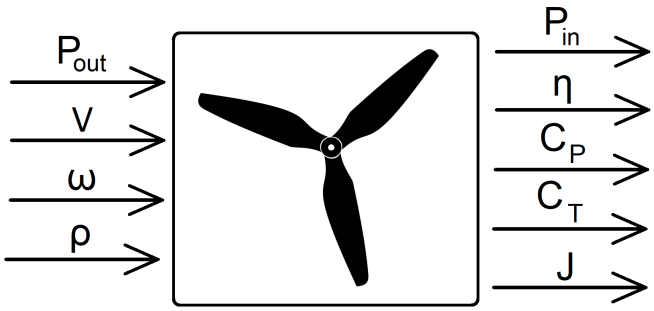

Figure 5.2: Schematic representation of propeller model

Because of the availability of this data it is chosen to model the propeller to this empirical data instead of using analytical models such as Actuator Disc Theory (ADT) or the Blade Element Method (BEM). When looking at the three dimensional data of the thrust coefficient versus the power coefficient and the advance ratio shown in figure 5.3, a kink in the curve is observed and there are some parts of the curve where a certain thrust coefficient can be achieved for two different values of power coefficient and advance ratio. The other side of this kink where the values for power coefficient are higher and advance ratio are lower, can be discarded from this data for the calculations of the performance. This is because it is always more efficient to get a thrust coefficient for a lower power coefficient if this is possible. For the case that there are two values of power coefficient for a certain thrust coefficient, the lower power coefficient would always yield in larger

efficiency. Therefore, for the optimization and calculations this data is deleted and the thrust coefficient is limited to that kink by means of non linear constraints. This is quite convenient for producing a smooth and continues model of the propeller.

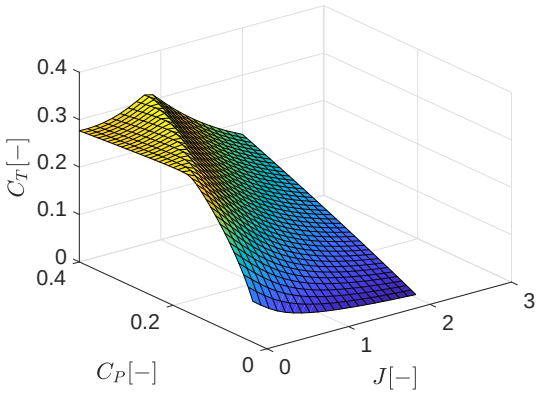

Figure 5.3: 3D representation of the thrust coefficient versus the power coefficient and the advance ratio

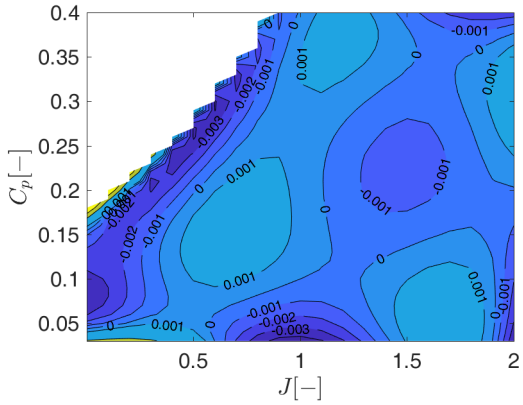

Figure 5.4: Contour plot of the error of the propeller model compared with the reference data

The output power is requested from the propeller for a certain segment of flight and is therefore the main input of the model. Together with the flight speed, rotational velocity of the main drive train and the surrounding air density at a certain altitude obtained by the standard atmosphere model, the basic propeller parameters are obtained. At first the thrust force that the propeller produces is determined by equation 5.3 and then the thrust coefficient by means of equation 5.4. In addition, the advance ratio is determined by equation 5.5. With the advance ratio and thrust coefficient known, the power coefficient can be obtained by means of a produced model of the obtained reference data. A contour plot of the error between the data and the model is presented in figure 5.4, where the white space represents the excluded data. In addition, the propeller model makes use of some assumptions and limitations which are listed below:

- The data does not change with the Reynold's number
- The data does not change with the Mach number
- The blade angle is automatically changed to meet the propeller power requirements for highest efficiency

$$T = \frac{P_{out_{prop}}}{V} \tag{5.3}$$

$$C_T = \frac{T}{\rho \omega^2 {d_{prop}}^4} \tag{5.4}$$

$$J = \frac{V}{\omega d_{prop}} \tag{5.5}$$

5.2 HEPS aircraft

Since both aircraft use the same airframe and propeller, the aircraft aerodynamic model and propeller model for both are identical. Consequently for the HEPS aircraft, the aerodynamic model is discussed in subsection 5.1.1 and the propeller model is discussed in 5.1.2. What remains for the HEPS aircraft modeling is the EM, battery, ICE, generator and inverter/converter which are described in this section.

5.2.1 EM

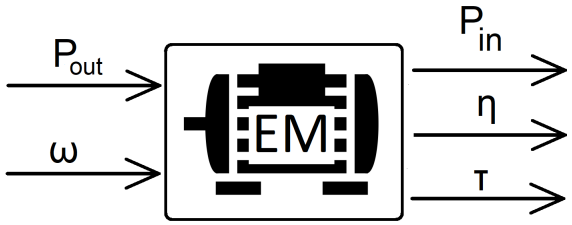

Figure 5.5: Schematic representation of Electric Motor model

Since the data for the EM is very coarse it is more challenging to model accurately. The main aspect of the EM that is going to be modeled is its efficiency. This means that the input for the model will be the power that is requested by the propeller and the rotational velocity of the main drive train. With both of these values known the required torque from the EM is determined by means of equation 4.4. With the coarse data that is obtained it is possible to produce a model that uses a three dimensional polynomial for the efficiency as a function of torque and rotational velocity. Because the data consist out of only four points in both torque and RPM, the order of the polynomial in both directions is at maximum also four. However, it is observed that a fit of the order four produces unrealistically peaks and valleys between the points, exceeding a perfect 100% efficiency, while the error still decreases at the data points. Therefore, a model fit at order three in both directions seems more realistic whilst having a significantly small error from the data points. The fit through these points together with the contour plot of the efficiency model of the EM are shown in figure 5.6 and figure 5.7, respectively. For the EM model some assumptions are made and these are listed below:

- No altitude effects
- No temperature effects

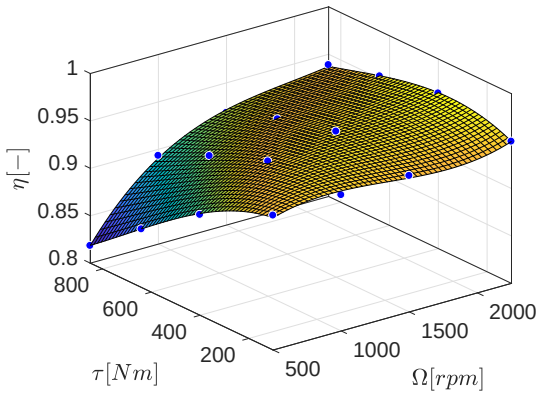

Figure 5.6: The efficiency model of a polynomial surface fit through the data points

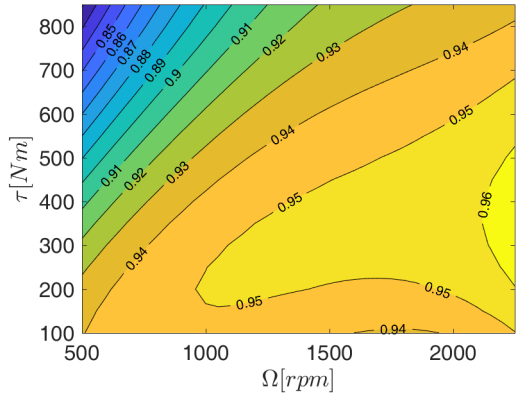

Figure 5.7: Contour plot of the efficiency model of the EM

5.2.2 Battery

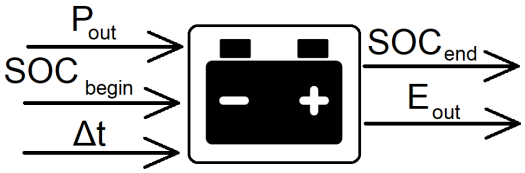

Figure 5.8: Schematic representation of discharge battery model

The performance of the battery can be considered as one of the hardest parts of the propulsion system to model. As can be observed from figure 4.11 and 4.12, the discharge and charge curves of the battery cell display some non-linear behavior, where the challenge originates to model this behavior. The discharge model of the battery requires the requested output power from the battery, the current SOC of the battery and the time for discharging the battery as input. The amount of output power states at what discharge current and consequently C-rate, each cell is discharged. Together with the amount of time the battery discharges, the energy output from the battery is determined and the SOC at which the discharging ends. For these calculations a model is required that calculates the voltage versus the capacity of each cell for different discharge currents. For the charge model the same is required except the voltage versus the capacity reverses. Tremblay et al. [31] developed an improved and easy to use dynamic battery model for the charge and discharge behavior of four different battery types, including a lithium based battery type. Here, the charge and discharge curve are divided into an exponential zone and a nominal zone as shown in figure 5.9. The voltage at the end of each zone is used to model the battery's dynamic behavior by using equation 5.6 and 5.7, respectively, where the actual battery charge (it) is given by equation 5.8. So this means these equations can be used for a specific charge or discharge current (i) to determine the dynamic behavior of the actual battery charge. The only constants that are unknown for these equations are the battery constant voltage (E_0), the polarization constant (K), the exponential zone amplitude (A) and exponential zone time constant (B), where the latter is assumed by

equation 5.9. The other three constants are obtained by equation 5.10, 5.11 and 5.12, where the voltages (U_{exp} and U_{nom}) are estimated by the graphic data supplied by the battery cell manufacturer. Consequently, the three equations have three unknowns which are the previously mentioned constants.

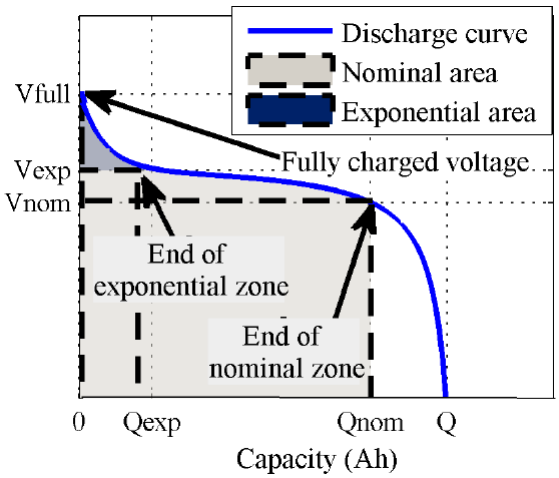

Figure 5.9: Typical discharge curve of a battery with the zones for the model [1]

$$U_{batt_{charge}} = E_0 - R \cdot i - \frac{K \cdot Q}{Q - (0.1) \cdot it} i^* - \frac{K \cdot Q}{Q - it} \cdot it + Ae^{-B \cdot it} \tag{5.6}$$

$$U_{batt_{discharge}} = E_0 - R \cdot i - \frac{K \cdot Q}{Q - it}(it + i^*) + Ae^{-B \cdot it} \tag{5.7}$$

$$it = \int idt \tag{5.8}$$

$$B = \frac{3}{Q_{exp}} \tag{5.9}$$

$$U_{full} = E_0 - R \cdot i + A \tag{5.10}$$

$$U_{exp} = E_0 - \frac{K \cdot Q}{Q - Q_{exp}} (Q_{exp} + i) - R \cdot i + Ae^{-3} \tag{5.11}$$

$$U_{nom} = E_0 - \frac{K \cdot Q}{Q - Q_{nom}} (Q_{nom} + i) - R \cdot i + Ae^{\frac{-3}{Q_{exp}} Q_{nom}} \tag{5.12}$$

Because the voltages for each zone are estimated there is an error in the model compared to the reference data. Consequently, the estimation of these voltages act as an initial guess for an optimization of the model with the objective to have the least amount of error from the reference data. Therefore, the error of each point on the graph with the reference data is summed and this sum is minimized, as represented by equation 5.13, where the variables of $\vec{x}$ are represented by the estimated points of each zone. The value of n is represented by the amount of data points that is used for the reference and calculated data. The variables are bound by the cut off voltage which is constant and the fully charged voltage which depends on the C-rate, shown equation 5.14 and 5.15, and are constraint by equation

5.16. The results of the optimization are given in Appendix C. From the graphs of the error it is observed that the error decreases in certain capacity ranges while increasing in other, however, the sum of all errors is decreased due to the optimization. In addition, from the graphs of the voltage versus the capacity it is observed that the model cannot precisely represent the reference data, even when it has been optimized to minimize the sum of errors. However, the model is considered to be sufficient because it can represent the battery data as a function of current which is required for a dynamic battery model, while interpolation of the data will not be able to implement current as a variable. In addition, there are some assumptions that are made and limitations that are set for this model and these are listed below:

- No lifetime cycle effects
- No self discharge effects
- No temperature effects
- No resistive losses in connections between the battery cells
- Constant current charing only

$$\min \sum_{i=1}^{n} \left| \vec{U}_{ref_i} - \vec{U}_{calc_i}(\vec{x}) \right| \tag{5.13}$$

$$U_{cutoff} \leq U_{exp} \leq U_{full}(C) \tag{5.14}$$

$$U_{cutoff} \leq U_{nom} \leq U_{full}(C) \tag{5.15}$$

$$U_{nom} - U_{exp} \leq 0 \tag{5.16}$$

5.2.3 HEPS ICE

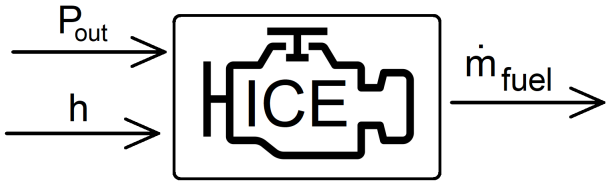

Figure 5.10: Schematic representation of Internal Combustion Engine model for HEPS

In this section the model for the Rotax ICE of the HEPS is described. The model uses the requested output power from the ICE as an input together with the altitude, and determines the fuel consumption. Because the influence of altitude is of great significance for the ICE, as shown previously in subsection 4.3.3, it is also an input for the model. The model is used during the optimization of the climb and cruise phase, meaning the power setting is at maximum continues. At first the model determines that rotational velocity that corresponds to the altitude and the requested output power. The model determines this by means of using the previously obtained data for power versus rotational velocity for different altitudes shown in figure 4.17, and producing a three dimensional polynomial fit through this data. The polynomial function uses the altitude and requested output power as input and determines the rotational velocity accordingly. It is assumed that the fuel

consumption is fixed to the rotational velocity and not influenced by the altitude since the power already is influenced. This means that at higher altitude higher BSFC is produced meaning lower efficiency is obtained. In this way the effect of altitude on the power output and fuel consumption is sufficiently modeled. To determine the fuel consumption corresponding to the rotational velocity that is determined, again a polynomial fit is used. For this a dual variable polynomial fit is used, as shown in equation 5.2.

5.2.4 Generator, Inverter/Converter

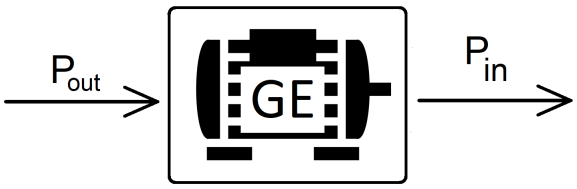

Figure 5.11: Schematic representation of generator model

Figure 5.12: Schematic representation of inverter/converter model

As mentioned previously, for the generator and the inverter/converter, not much data is available because the parts are still in development. It is therefore chosen to model these to parts very simple, by means of a power conversion with a fixed efficiency. For the generator, efficiency will most definitely be influenced by rotational velocity and torque, however, like the EM the efficiency does not differ by a lot over a wide range of these influential variables. Since the efficiency at nominal operation of the generator is estimated higher than 95%, the efficiency is set at a constant 95%. For the inverter/converter the efficiency is influenced by the by the number of switches in parallel and series, which is unknown as of current state. Accompanied by the fact that usually these losses are substantially low as stated in subsection 2.2.4, the efficiency is assumed at 99.5% which can be rounded off to 100% since this will not influence the results much.

Chapter 6

Mission Analysis

In this chapter the mission analysis of the conventional and HEPS aircraft are presented. Accompanied by the optimization of the climb flight path, cruise flight path and the coupling of both these segments to yield a total mission optimization. The optimization are run for different objectives stated in each section. For the beginning of each mission, the weight of the aircraft is considered to be equal to the MTOW.

6.1 Basic aircraft performance

At first the basic aircraft performance is reviewed. Figure 6.1 shows the maximum power available and minimum power required for steady horizontal symmetric flight at MTOW versus the flight velocity for different altitudes, for both the aircraft with the conventional propulsion system and with the HEPS. The maximum power available for the conventional propulsion system is the maximum thrust that the propulsion system is able to deliver at each altitude multiplied by the flight velocity. This means that the ICE is operating at its highest continuous power output. The maximum power available for the HEPS is defined similar, however in this case the ICE and battery are both operating at there maximum continuous power output. For the power required the conventional case and HEPS case are similar since the lift and drag characteristics of the aircraft do not vary. The main observation here is that the effect of altitude on the maximum power available is far more substantial on the conventional propulsion system then on the HEPS. This is one of the inherent advantages of a HEPS, the electrical components are not influenced by altitude as much as the ICE. However, the ICE of the HEPS has a turbocharger which compresses the air before it goes into the combustion chamber meaning it is less effected by altitude than the conventional ICE which does not have a turbocharger. Therefore, the maximum altitude for the aircraft with the HEPS can be potentially higher and the maximum velocity the aircraft is able to achieve is less influenced by altitude as well for the HEPS aircraft. Contrary, the maximum power available of the HEPS depends largely on how it is operated and thus on the battery capacity. Figure 6.2 shows the difference in maximum power available for these different propulsion system operations. Here, one of

the inherent disadvantages of a HEPS is illustrated. Once the battery is drained the power output becomes significantly small. It can be concluded that the size of the ICE is quite limiting to the flight envelope of the aircraft. A larger ICE would increase the weight of the aircraft limiting payload capabilities, however the higher output power would increase the performance of the aircraft significantly.

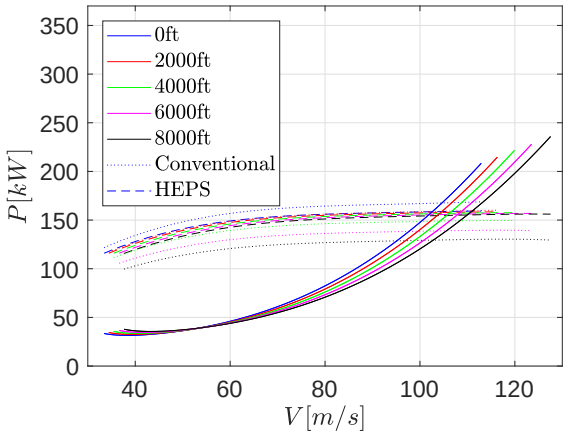

Figure 6.1: The maximum power available and minimum power required for steady horizontal symmetric flight versus the flight velocity for different altitudes

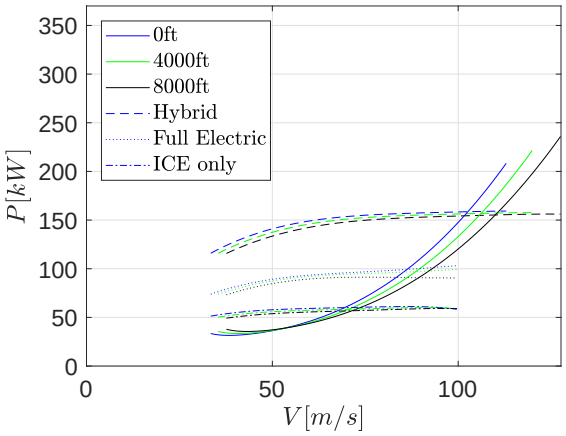

Figure 6.2: The maximum power available for the HEPS aircraft and minimum power required for steady horizontal symmetric flight versus the flight velocity for Hybrid, full electric and ICE only operation and for different altitudes

6.1.1 Climb

Another inherent advantage of the fact that altitude does not influence maximum power available for the HEPS by much, is that the maximum rate of climb of the aircraft is also less affected by altitude. By observing the graph previously mentioned, the velocity at which the maximum rate of climb occurs changes with altitude and also the amount of excess power at this velocities changes with altitude. Figure 6.3 shows the changing flight velocity and flight path angle at which maximum rate of climb occurs versus the altitude for the conventional and HEPS case. In addition, the maximum rate of climb versus the altitude of both cases is illustrated in figure 6.4. The difference between the conventional case and the HEPS case is quite significant, especially at higher altitude. This means that the minimum time to climb for the HEPS case can potentially be significantly less as well, depending if the battery capacity is able to last until reaching the final altitude, and the final altitude itself since the rate of climb of the conventional case is more than that of the HEPS case for low altitudes.

6.1.2 Cruise

For the cruise phase the basic performance that is determined are the endurance and range parameters. The velocity at which the maximum range and endurance occurs is

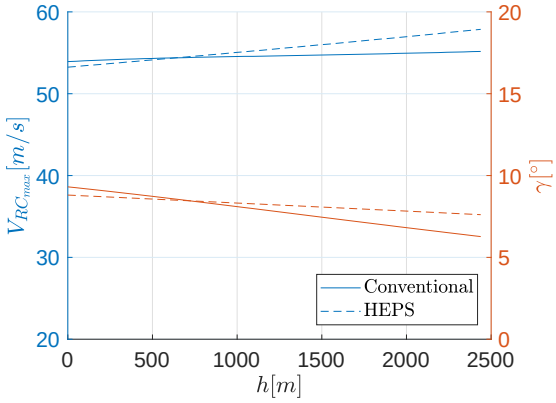

Figure 6.3: Velocity and flight path angle at which maximum rate of flight occurs versus altitude

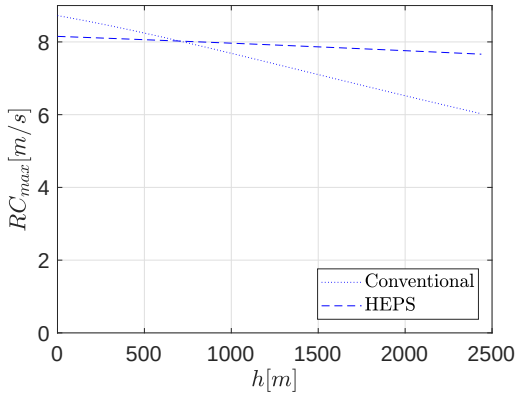

Figure 6.4: Maximum rate of flight versus altitude

drag-based, meaning it does not differ between the conventional and HEPS case for this study. The maximum range for propeller aircraft occurs at the velocity where the drag is minimum. With the assumption that Mach number and Reynold's number effects do not influence the lift-drag polar, the magnitude of drag force that occurs at the minimum point does not change with altitude. However, the velocity and power required for horizontal steady symmetric flight where this minimum drag occurs does change with altitude and this is shown in figure 6.5. Thus, the maximum range point is also the point where the least amount of energy is required from the output of the propeller. This does not necessarily mean that this is similar to the point where the least amount of energy is consumed by the propulsion system since the propeller efficiency depends not only on aerodynamic properties but also drive train rotational velocity. The maximum endurance for propeller aircraft occurs at the lowest value of power required for steady symmetric horizontal flight. Hence, this is not similar to the point where drag is minimum. The velocity and power required at which the maximum endurance occurs changes with altitude and the relation is shown in figure 6.6.

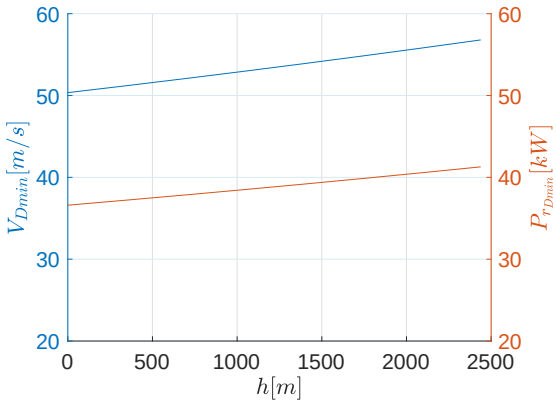

Figure 6.5: Maximum range velocity and power required versus altitude

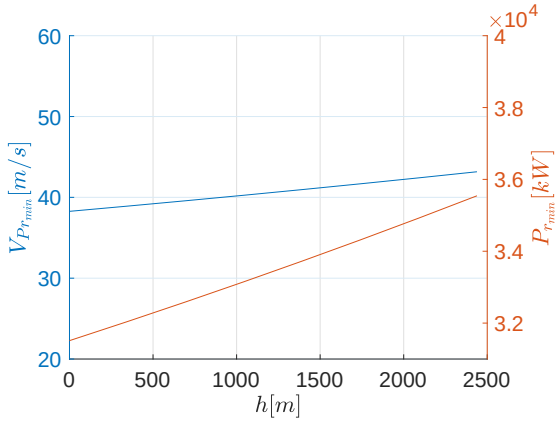

Figure 6.6: Maximum endurance velocity and power required versus altitude

6.2 Taxi and take off performance

In this section the taxi and take off performance of the conventional and HEPS aircraft are presented. The taxi and take off are not optimized due to the small influence these segments of the mission have on the total amount of energy use or time for the mission, especially the taxi segment. Furthermore, for the take off it is usually more important to minimize the runway length that is required and hence, the propulsion system operates at its maximum power it is able to achieve. Because taxiing will most probably occur in full electric mode, and take off will occur in hybrid mode with both power sources operating at its maximum, the influence of this segments on the mission and the battery SOC is of importance. Therefore, the performance for these section is determined prior to the climb phase and act as a fixed input for the climb or mission optimization.

6.2.1 Taxi performance

For the reference mission taxi segment for both the conventional and HEPS aircraft, a taxi length of 500 meters is considered since the required runway length is about the same. The taxi speed that is considered for these calculations is 30 kts. The airfield is considered to be a grass strip airfield and hence the rolling friction coefficient is set accordingly. The input values for the calculations are the fixed values mentioned previously in chapter 4 and the additional data is given in table 6.1. The lift coefficient is obtained by the aerodynamic model of the aircraft by assuming that the aircraft's attitude remains constant during a ground run, the incidence angle is 0°, flaps in take off position and obviously the gear is down. For the performance of the taxi segment some assumptions are made and these are presented below:

- The airfield consists out of a grass strip
- No turns during taxi
- No wind
- The flaps are in retracted position
- The ground run attitude of aircraft is constant
- The airfield is situated at 0m above sea level

Parameter	Value	Unit
$C_{L_{taxi}}$	0.38	–
$S_{max_{taxi}}$	500	m
$V_{max_{taxi}}$	15.43	m/s
μ_{grass}	0.05	–
$SOC_{begin_{taxi}}$	1.0	–

Table 6.1: Fixed input values for taxi performance calculations

The taxi performance calculations are set up according to the FBD presented in figure 2.25 and make use of equation 2.16, 2.17 and 2.18. The taxi performance calculations are split into two sections. The first section is where the aircraft is at stand still and accelerates to the maximum taxi speed. The second section is where the aircraft keeps taxiing at the constant maximum taxi speed for the remaining distance. For the conventional aircraft,

the power output of the ICE during the accelerating section, is set to its lowest economic value of 87.11 kW. This value corresponds to the best economic mixture setting and the lowest rotational velocity of 1800 RPM and therefore the rotational velocity of the directly coupled propeller is the same. Together with an array of velocities ranging from zero to V_{taxi}, the power that comes out of the propeller is determined. With this power known the thrust can be determined for each velocity and with the velocities known the aerodynamic drag, ground drag and lift. With all of these combined the acceleration is determined. With the acceleration and velocity profile known, the time profile of the acceleration section is determined and with that the distance as well. The time is necessary to determine the amount of fuel that has been burned and the distance is required to determine the remaining distance of the second section. For the second section the calculation procedure is somewhat reversed. The aircraft taxi's at a constant speed so the power out of the propeller that is required for that is determined first. Again at the constant taxi speed the aerodynamic drag, ground drag and lift are determined. Since the aircraft moves at constant speed, the thrust force must equal the sum of the aerodynamic drag and ground drag. Thereby, the power out of the propeller is determined. For the HEPS the same procedure is performed, by splitting the taxi into two sections. The taxi is considered to be full electric to make use of the advantages of the series architecture at an airport. This means that all of the power comes from the battery through the EM and is delivered to the propeller. To increase the battery discharge efficiency and ride comfort the power from the battery during the first section is set to 40% of its maximum and the drive train rotational velocity is set to 1400 RPM to so that the system operates in the regions of high efficiency of both components without a large acceleration. With this known, the power out of the EM is determined. The results of both calculations are given in table 6.2 and the power output for the propeller profiles are illustrated in figure 6.7.

Parameter	Conventional	HEPS	Unit
Total energy consumed	1.93	0.42	kWh
SOC end of taxi	N/A	0.97	–
Time for taxi	40.67	41.46	s
Fuel burned during taxi	0.16	0	kg

Table 6.2: Results from taxi performance calculations

6.2.2 Take off performance

The take off performance calculations consists of two main part, the ground run and the airborne section. The FBD and equations of motion are given by figure 2.25 and equation 2.16, 2.17 and 2.18, respectively. The airborne section is from the lift off point until the aircraft reaches 50ft above the ground, given by regulations. The FBD and equations of motion for this segment are given by figure 2.26 and equation 2.20, 2.21 and 2.22, respectively. The sum of the horizontal distance of both section is the required runway length for the situation that there is no failure in the ICE or battery. The fixed input values for the take off calculations are given in table 6.3. The lift coefficient is obtained similarly as the taxi calculations where the flaps are now in take-off position. In addition,

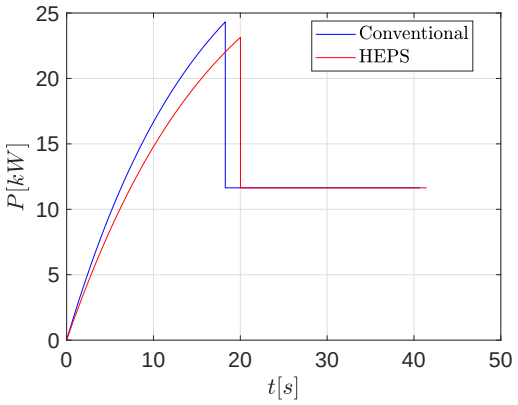

Figure 6.7: Power out of the propeller versus time for the taxi performance

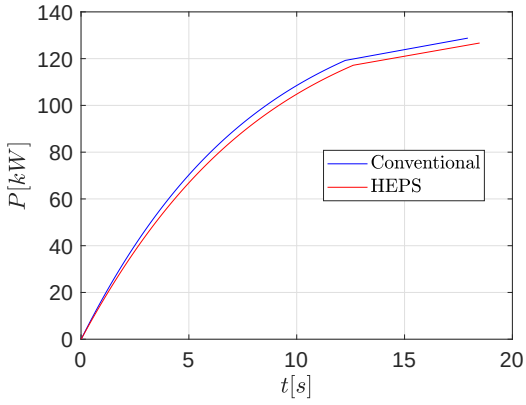

Figure 6.8: Power out of the propeller versus time for the take off performance

some assumptions are made for the take off performance calculations and these are listed below:

- The airfield consists out of a grass strip
- No wind
- No slope in the runway
- Weight is constant during take off
- The airfield is situated at 0m above sea level
- Thrust minus drag during airborne segment is averaged
- There is no ground effect
- The distance for rotating the aircraft is assumed zero
- The ground run attitude of aircraft is constant
- The incidence angle of the main wing is zero
- $V_{lof} = 1.05 \cdot V_{stall}$
- $V_2 = 1.2 \cdot V_{stall}$

Parameter	Value	Unit
$C_{L_{ground}}$	1.12	–
μ_{grass}	0.05	–
δ_f	15	°
h_{scr}	50	ft
a_{scr}	0	m/s^2

Table 6.3: Fixed input values for Take off performance calculations

Again the take off performance for both the conventional aircraft and the HEPS aircraft is determined. For the conventional case the power output of the ICE is set to it's maximum take off value together with the corresponding drive train rotational velocity and fuel consumption. For the ground segment an array of velocity is produced from zero to V_{lof}. For each velocity in this array the power out of the propeller is determined. With the power known, the thrust is determined and with the velocities known the lift, aerodynamic drag and ground drag is determined. With all of the active forces known

the acceleration is determined, and hence the time. With these known, the horizontal distance of the ground run is determined together with the mass of fuel that has been burned during the ground run. For the airborne segment, the calculation procedure is somewhat different. The point performance of the aircraft at lift off and at the screen height is determined and with that the thrust minus drag is averaged over the airborne segment. Since, the acceleration at screen height is assumed to be zero, the average acceleration over the airborne section is determined. Then, with an array of velocities from V_{lof} to V_2 the time and the mass of fuel burned is determined. For the HEPS aircraft the same procedure is done for the take off performance calculations. The output power from the battery is set to its maximum together with the output power from the ICE. The rotational velocity and torque of the main drive train are set to the maximum values to correspond with the power input from the summation of battery power and ICE power. The SOC of the battery at the beginning of the take off is set to the SOC of the battery at the end of the taxi phase. The results are given in table 6.4 and the power output for the propeller profiles are illustrated in figure 6.8.

Parameter	Conventional	HEPS	Unit
Total energy consumed	3.85	2.35	kWh
Energy consumed battery	N/A	0.74	kWh
Energy consumed fuel	3.85	1.61	kWh
Fuel burned during take off	0.32	0.13	kg
SOC end of take off	N/A	0.92	$-$
Time for take off	19.41	20.05	s
Total take off distance	476.55	492.57	m
Flight path angle at V_2	7.50	7.23	$^\circ$

Table 6.4: Results from take off performance calculations

6.3 Climb optimization

In this section the optimization of the climb is presented. The methodology of optimizing the flight path is presented at first. Thereafter, the optimization problem is stated with the different objectives with the variables of the problem. Alongside, the bounds on these variables are presented together with the constraints on the objective function. Finally, the results from the optimization procedures are presented. The reference climb is considered to be from 0ft above sea level to 8000ft above sea level,so that the cruise altitude is sufficient when flying over mountainous terrain. The assumptions for the climb optimization are presented below:

- There is no influence of wind
- Weight at beginning of climb phase is equal to MTOW
- Climb path is two dimensional (heading does not change)
- Climb is performed in standard atmosphere conditions
- Climb is not performed in full electric mode
- Velocity increases linear between points
- Flaps and gear are both retracted

6.3.1 Methodology

For the calculations of the total energy consumed during the climb, the flight path is divided into segments of equal spacing in altitude, illustrated in figure 6.9 and for each segment the performance is determined. Each segment has four variables that the optimizer changes. These variables are velocity, flight path angle, rotational velocity of main drive train and the power split factor. The power split factor is given by equation 2.3 and states how much power that goes into the EM is gained from the battery and from the generator with the ICE.

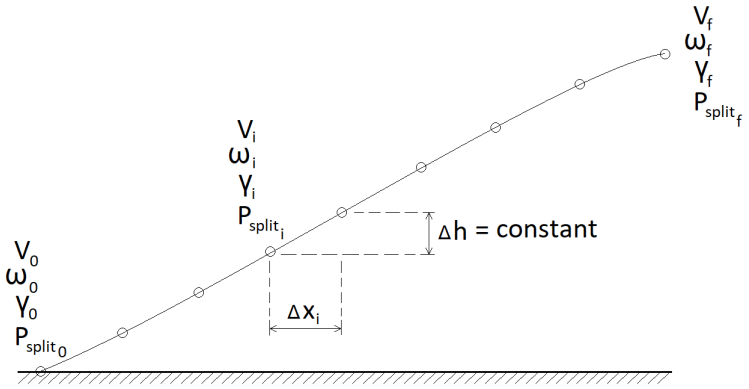

Figure 6.9: Schematic representation of the climb flight path optimization methodology

With the altitude, velocity and flight path angle known for each point, the horizontal distance between the points is determined by equation 6.1, where the flight path angle is set equal to the flight path angle at the beginning of the segment. This means that the flight path is considered to be straight and linear for each segment, so by increasing the number of segments the flight path will approach a continues change. With the horizontal distance known the flight path distance for each segment is also determined by means of equation 6.2. With the assumption that the velocity remains constant for each segment (but does increase or decrease from point to point) the time for each segment is determined by means of equation 6.3. The time between the points is required to determine the power required to increase the kinetic energy and potential energy of the aircraft. The FBD used for the calculation of the aircraft performance for the climb phase is shown in figure 2.26. For each segment, at first the lift force is determined by means of equation 6.4 where the velocity of the initial point of the segment is taken. With the lift force known, the lift coefficient is determined at each altitude with the standard atmosphere model. The aerodynamic model of the aircraft then determines the drag coefficient and hence the drag force. With all of these known, the power required for each segment is determined by equation 6.5, which is the power the aircraft must produce with the propeller. The first part of the equation is the power for steady straight symmetric flight. Added to this is a term which accounts for the power required to climb and the power required is accelerate. These last two terms can become negative for the segments, meaning the aircraft descents or decelerates. With the power required for each segment known, the models for the propulsion system are used to determine the efficiency of the HEPS and the energy or fuel consumption. For each segment the fuel consumption is determined as well and hence the weight of the aircraft is updated each time. The Design Structure

Matrix (DSM) is illustrated in Appendix D.

$$\Delta x = \frac{\Delta h}{\tan \gamma} \tag{6.1}$$

$$\Delta s = \sqrt{\Delta x^2 + \Delta h^2} \tag{6.2}$$

$$\Delta t = \frac{\Delta s}{V} \tag{6.3}$$

$$L = W + \frac{W}{g} V \frac{\Delta \gamma}{\Delta t} \tag{6.4}$$

$$P_r = DV + WV \sin(\gamma) + WV \frac{\Delta V}{\Delta t} \tag{6.5}$$

6.3.2 Optimization problem

In this section the optimization problem statement is given for different objectives. Alongside, the bounds and constraint of the problem are stated together with the optimizer settings. Three different objectives are chosen to be minimized for the climb flight path; minimum total energy use, minimum fuel burned and minimum time. All three are determined by the same method described in the previous subsection, called function J and are given by equation 6.6 to 6.8. Here, the vector $\vec{x}$ is given by equation 6.9, which consist out of individual vector at each point in the flight path $\vec{x}_i$ given by equation 6.10. The objective is always to minimize the function J.

$$J_1 = E_{tot}(\vec{x}) = E_{out_{batt}}(\vec{x}) + E_{fuel}(\vec{x}) \tag{6.6}$$

$$J_2 = m_{fuel}(\vec{x}) \tag{6.7}$$

$$J_3 = t_{c\lim b}(\vec{x}) \tag{6.8}$$

$$\vec{x} = \begin{bmatrix} \vec{x}_1 \\ \vec{x}_2 \\ \vdots \\ \vec{x}_n \end{bmatrix} \tag{6.9}$$

$$\vec{x}_i = \begin{bmatrix} V_i \\ \gamma_i \\ \Omega_i \\ f_{p_{split}i} \end{bmatrix} \tag{6.10}$$

Obviously, the design variables are bound for each individual point. These bounds are given by 6.11 to 6.14. The velocity is bounded by the minimum (stall) speed and the maximum structural cruise speed which are both depending on the altitude. The velocity

bounds as a function of altitude are determined by the conversion from IAS to TAS. IAS is the speed that is given by the airspeed indicator of the aircraft and is driven by measuring the difference between the static pressure and total pressure. Consequently, the dynamic pressure is measured. To determine airspeed, the density must be factored out and since the airspeed indicator cannot measure air density it uses the density at sea level. For an incompressible flow the IAS can be assumed equal to the Equivalent Air Speed (EAS), which is the airspeed at sea level that will result in the same dynamic pressure. Since the maximum cruise speed and altitude result in a Mach number of 0.39 it can be assumed that the aircraft will fly in and incompressible flow for these calculations. The maximum and minimum TAS as a function of altitude are illustrated in figure 6.10. Here, the economic cruise speed of the conventional as given by Pipistrel is also shown.

$$V_{stall}(h) \leq V_i \leq V_c(h) \tag{6.11}$$

$$1 \leq \gamma_i \leq 30 \tag{6.12}$$

$$500 \leq \Omega_i \leq 2250 \tag{6.13}$$

$$0 \leq f_{p_{split}i} \leq 1 \tag{6.14}$$

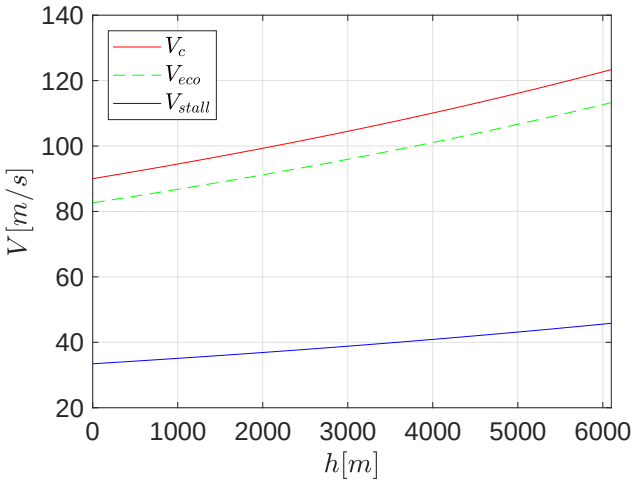

Figure 6.10: The minimum and maximum flight velocities given in TAS versus the altitude

The constraints are also important since each component of the HEPS has its own constraints that are influenced by the design variables. The power that comes out of the battery is constraint at 120 kW as given by a battery requirement from Pipistrel, given by equation 6.15. In addition, the battery model is not made to give a larger power out of the battery so the model will fail if this constraint is not satisfied. For the climb, the SOC at the end of the climb phase must not be lower than a certain number, given by equation 6.16. This value has been chosen so that at the beginning of the cruise the battery is not fully discharged resulting in a large charge cycle during the cruise and of course to make sure there is enough power left te perform a reserve mission would an anomaly occur. The power that is requested from the ICE is constraint to its minimum and maximum value which depends on the altitude, given by equation 6.17. In addition, the propeller

is constraint to the minimum and maximum values that are stated by the available data. The propeller constraints are given by equation 6.18, 6.19 and 6.20. Furthermore, the EM's torque is constraint to the minimum and maximum values that are stated by the available data as well, given by equation 6.21.

$$P_{out_{batt}}(\vec{x}) \leq 120kW \tag{6.15}$$

$$0.3 \leq SOC_{end_{c\,\mathrm{lim}\,b}}(\vec{x}) \tag{6.16}$$

$$P_{out_{ICE}\,\mathrm{min}}(h) \leq P_{out_{ICE}}(\vec{x}) \leq P_{out_{ICE}\,\mathrm{max}}(h) \tag{6.17}$$

$$0.03 \leq C_P(\vec{x}) \leq 0.4 \tag{6.18}$$

$$0.01 \leq C_T(\vec{x}) \leq 0.32 \tag{6.19}$$

$$0 \leq J(\vec{x}) \leq 2 \tag{6.20}$$

$$100 \leq \tau_{EM}(\vec{x}) \leq 850 \tag{6.21}$$

The optimizer used to solve this problem is *fmincon* from Matlab. The algorithm used is the Sequential Quadratic Programming (SQP) algorithm. Most of the options for *fmincon* are left unchanged, so to their default value. However, the constraint tolerance is set to 10^{-4}, the optimality tolerance to 10^{-2}, the step tolerance to 10^{-5} and the finite difference step size to 10^{-3}. The constraint tolerance is changed to a larger value so that the algorithm converges faster and a value that is 0.0001% over the constraint does not influence the solution in a negative way and may be considered as realistic. For the optimality tolerance, the step tolerance and the finite difference step size the same logic applies. If the solution is still within 0.01% of its optimum value it is considered to be satisfactory so these values are increased slightly as well to ensure faster convergence to the local optimum point. In addition, the models use smooth functions that represent there performance resulting in a smooth objective function so very small tolerances are not required. The main options that are set for *fmincon* are summarized in table 6.5. Of course, the objective function is normalized to its initial point value and the bounds and constraints are normalized as well.

Option	Setting
Algorithm	SQP
Constraint tolerance	10^{-4}
Finite difference step size	10^{-3}
Optimality tolerance	10^{-2}
Step tolerance	10^{-5}
Finite difference type	Forward
Max function evaluations	$100 \cdot numberofvariables$
Max iterations	400
Objective limit	10^{-20}

Table 6.5: Option settings for fmincon for climb optimization

6.3.3 Results

The number of segments for this method influences the solution substantially. More segments most likely results in better accuracy, however the number of variables for the optimization increases and the time step between the points becomes smaller requiring a more accurate battery model. Therefore, more points makes the optimization more computationally expensive. Consequently, it is investigated which amount of points is acceptable. Figure 6.11 shows the optimum distribution for one of the variables for the minimum fuel objective. It clearly shows that by increasing the number of points, the optimum flight velocity approaches a certain profile. The same is investigated for each objective for the climb phase optimization and for each 50 segments seems to result in a relatively satisfying curve. Increasing the points more results in a exponential increase of the time to run the optimization since the battery precision must be adjusted as well.

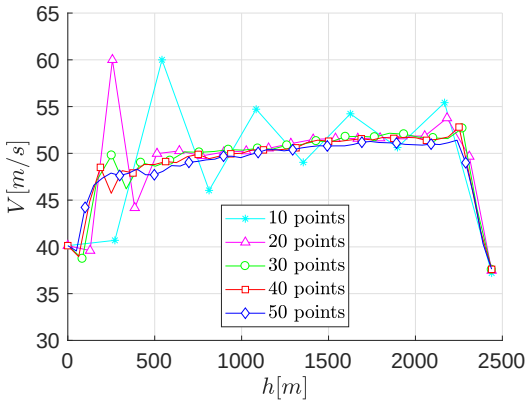

Figure 6.11: Optimum flight velocity versus altitude for different number of points, for minimum fuel to climb objective

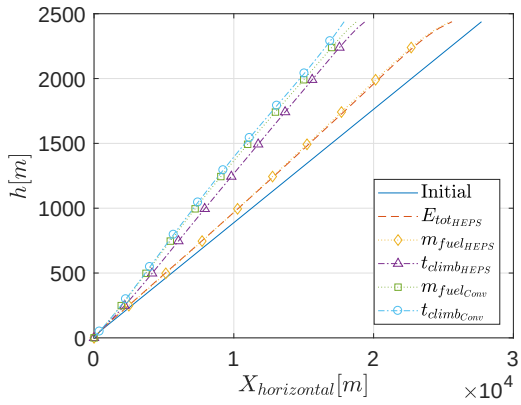

Figure 6.12: Altitude versus horizontal distance for initial point and optimum points for different objectives and both conventional and HEPS

For reference and comparison, the conventional aircraft and propulsion system model is optimized similarly. The first point of the climb is not included in the optimization as a variable and is fixed to the end point of the take off phase. In addition, the variables must be set to an initial value in order to determine the initial point of the optimization procedure, so where the algorithm starts searching for a direction towards a local minimum. This initial point consists of values that are also based on an engineering guess by the author. The velocity at each point is set to 50 m/s which is slightly based on the minimum time to climb velocities determined in the beginning of this chapter. The author suspects that the minimum energy and minimum fuel to climb optimum point lies at a lower velocity, hence this value is chosen. To same logic applies to the initial flight path angle. The main drive train rotational velocity is set slightly lower than its maximum value as well. This done because the author suspects that the drive train rotational velocity will be high (low advance ratio) because the output power from the propeller will be high as well for the climb. The power split factor is set to 0.4 for each variable as well for the HEPS, based on an engineering guess. The first point which is fixed, together with the initial values of the variables are given in table 6.6.

Parameter	Value	Unit
V_0	40.13	m/s
γ_0	7.23	$^\circ$
Ω_0	2250	RPM
$f_{p_{split}0}$	0.4	–
V_i	50	m/s
γ_i	5	$^\circ$
Ω_i	2000	RPM
$f_{p_{split}i}$	0.4	–

Table 6.6: First fixed points values and initial variable values for the climb optimization

	Total energy	Fuel		Time to climb		Unit
Parameter	HEPS	Conv	HEPS	Conv	HEPS	
t_{climb}	8.78	8.26	8.77	8.16	6.36	min
E_{tot}	37.28	51.70	37.24	53.53	44.56	kWh
E_{fuel}	28.11	51.70	28.07	53.53	35.68	kWh
E_{batt}	9.17	N/A	9.17	N/A	8.88	kWh
m_{fuel}	2.30	4.23	2.30	4.38	2.92	kg

Table 6.7: Basic results for the climb optimization

The convergence history of the climb optimization are shown in Appendix E in the form of normalized function value versus the iterations. The basic results from the climb optimization are presented in table 6.7. Here, the conventional propulsion system optimum climb values are shown with the HEPS optimum values for each objective. The minimum total energy and minimum fuel objective are almost the same for the HEPS, so most likely this is a local minimum in the function to which both objectives seem to converge. For the conventional propulsion system the total energy would be similar to the total fuel objective since there is no use of a battery. The minimum time to climb objective does differ from the other results. Obviously, the time to climb is less and the total energy is more. However, the energy from the battery is less for the minimum time to climb than for the other objectives. Contrary, the energy from the fuel and mass of the fuel used is significantly higher for the minimum time to climb. This is due to the constraint on the battery SOC at the end of the climb. The power output from the battery is higher resulting in less efficiency from the battery resulting in less energy subtracted from the battery. For illustration purposes the flight paths for the initial and optimum points are shown in figure 6.12, note that the axis are not to scale.

The resulting optimum velocity distribution versus the altitude during the climb is shown in figure 6.13. Note that the final altitude point is free meaning the optimizer decreases the velocity and flight path angle towards there lower bound. The optimizer does this because there is no acceleration or climb rate required at this last point meaning this term wants to go to zero because that saves power and thus energy. Another thing that is observed is that the minimum time to climb optimum yield in a higher velocity and flight path angle distribution than the other objectives for the HEPS case, and approaches the maximum rate of climb velocity and flight path angle distribution. For the conventional

case however, it does not and the minimum time to climb and minimum fuel burned curves coincide. This is most likely caused by the effect that the ICE is directly coupled to the main drive train in the conventional case while for the HEPS case it is decoupled. If the battery SOC constraint would not be active due to a higher battery capacity, the optimum time to climb distribution would most likely coincide with the maximum rate of climb velocity and flight path angle distribution. In addition, the rate of climb distribution is shown in figure 6.14.

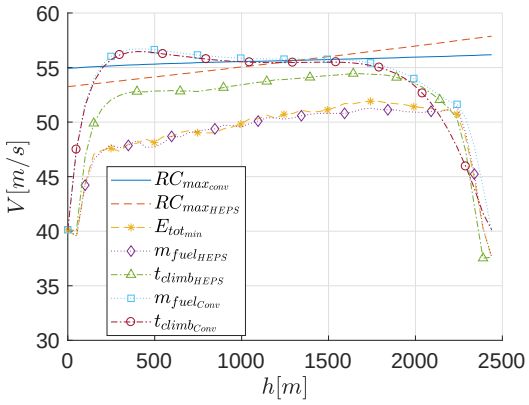

Figure 6.13: Optimum velocity versus altitude for different objectives for a climb to 8000ft with the HEPS aircraft

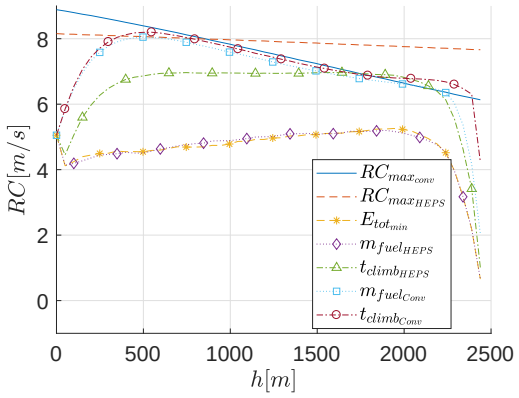

Figure 6.14: Optimum rate of climb versus altitude for different objectives for a climb to 8000ft with the HEPS aircraft

Figure 6.15 shows the optimum profile for the main drive train rotational velocity and power split factor versus the altitude. It is observed that the rotational velocity of the drive train for these objectives starts to increase with altitude until it reaches its maximum bound. For the minimum time to climb objective the rotational velocity for each altitude is at its maximum to obtain maximum power everywhere. At the very end of the climb phase different effects occur. One of these effects is that the optimizer decreases the potential and kinetic energy term towards zero because at the last point there is no increase in these two terms necessary. Therefore, the rotational velocity drops at the very end of the climb phase. Another effect is that the optimizer satisfies the SOC constraint at the very end of the climb phase, meaning that the power from the battery at the end goes to zero. The power profiles of the EM, the battery and the ICE are shown in figure 6.16. For the minimum total energy (solid line) and minimum fuel (dashed line) objective the power going into the EM increases during the climb. This is mainly due to the increasing power from the battery. The power from the ICE is lower and slightly decreases during the climb due to altitude effects.

The variation of propeller efficiency during the climb for each objective is shown in figure 6.17. For the efficiency of the propeller, most of the points are centered around the same value of about 0.78. This is definitely not the highest efficiency achievable but still quite sufficient. The problem arises that the propeller is designed for a high advance ratio (low RPM or high flight velocity). The optimizer wants the aircraft to fly at low drag so at low speed while increasing the rotational velocity to obtain high output thrust to climb faster. A larger flight velocity would increase the drag resulting in more energy lost during flight. For the EM the results for the climb are somewhat different as shown in figure 6.18. The

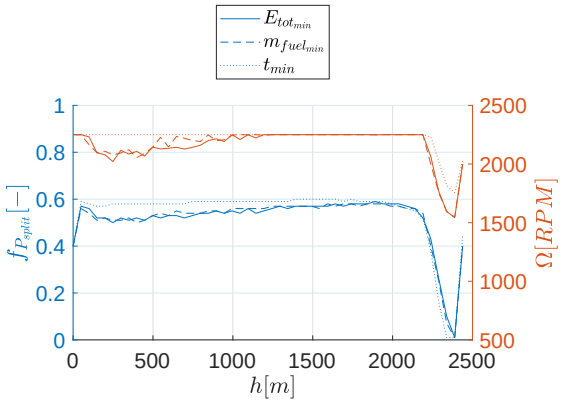

Figure 6.15: Optimum power split factor and rotational velocity versus altitude for different objectives for a climb to 8000ft with the HEPS aircraft

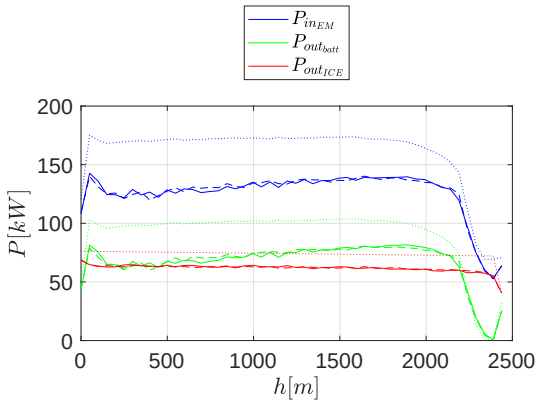

Figure 6.16: Optimum Power into EM, out of battery and out of ICE versus altitude for different objectives for a climb to 8000ft with the HEPS aircraft

cluttering of the points is where the climb is really being performed and the outer points represent the beginning and end of the climb phase. The author suspects that the SOC at the end of the climb constraint is responsible for limiting the torque values because in the upper right corner of the graph the maximum power occurs and the battery capacity is not able to cope with that amount of power over the time.

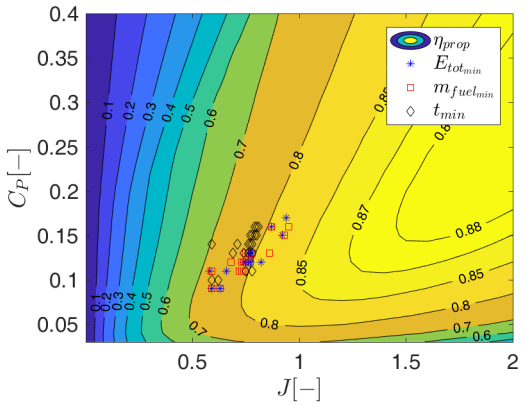

Figure 6.17: Contour plot of propeller efficiency with optimum climb points

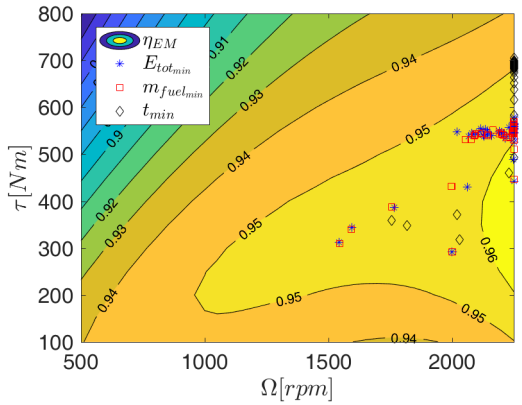

Figure 6.18: Contour plot of EM efficiency with optimum climb points

6.3.4 Intermediate conclusion for climb

In this subsection a short overview is given of the climb results and a few conclusions are drawn. From the results it is observed that there is a significant difference between the conventional case and the HEPS case. Figure 6.19 shows the normalized results for the minimum total energy and minimum time objectives. Compared to the conventional case both objectives use less total energy (and fuel) to perform the reference climb to 8000 ft.

However, this might be penalized by other performance characteristics. Therefore, the normalized time to climb is shown for both objectives in figure 6.20. For the minimum total energy case indeed the time to climb exceeds the value of the conventional case, however only by a small amount. The minimum time to climb objective for the HEPS is better in performance for time and total energy compared to the conventional case.

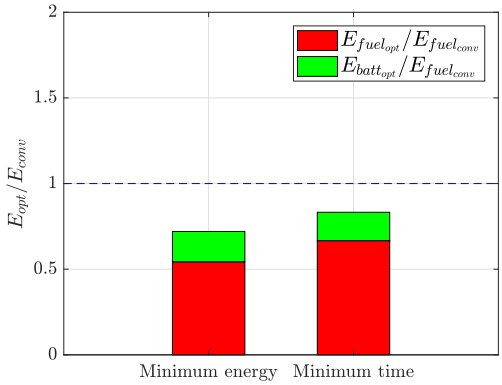

Figure 6.19: Bar plot of different objectives for energy use during climb, normalized to conventional case

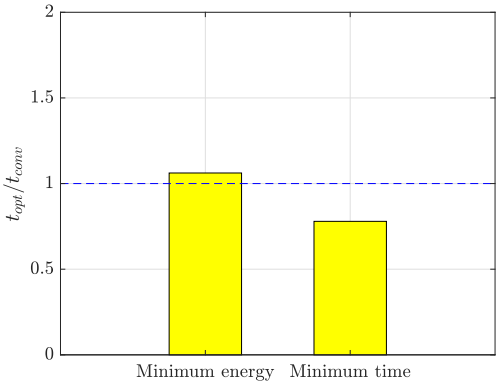

Figure 6.20: Bar plot of different objectives for time to climb, normalized to conventional case

6.4 Cruise optimization

For long flights (normal flight missions) the cruise is the longest part of the flight path, but the aircraft can potentially use significantly less power during this phase. Several parameters and objectives are considered in this chapter starting from simple optimization to more advanced. For the cruise phase, three different strategies are considered and are described in subsection 6.4.1. The main input to the cruise phase calculations results from the climb phase optimization. The key effect is in this case the battery SOC which has been drained to its lower limit during climb. This means that if electrical power from the battery is required that the battery first must be recharged during the cruise.

6.4.1 Methodology

The methodology of determining the optimum cruise phase is described in this section. At first the optimizer is ran to optimize the amount of energy that comes out of the propeller and it is therefore expected that the optimizer will converge to the minimum drag velocity since that is the velocity at which the least amount of energy is dissipated through drag. Secondly, an optimization is ran for the least amount of energy going into the EM, meaning the influence of the main drive train rotational velocity is added to the problem. This extra parameter might influence the most efficient velocity of the aircraft. Then finally the power sources are added to the problem. With the implementation of that, the optimum solution and objective for the cruise phase depends largely on the strategy that is applied. Therefore, three different strategies are investigated and for each the cruise phase is optimized. The three strategies are described below:

Strategy #1: During the first part of the cruise the ICE is running at the most efficient rotational velocity meaning the lowest amount of BSFC. The power output from the ICE and generator combination is than given to the controller which is able to split this power if possible. If the EM requires less amount of power than the ICE and generator combination supplies, the rest of this power is used to charge the battery. If the battery is than charged to a certain SOC constraint, the ICE is turned off and the aircraft flies fully electric until the batteries are discharged to the lower SOC constraint. If possible, this cycle is repeated during the cruise. The objective is than to minimize the energy consumed by the HEPS for each section.

Strategy #2: In this mission the assumption is made that the airport of arrival does not have recharging capabilities, but obviously does have a refueling point. This means that a return mission must be possible and the battery should be recharged completely at the end of the cruise phase. Therefore, during the first part of the cruise the ICE is running at a variable rotational velocity and the left over power is used to recharge to battery completely and should be at SOC of 1.0 at the end of the cruise. The velocity can therefore be a little bit higher than for strategy #1 since the battery does not need to be charged quickly.

Strategy #3: Generally, when a pilot plans a mission the velocity is selected. This way the pilot knows the estimated time of arrival and can calculate how much fuel is required. With the selected velocity the power for flight during the cruise is also known. The requirement on the battery at the end of the cruise phase for this strategy will be the same as strategy #1, a SOC of 0.3. Therefore, the battery does not have to be recharged during the cruise.

For each strategy different operating modes can be used, i.e. Hybrid mode, full electric mode and ICE only mode. For each of the strategies the flight path is optimized separately, to determine what flight velocity, flight path angle and drive train rotational velocity is most advantageous. Therefore, the flight path is divided into separate sections, similar to the methodology for the climb optimization. However, for this methodology a fixed horizontal distance instead of fixed altitude gain is used to discretize the flight path, as shown in figure 6.21.

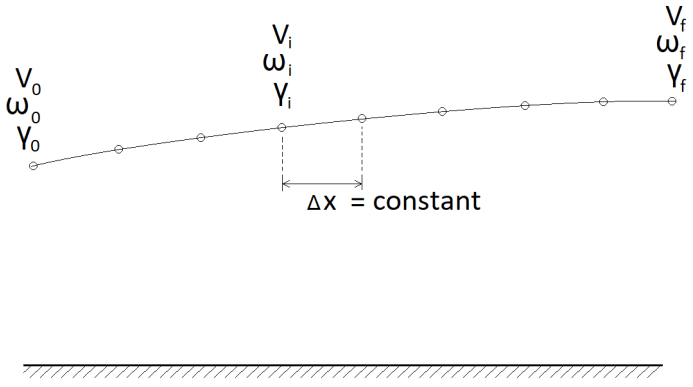

Figure 6.21: Schematic representation of the cruise flight path optimization methodology

6.4.2 Optimization problem

In this section the optimization problem statement is given together with the bounds and constraints of the problem and with the optimizer settings. Because for the cruise different kinds of optimizations are run for different strategies the optimization problem for each is stated. Like mentioned previously, two initial optimizations are run to observe some of the effects the aircraft and its main drive train have on the optimum point. This first optimization is to minimize the energy that comes out of the propeller, shown in equation 6.22. For this problem only the velocity and flight path angle are taken as a variable so the design variable vector is given by equation 6.9 where each individual vector $\vec{x}_i$ is given by equation 6.23. For the next preliminary optimization the energy going into the EM is optimized resulting in the objective function given by equation 6.24. Because the main drive train is included in this problem, the main drive train rotational velocity is added as a variable as well resulting in each individual vector $\vec{x}_i$ given by equation 6.25.

$$J = E_{out_{prop}}(\vec{x}) = \int P_{out_{prop}}(\vec{x})dt \tag{6.22}$$

$$\vec{x}_i = \begin{bmatrix} V_i \\ \gamma_i \end{bmatrix} \tag{6.23}$$

$$J = E_{in_{EM}} = \int P_{in_{EM}}(\vec{x})dt \tag{6.24}$$

$$\vec{x}_i = \begin{bmatrix} V_i \\ \gamma_i \\ \Omega_i \end{bmatrix} \tag{6.25}$$

The bounds of the variables are similar to the bounds used during the climb optimization except for the flight path angle, which lower bounds is now set at $0^/circ$. For the constraints of the problem the same applies as for the climb for the maximum power out of the battery, the propeller's advance ratio, thrust coefficient and power coefficient and for the EM's rotational velocity. The additional constraint that is added to this problem is the power going into the battery which is shown by equation 6.26. In addition, the same optimization algorithm is used as for the climb optimization however the settings are changed slightly to ensure a more sufficient convergence. These settings are shown in table 6.8.

$$P_{in_{batt}}(\vec{x}) \leq 45kW \tag{6.26}$$

6.4.3 Preliminary results

Like mentioned previously, at first an optimization is ran for the minimum energy out of the propeller. For this initial optimization the velocity and flight path angle are variable for each section. Similar to the climb the first point of the cruise phase is fixed and the

Option	Setting
Algorithm	SQP
Constraint tolerance	10^{-4}
Finite difference step size	10^{-3}
Optimality tolerance	10^{-4}
Step tolerance	10^{-5}
Finite difference type	Forward
Max function evaluations	$100 \cdot numberofvariables$
Max iterations	400
Objective limit	10^{-20}

Table 6.8: Option settings for fmincon for cruise optimization

Parameter	Value	Unit
V_0	50	m/s
γ_0	0	$^\circ$
V_i	50	m/s
γ_i	0.1	$^\circ$

Table 6.9: First fixed points values and initial variable values for the cruise optimization

rest of the points are set as variables. The first fixed point and initial variable values for this cruise optimization at each point are given by table 6.9.

The resulting velocity and flight path angle profile are shown in figure 6.22. The initial and optimum energy that comes out of the propeller is given in table 6.10. In addition, the time to cruise is also given for interpreting the influence time has on the lower optimum velocity. Although the problem is constraint, there are no constraints active for this optimization.

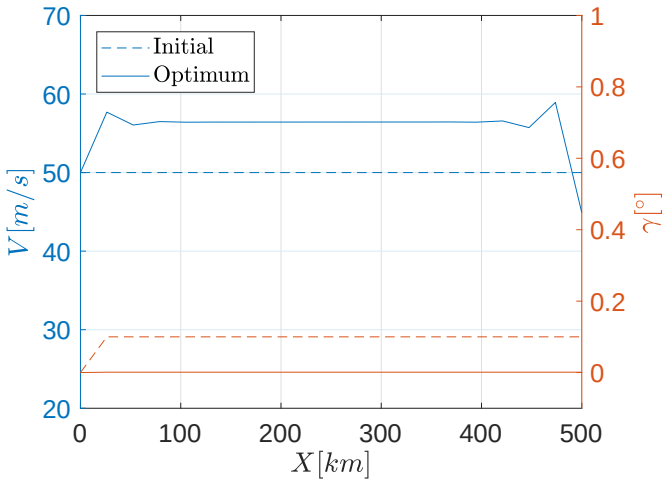

Figure 6.22: Velocity and flight path angle versus the horizontal distance of the cruise phase for the energy out of the propeller optimization

Parameter	Initial point	Optimum point	Unit
$E_{out_{prop}}$	107.34	100.64	kWh
t_{cruise}	2.78	2.46	hr

Table 6.10: Basic results for the cruise optimization of the energy out of the propeller

Secondly, an optimization is performed to observe the influence of drive train rotational velocity as well on the total amount of energy the EM uses during cruise. The basic drive train for this optimization is presented schematically by figure 6.23 and does not include the energy sources.

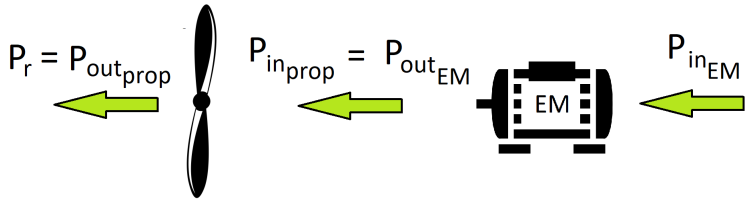

Figure 6.23: Simple drive train representation for initial optimizations

The values for the first fixed points and the initial variables are the same as that of the previous optimization and are therefore presented by table 6.9. Again the weight is considered constant during this optimization and it is therefore expected that the optimum flight path is flat as well. The resulting velocity and flight path profile are shown in figure 6.24. Again the flight path angle goes to zero everywhere. The velocity however is at a slightly higher value than for the energy out of the propeller optimization of 58.00 m/s. This means that the main drive train influences the most efficient flight velocity. The main drive train rotational velocity seems to converges to an optimal value of 1437 RPM and stays almost constant for each point, as shown in figure 6.25 and the power into the EM converges to approximately 51 kW. Due to the fact that the ICE is able to deliver slightly more, it is possible to recharge the battery at this velocity. The value of the optimum energy going into the EM and the time it takes to complete the cruise is given in table 6.11. The constraint that is active is the maximum power coefficient of the propeller. This is mainly due to the fixed first point because after that the algorithm wants the aircraft to accelerate to the most efficient velocity as quick as possible but is constraint by the maximum power coefficient.

Parameter	Initial point	Optimum point	Unit
$E_{in_{EM}}$	132.63	122.11	kWh
t_{cruise}	2.78	2.41	hr

Table 6.11: Basic results for the cruise optimization of the energy into the EM

Figure 6.26 shows a contour plot of the propeller efficiency together with the optimum energy into the EM points. In figure 6.27 the efficiency of the EM model is shown and here most of the points do not lie around the highest achievable efficiency. The main reason for this is that the highest efficiency of the EM is at high rotational velocity while the highest efficiency for the propeller is at low advance ratio or low rotational velocity

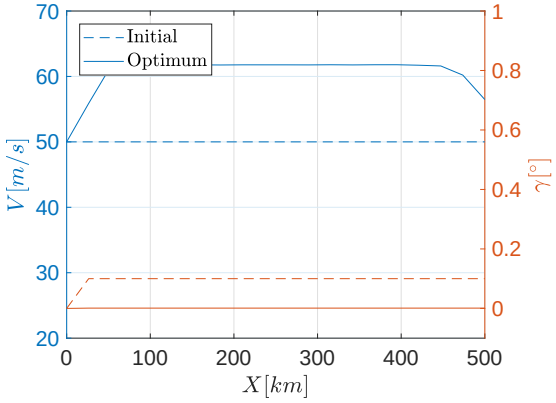

Figure 6.24: Velocity and flight path angle versus the horizontal distance of the cruise phase for the energy into the EM optimization

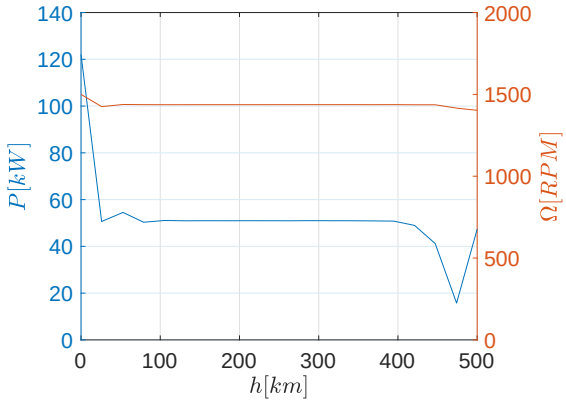

Figure 6.25: Power into EM and main drive train rotational velocity versus the horizontal distance of the cruise phase for the energy into the EM optimization

for a fixed flight velocity. The optimizer clearly makes a trade off between flying at a low drag speed, while maximizing the efficiency of the complete main drive train.

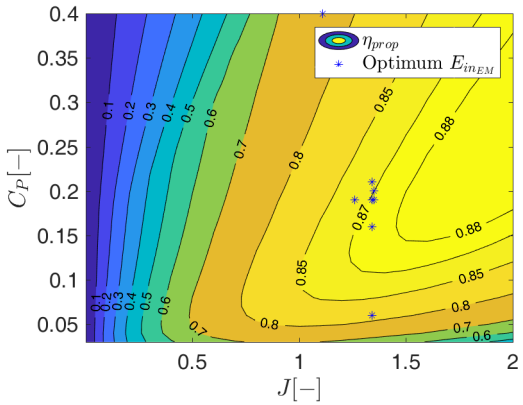

Figure 6.26: Contour plot of propeller efficiency with optimum energy going into EM for cruise points

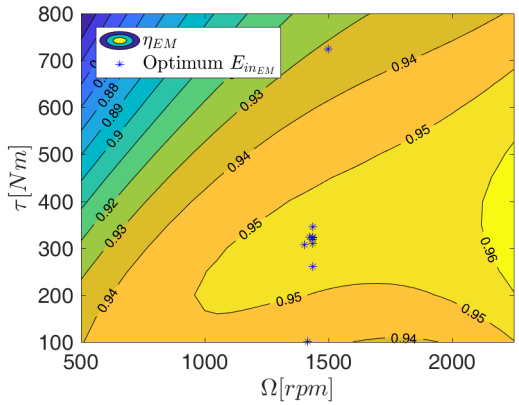

Figure 6.27: Contour plot of EM efficiency with optimum energy going into EM for cruise points

6.4.4 Strategic results

In this section, the optimization results for each strategy are presented. The reference cruise phase begins at altitude of 8000 ft above sea level. During the cruise the optimization is able to increase or decrease the altitude if that is more efficient. The convergence history of the cruise optimizations is shown in Appendix E again in the form of normalized function value versus the iterations.

Strategy #1 The basic parameters for the most efficient point of the Rotax ICE are given by table 6.12. This means that for this strategy when the ICE is running these

values are used. Because the generator model uses a fixed efficiency of 95% the output power from the combination of the ICE with the generator is 63.51 kW. Another aspect of this strategy is that the aircraft flies at the velocity and main drive train rotational velocity determined previously to be most efficient in energy use of the EM. This means that the required power input for the EM is less than the output form the generator and thus there is left over power to recharge the battery.

Parameter	Value	Unit
Ω	5280	RPM
$\dot{m}_f$	18.24	kg/h
$P_{out_{8000\,ft}}$	66.85	kW

Table 6.12: Most efficient point values of Rotax ICE

So for the first part of the cruise the battery is recharged to a SOC of 0.9. This boundary has been chosen to assure a high efficiency of the charge and discharge cycles and thereby maximizing the life time of the battery by not putting too much stress on the component. Once the battery is recharged, the ICE is turned off and the aircraft flies full electric until the battery is discharged to SOC of 0.3 again. This cycle is repeated until the final range of 500 km is obtained. The results in this section are for a flight path divided into 50 segments. The initial point for the flight velocity and rotational velocity of the main drive train at each point is set at the value at which the energy into the EM is most efficient, determine previously. Similar to the climb phase the first point of the flight path is fixed and the rest is free. One of the reasons for this is the ability to couple the climb phase to the cruise phase. If this point would not be fixed the optimization algorithm will increase the velocity to the maximum bound at the first point because the kinetic energy to reach that first point is not included in the cruise analysis. The initial flight path angle at each point is set to 0.1° again to observe what the optimization wants to do with the flight path. The values of the first fixed point and the initial variables are given in table 6.13. Since the energy sources are included in these calculations, the weight influence is included. As the aircraft burns fuel it loses weight and this might influence the optimum point. The aircraft weight and battery SOC at the beginning of the cruise are obtained from the climb optimization and acts as a fixed input to the problem.

Parameter	Value	Unit
V_0	57.99	m/s
γ_0	0	°
Ω_0	1437	RPM
V_i	57.99	m/s
γ_i	0.1	°
Ω_i	1437	RPM

Table 6.13: First fixed points values and initial variable values for the cruise optimization of strategy #1

Similar to the climb optimization different objectives are used to observe how these influence the flight path. Since for this strategy different operating modes are used for the HEPS (recharge and full electric) the total amount of energy comes form the fuel source.

Therefore, two different objectives are used, minimizing the total energy that goes into the EM and minimizing the fuel that is being burned. The basic results for the cruise optimization of strategy #1 are shown in table 6.14. No constraints are active for these optimum solutions.

Parameter	Initial	Energy into EM	Fuel	Unit
$E_{in_{EM}}$	124.11	120.21	120.40	kWh
t_{cruise}	2.40	2.42	2.36	hr
m_{fuel}	40.11	38.80	37.75	kg

Table 6.14: Basic results for the cruise optimization for strategy #1

Figure 6.28 shows the optimum profiles for the flight velocity and drive train rotational velocity versus the horizontal distance of the cruise. There is some difference between both objectives where the optimum fuel speed is somewhat larger for the recharging mode and for the full electric modes the velocity almost coincide. During recharging mode the optimum fuel leads to a larger speed since that minimizes the time for that section yielding in less fuel being burned. During full electric mode the fuel consumption becomes zero meaning the velocity stays at the most efficient for the energy into the EM. Figure 6.29 shows the aircraft's weight normalized to the MTOW versus the horizontal distance in the cruise phase. Due to the hybridization of the aircraft's propulsion system the weight decreases only by a small amount ($\approx$ 3%) and therefore the weight has a smaller influence on the optimum flight path than for a conventional aircraft.

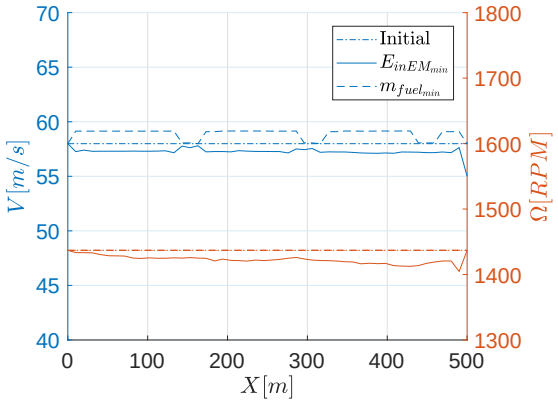

Figure 6.28: Velocity and drive train rotational velocity of the cruise optimization for strategy #1

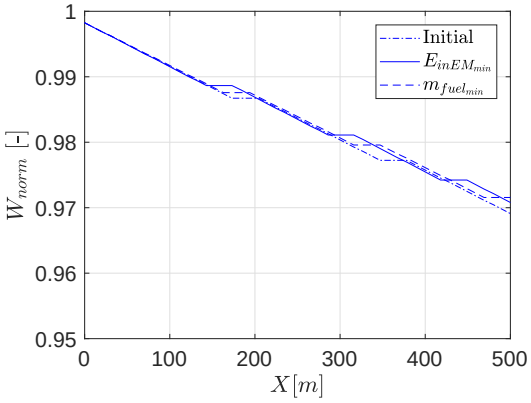

Figure 6.29: Normalized aircraft weight versus the horizontal distance of the cruise optimization for strategy #1

Figure 6.30 shows the initial and minimum energy into the EM profiles for the power going into the battery and the power going out of the battery versus the horizontal distance. For full electric flight the power out of the battery is quite high resulting in a short full electric flight. Contrary, the power into the EM during recharge mode, results in a significantly smaller power left to charge the battery and hence it takes longer to recharge the battery. Furthermore, the same graph is shown for the minimum fuel objective in figure 6.31. The initial points for the two cases are the same and consist of three recharge sessions and two full electric sessions. The minimum energy into the EM objective results

in one additional full electric session and end the cruise during the fourth recharge session, whilst the minimum fuel objective yields into one additional full electric session as well, but does not put another partly recharge session.

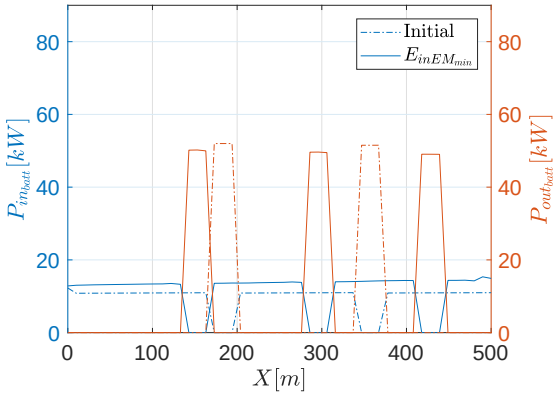

Figure 6.30: Power into the battery and power out of the battery versus the horizontal distance for the cruise optimization of the energy into the EM for strategy #1

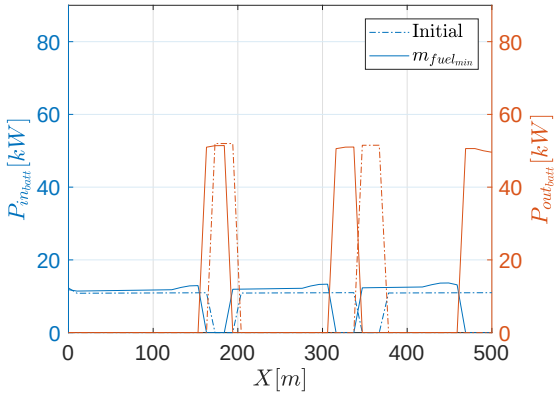

Figure 6.31: Power into the battery and power out of the battery versus the horizontal distance for the cruise optimization of fuel for strategy #1

Figure 6.32 shows the power into the EM and power out of the propeller (power required for the flight segment) versus the horizontal distance. The clear difference between the initial and both objectives is that the power for the optimum points is slightly lower. Just like with the velocity the recharge sessions have a higher power than the full electric sessions. Overall, the power for both components is decreasing during the cruise due to the decrease in weight. Like mentioned before, with decreasing weight the optimum drag point. It is therefore of interest to observe what happens to the actual thrust the propeller delivers. Figure 6.33 shows this thrust force for the initial and both objectives and it is observed that indeed the thrust also decreases during the cruise. The minimum drag velocity is never reached during the cruise by the velocity profile yet does come significantly close. In addition, the power coefficient from the propeller and torque from the EM points during the cruise are illustrated in the efficiency contour plots shown in figure 6.34 and 6.35, respectively. It can be stated that the propulsion system wants to operating in the most efficient condition for the main drive train.

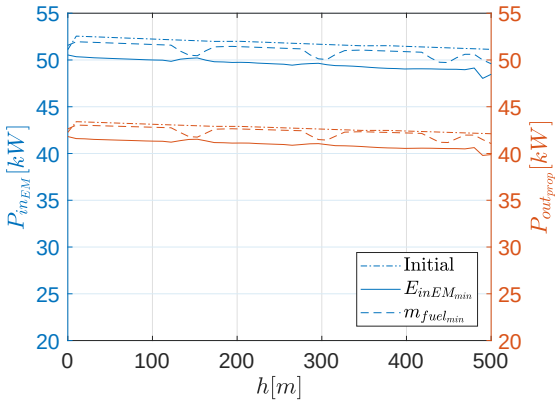

Figure 6.32: Power into the EM and power out of the propeller versus the horizontal distance for the cruise optimization of the energy into the EM for strategy #1

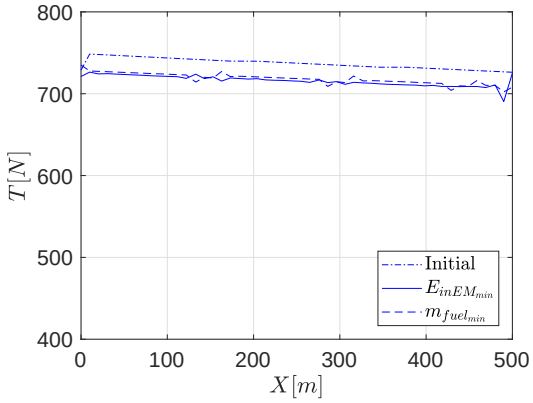

Figure 6.33: Thrust versus the horizontal distance for the cruise optimization of fuel for strategy #1

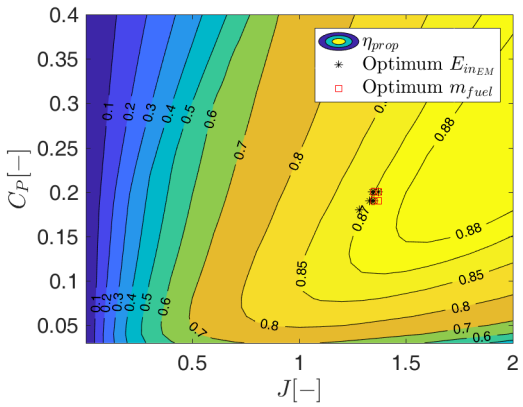

Figure 6.34: Contour plot of propeller efficiency with optimum energy going into EM and fuel for cruise points and strategy #1

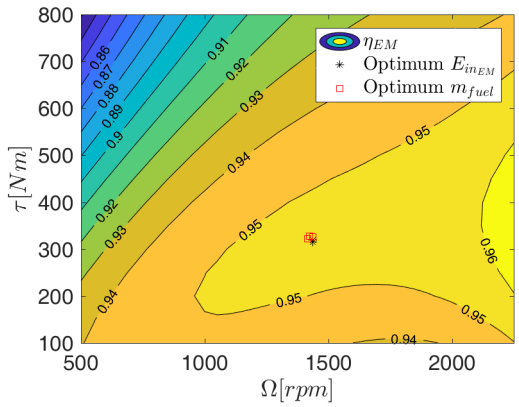

Figure 6.35: Contour plot of EM efficiency with optimum energy going into EM and fuel for cruise points and strategy #1

Strategy #2 For this strategy the first part of the cruise the battery is recharged fully where after the HEPS operates on ICE only. The variables for the optimization for this strategy are velocity, main drive train rotational velocity and rotational velocity of the ICE. The flight path angle is left out of the optimization as a variable due to the previously obtained results for the first strategy where the flight path angle goes to zero for every point. Therefore, the altitude for the cruise remains constant. The results for this strategy are also obtained for a flight path divided into 50 segments. The first point of the cruise is fixed and the other points are variables for the cruise phase. The initial values of the variables for the optimization are set at the same values as for strategy #1, given by table 6.13. The initial rotational velocity of the ICE for each point is set at 5200 RPM based on an engineering guess and close to the rotational velocity where the ICE performs most efficiently. Again the aircraft weight is updated each section since the ICE

burns some of the fuel mass. Similar to the previous optimization different objectives are investigated and for this strategy minimum fuel and minimum time are used. Minimum fuel because the only energy source for this strategy is the fuel tank (the battery is not discharged) and minimum time because economically speaking this might yield in a better performance. The basic results for this optimization are shown in table 6.15.

Parameter	Initial	Fuel	Time	Unit
t_{cruise}	2.40	2.87	2.07	hr
m_{fuel}	48.53	30.14	51.48	kg

Table 6.15: Basic results for the cruise optimization for strategy #2

Figure 6.36 shows the velocity and rotational velocity of the main drive train distribution over the horizontal cruise distance. The velocity profile for both objectives show two distinct regions. The lower region is the velocity where the battery is recharged and the higher velocity region at the end of the cruise phase is where the HEPS performs with ICE only mode. Figure 6.37 shows the weight of the aircraft relative to the MTOW versus the horizontal distance of the cruise phase.

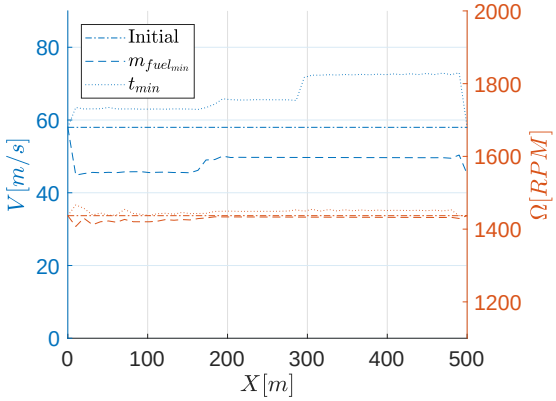

Figure 6.36: Velocity and drive train rotational velocity of the cruise optimization for strategy #2

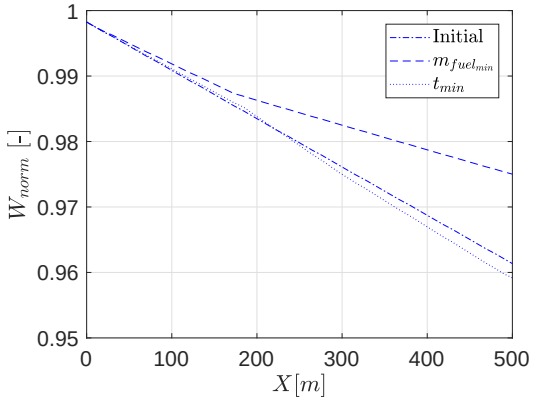

Figure 6.37: Normalized aircraft weight versus the horizontal distance of the cruise optimization for strategy #2

In figure 6.38 the power into the battery and the battery efficiency profiles are shown for each objective. It is observed that for the minimum fuel objective the power used to recharge the battery is somewhat similar to the initial point. Because the first point of the cruise phase has a fixed velocity which is higher than the velocity the optimization wants to obtain for the recharging part, the aircraft first decelerates during which a slightly higher charge power can be obtained. Therefore, the power into the battery for this objective is slightly smaller and the battery is recharged a little bit quicker. The most significant difference occurs at the minimum time objective where the power into the battery becomes even lesser resulting in a longer recharging cycle. With lower power going into the battery more power is used to fly the aircraft at a higher velocity. Therefore, when the battery is recharged completely the velocity for the minimum time requirement goes to its maximum obtainable value of about 72 m/s for ICE only mode at 8000 ft which can be observed in figure 6.2. The battery recharging efficiency is quite high due to the

relatively low charging power. During ICE only mode it is considered to be 1.0 since the power becomes zero. The power into the EM and out of the propeller is shown in figure 6.39 for both objectives. Again two distinct regions are observed where the first region of the minimum time objective shows a step in the results, most likely due to the influence of the initial guess. For the minimum fuel objective both power profiles show a slightly decreasing power for both regions, most likely due to the small decrease in weight. The minimum time objective also shows this small decrease except for the ICE only region where the power is set to the maximum value obtainable for ICE only mode.

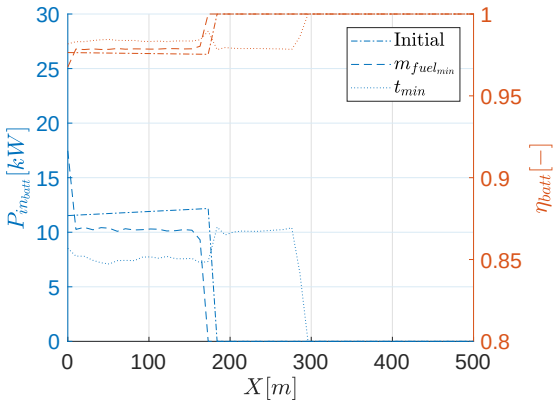

Figure 6.38: Power into the battery and battery efficiency versus horizontal distance of the cruise optimization for strategy #2

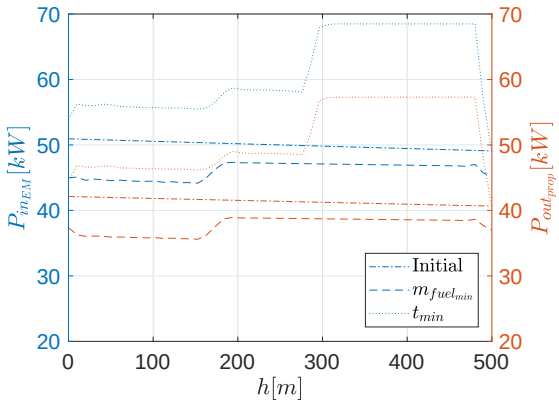

Figure 6.39: Power into the EM and out of the propeller versus the horizontal distance of the cruise optimization for strategy #2

Figure 6.40 and 6.41 show the contour plots of the efficiency of the propeller and EM respectively. The results for both objectives are shown in the form of points in the contour plots. It is observed that for the minimum fuel objective the propeller performs at a smaller efficiency than for the minimum time objective. For the EM there is a difference observed as well yet it remains very small so the propeller influences the problem more than the EM, which is expected. The group of point at the lower advance ratio for the minimum time objective is where the battery is recharged and the group at the higher advance ratio is where the HEPS performs on ICE only mode.

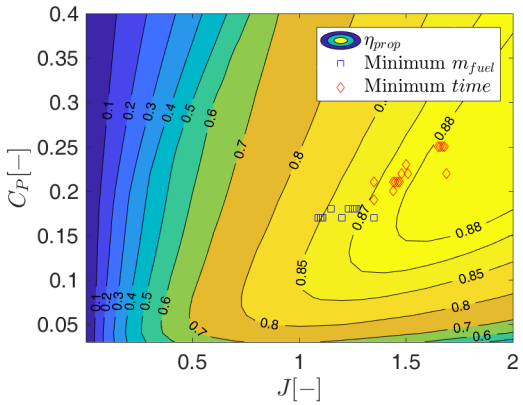

Figure 6.40: Contour plot of propeller efficiency with minimum fuel and minimum time for cruise points and strategy #2

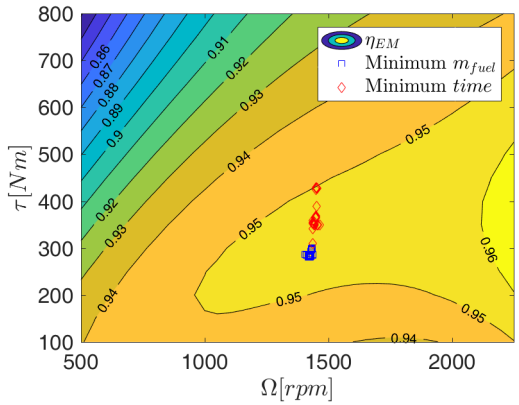

Figure 6.41: Contour plot of EM efficiency with minimum fuel and minimum time for cruise points and strategy #2

Strategy #3 For this strategy the velocity is kept constant during the cruise. However, the value of the constant velocity is set free during the optimization. Therefore, the first variable in $\vec{x}$ is the constant cruise velocity. During the cruise of this strategy the battery is not charged so the HEPS is in ICE only mode. This means that the battery SOC stays at 0.3 and must be recharged either during descent or at the destination airport. The other variables during this optimization is the main drive train rotational velocity. The rotational velocity of the ICE and generator combination is determined by the demand of the EM. Again the flight path angle is kept constant at zero degrees so the cruise phase altitude is constant as well. In addition, the results for this optimization are also obtained for a cruise flight path consisting out of 50 segments. The first point of the cruise phase is also fixed, and the initial values of the variables are given by table 6.13. Furthermore, the weight is updated at the end of each segment and the objectives used for the optimization are minimum fuel and minimum time. The basic results of the optimization are given in table 6.16 and includes the constant velocity.

Parameter	Initial	Fuel	Time	Unit
t_{cruise}	2.40	2.79	1.93	hr
m_{fuel}	27.19	24.49	51.62	kg
V_{cruise}	57.99	49.72	71.93	m/s

Table 6.16: Basic results for the cruise optimization for strategy #3

Figure 6.42 shows the initial and both optimum rotational velocity profiles for the ICE and the main drive train. The first observation made is that for the minimum fuel objectives both rotational velocities decreases during the cruise in a similar manor as the weight. In addition, for the minimum time objective the rotational velocity of the ICE combustion engine decreases as well during the cruise while the rotational velocity of the main drive train stays constant at the initial value. The power going into the EM and power going out of the propeller is shown in figure 6.43 and shows a similar behavior due to the constant velocity during the cruise.

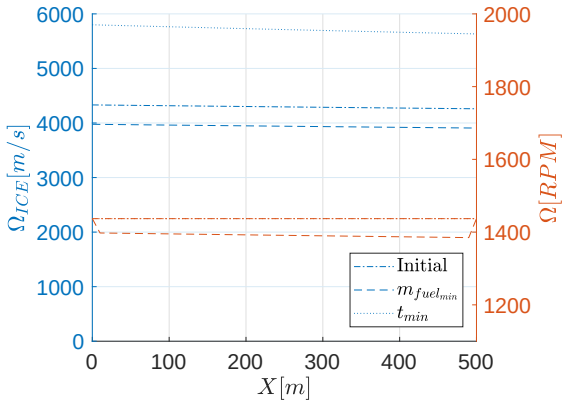

Figure 6.42: Rotational velocity of the ICE and main drive train versus the horizontal distance for the cruise optimization for strategy #3

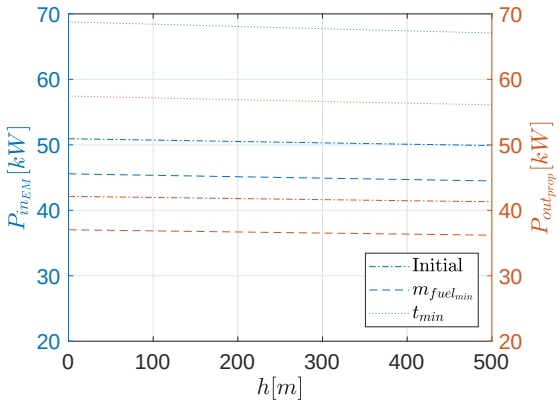

Figure 6.43: Power into the EM and out of the propeller versus the horizontal distance of the cruise optimization for strategy #3

The contour plot of the propeller efficiency with the points during the cruise phase for each objective, is shown in figure 6.44. The minimum time objective results in a higher advance ratio due to the higher velocity and therefore a higher efficiency for the propeller. However, the rotational velocity of the main drive train remains almost constant and close to the initial value so for the EM only the torque changes significantly for the minimum time objective. This results in a slightly less efficiency for the EM compared to the minimum fuel objective. The minimum fuel objective for this strategy results are in the same region as for the other strategies.

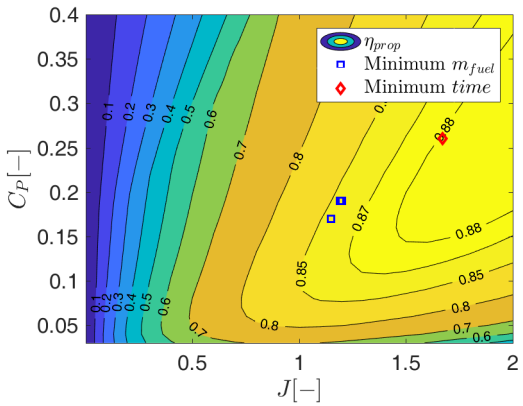

Figure 6.44: Contour plot of propeller efficiency with minimum fuel and minimum time for cruise points and strategy #3

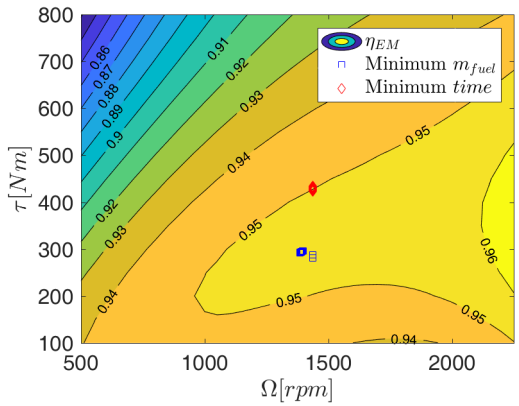

Figure 6.45: Contour plot of EM efficiency with minimum fuel and minimum time for cruise points and strategy #3

6.4.5 Intermediate conclusion for cruise

For visualization purposes results are shown in a bar chart with values normalized to the conventional mission. For the energy from the fuel this is shown in figure 6.46. It

can clearly be observed that strategy #3 is the best strategy in term of minimum fuel compared to the other strategies. However, in terms of time it is not. There is clearly a connection between the decrease of the fuel consumed and the increase of the time to perform the cruise. In addition, it can be stated that strategy #1 is not efficient in term of fuel, so it is not recommended to perform multiple discharge/charge cycles for the battery during the cruise. Contrary, strategy #2 does have a completely charged battery at the end of the cruise allowing for return mission from airfields without charging capabilities. However, the difference in energy from fuel between strategy #2 and strategy #3 is more than the energy going into the battery. This means that more of the energy is lost in strategy #2 due to lower efficient operation of the drive train. However, this is paid back in time since strategy #2 performs the cruise in a smaller time than strategy #3. The velocity profile for the minimum fuel objective for cruise and for the different strategies is shown in figure 6.48. For the minimum time objective the results are shown in a bar chart as well in figure 6.47. For strategy #1 the minimum time objective is not used because it would result in no charge at all, so it is left out of this chart. As can be observed, the difference between both strategies is rather minor in fuel. The velocity for the minimum time objective for cruise and for the different strategies is shown in figure 6.49. It is observed that the velocity during recharging is smaller so power is left to recharge the battery for strategy #2.

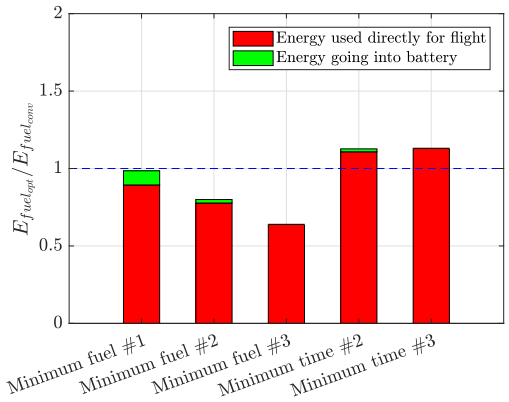

Figure 6.46: Bar chart of cruise optimization results for different objectives and strategies for energy from fuel, normalized to conventional case

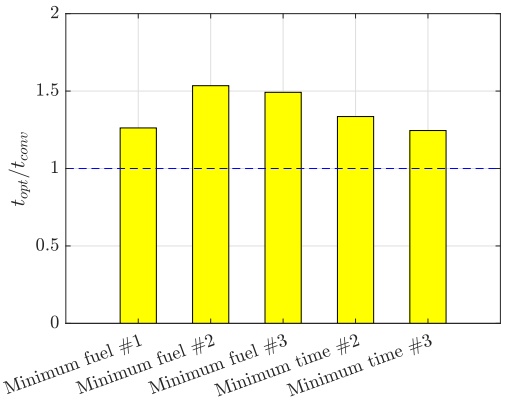

Figure 6.47: Bar chart of cruise optimization results for different objectives and strategies for time to cruise, normalized to conventional case

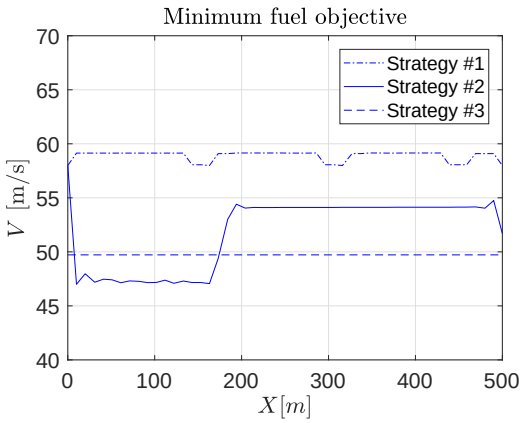

Figure 6.48: Velocity versus horizontal cruise distance for different strategies and minimum fuel objective

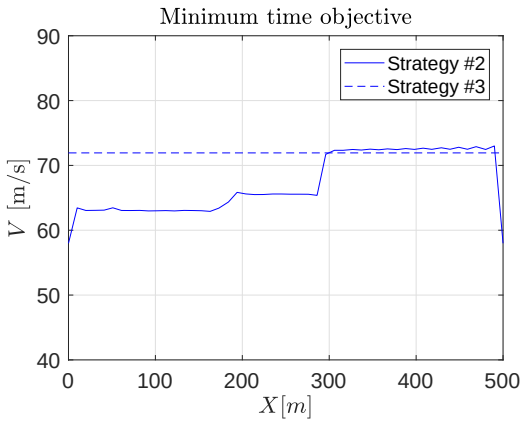

Figure 6.49: Velocity versus horizontal cruise distance for different strategies and minimum time objective

6.5 Mission optimization

In this section the total mission is optimized. The climb and cruise phase are connected together to observe any difference in optimum flight profiles. This connection means that the last point of the climb phase is set equal to the first point of the cruise phase and the total mission properties are optimized. The methodology is described below, followed by the optimization results.

6.5.1 Methodology

For the total mission optimization the climb and cruise phase are coupled together and the objective is set for the total mission. With that the taxi and take off are not considered variable for the optimization and act as a fixed input for the problem. At first a strategy from the cruise optimization is chosen for the total mission optimization and strategy #2 is selected. With this strategy the battery is always fully recharged at the end of the cruise phase resulting in a very quick turn around time and the possibility for a return mission at low utility airfields with no charging facilities. Because of the fully recharged battery requirement at the end of the cruise phase, the minimum SOC constraint is lowered to 0.1, which is the lowest boundary for the battery to operate nominal, while the fully charged constraint at the end of the cruise phase still applies in this case. The methodology of the mission optimization consists of the combination of the climb and cruise optimization methodology where the last point of the climb phase coincides with the first point of the cruise phase. Because the battery is recharged during flight, the objectives used in this optimization includes minimum fuel. In addition, the time to fly a certain mission can be crucial to the aircraft performance as well so the minimum time objective is also investigated. For the cruise phase two different operating modes are made available for the aircraft, recharging mode and ICE only mode. During the climb the aircraft performs in hybrid mode. For the optimization the same settings are used as for the climb and cruise phase optimizations.

6.5.2 Results

The convergence history of the mission optimization are shown in Appendix E again in the form of normalized function value versus the iterations. The basic results of the mission optimization for each objective are shown in table 6.17. By observing the results it can be concluded that the cruise phase has a significant larger impact on the overall performance parameters than the climb phase.

Table 6.17: Basic results for the mission optimization with strategy #2 for cruise

Parameter	Minimum fuel	Minimum time	Unit
$m_{fuel_{climb}}$	2.15	2.91	kg
$m_{fuel_{cruise}}$	31.96	51.33	kg
$m_{fuel_{climb+cruise}}$	34.11	54.25	kg
t_{climb}	0.10	0.11	hr
t_{cruise}	2.61	1.95	hr
$t_{climb+cruise}$	2.71	2.06	hr

The resulting velocity profile for the climb and cruise phase are presented in figure 6.50 and 6.51, respectively. Here, the velocity profile of the minimum time objective for the climb phase coincides with that of the theoretical maximum rate of climb velocity profile. Contrary, the optimum flight path angle, shown in figure 6.52, is lower for this objective, even lower than the minimum fuel objective flight path angle profile. The main reason that the flight path angle does not coincide with the theoretical maximum rate of climb is due to the coupling with the cruise phase. If the battery is not fully discharged some time advantage is gained during the cruise phase resulting in an overall less time to perform the mission. Therefore, the resulting rate of climb is lower than the theoretical maximum and the minimum fuel objective. For the power split factor the same can be stated, whereas the main drive train rotational velocity does not differ much between both objectives and stays rather constant at round 2000 RPM, as illustrated in figure 6.53.

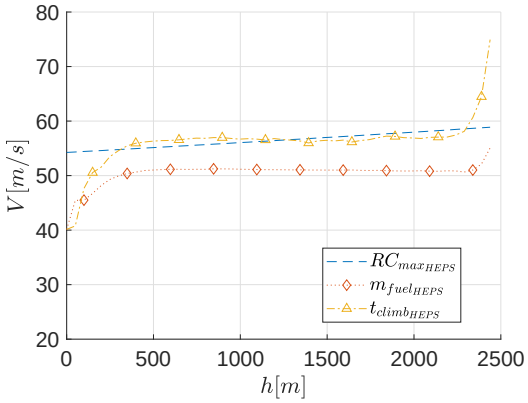

Figure 6.50: Optimum velocity versus altitude for different objectives for the climb phase of the mission optimization

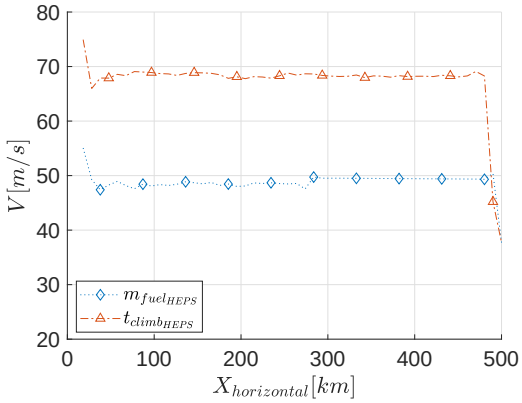

Figure 6.51: Optimum velocity versus altitude for different objectives for the cruise phase of the mission optimization

Figure 6.54 shows the profiles of the power out of the battery and the power out of the

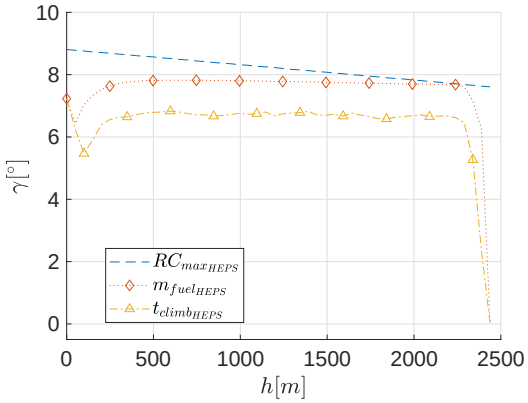

Figure 6.52: Optimum flight path angle versus altitude for different objectives for the climb phase of the mission optimization

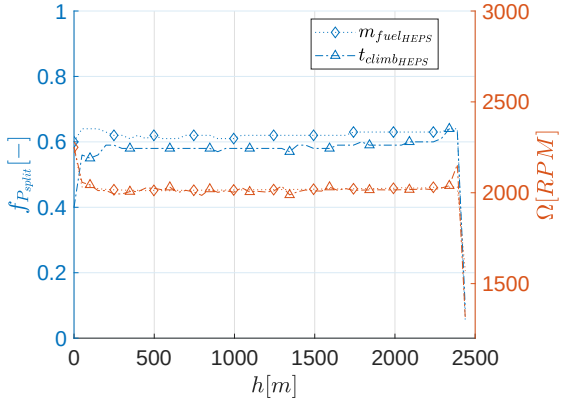

Figure 6.53: Optimum power split factor and main drive train rotational velocity versus altitude for different objectives for the climb phase of the mission optimization

ICE for the climb phase for each objective. For the minimum time objective the ICE power is at its maximum power constraint almost at every point meaning this constraint is active. The minor slope in the profile is due to the influence of altitude on the ICE. For the battery the maximum power constraint is not active in this case. It is observed that the minimum fuel objective results in a higher output power from the battery yet a lower power output from the ICE, for the same reason discussed earlier. The main drive train and ICE rotational velocity of the cruise phase is shown in figure 6.55. For the minimum fuel objective there is clearly a distinct region for the recharge and the ICE only flight modes. Contrary, for the minim time objective there is not due to the recharging occurring at a lower power into the battery meaning the recharge region is the entire cruise.

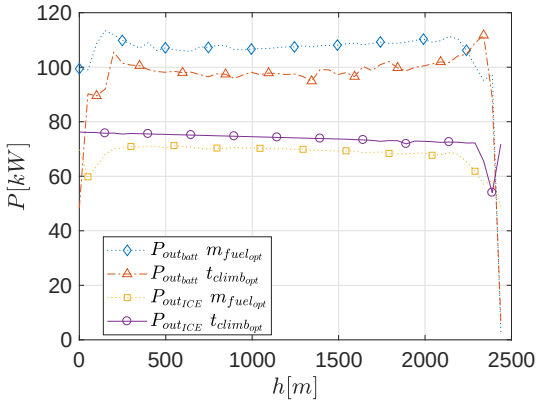

Figure 6.54: Optimum Power out of battery and out of ICE versus altitude for different objectives for the climb phase of the mission optimization

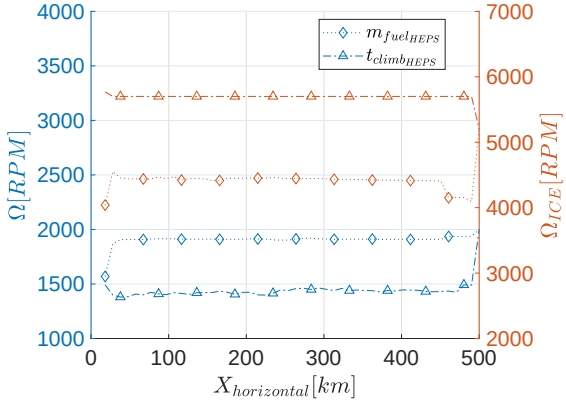

Figure 6.55: Optimum drive train and ICE rotational velocity versus altitude for different objectives for the cruise phase of the mission optimization

The difference between the optimum climb profile of the combined phase or mission optimization and the climb optimization separately is illustrated by figure 6.56, by means of the actual flight path. In addition, the corresponding optimum velocity profiles are shown in figure 6.57. For both minimum fuel objective the optimum profile lies almost at the same points. The real difference here is for the minimum time profiles, where the coupling of the cruise phase to the climb phase results in a significantly different results. One must keep in mind that the minimum SOC constraint for the climb optimization is higher than for the mission optimization which means that there is more energy available for the climb during the mission optimization which also explains the differences.

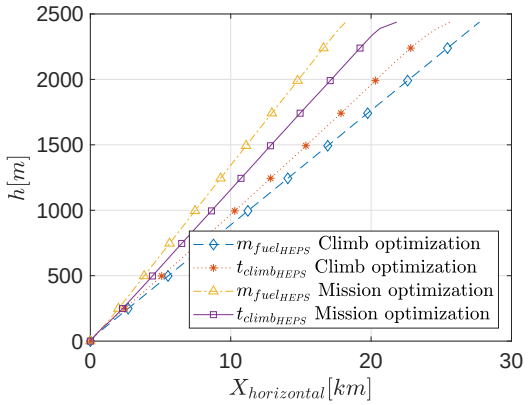

Figure 6.56: Optimum flight path for different objectives for the climb phase of the climb and mission optimization

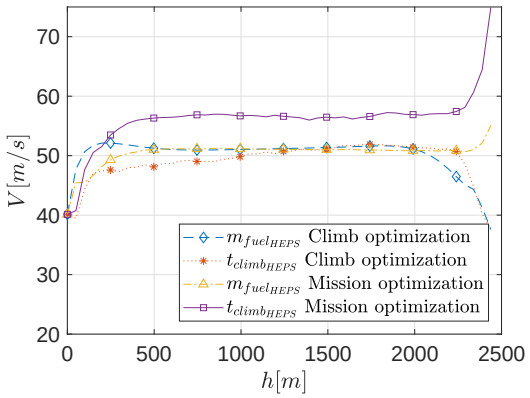

Figure 6.57: Optimum velocity versus altitude for different objectives for the climb phase of the climb and mission optimization

Chapter 7

Sensitivity analysis

To observe which parameters influence the optimum results for each objective in what manner, some parameters that define the optimization or the HEPS are varied. The main parameters that are chosen to perform this investigation are the battery capacity, range of the mission or cruise and the cruise altitude.

7.1 Battery rated capacity

For the battery rated capacity, the climb phase performance has proven to be the most influential on the minimum fuel objective. To investigate the influence battery capacity has on the optimum conditions, the same reference mission is used except now two other battery models are used. The original battery model has a rated capacity of 14.9 kWh and consists out of 55 cells. Doubling this number of cells leads to a 110 battery cell with a rated capacity of 30.5 kWh. Decreasing the number of cells to 25 leads to a battery with a rated capacity of 6.9 kWh. In these battery models, all other inherent battery properties, like maximum C-rate are kept constant to observe the influence of battery capacity in particular. In addition, it should be noted that when adding twice as much battery cells the empty weight of the aircraft increases by about 100 kg which could result in a significant decrease in payload capabilities or range. Figure 7.3 illustrates the optimum rate of climb for minimizing fuel for the different battery capacities. The main observation that is made here is that the larger the battery capacity the faster the aircraft climbs to altitude and thereby keeping the fuel burned at a minimum. Figure 7.2 shown the fuel burned during climb to altitude versus the battery capacity. Clearly, the behavior is not linear and the main reason for this are the constraints of maximum battery output power and minimum power from ICE. To minimize fuel the optimizer wants to maximize the energy from the battery. However, for the largest battery capacity running at the maximum output power the SOC constraint of 0.3 is not reached. In addition, the optimizer wants to decrease the output power by the ICE as much as possible to lower the fuel consumption until it is constraint by the lower value.

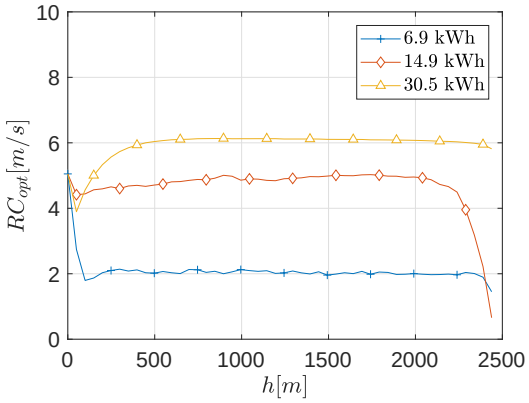

Figure 7.1: Optimum climb velocity profiles for minimum fuel objective for different battery capacities

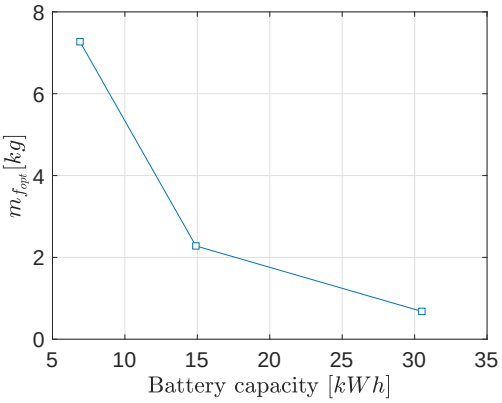

Figure 7.2: Optimum fuel to climb versus battery capacity

Figure 7.3 shows the rate of climb versus the battery capacity. It is observed that the rate of climb profiles increase with battery capacity as well. With the largest battery the aircraft is able to fly at the maximum rate of climb during most of the climb phase. It can therefore be concluded that for a mission to 8000 ft a larger battery would result in better climb performance. The author therefore expects that Pipistrel selected the battery capacity of 14.9 kWh on a different mission cruise altitude, most likely less than 8000 ft. Figure 7.4 shown the optimum time to climb versus battery capacity. Again the behavior is non linear due to the same reasons as discussed earlier.

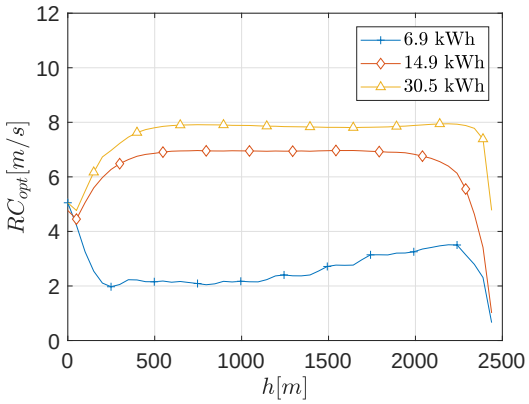

Figure 7.3: Optimum climb velocity profiles for minimum time objective for different battery capacities

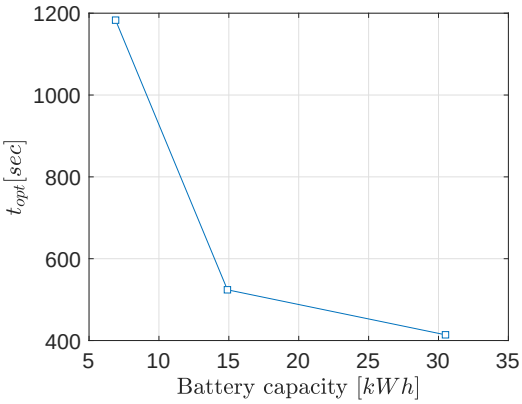

Figure 7.4: Optimum time to climb versus battery capacity

7.2 Cruise altitude

The cruise altitude has proven to be most influential on both climb and cruise phase performance so both are reported here. For the decoupled climb phase, the cruise altitude influences the problem by the final altitude to which the climb is performed. Therefore, for the climb optimization different final altitudes are used to observe how this influences

the optimum solution. For the minimum time optimization the different rate of climb profiles are shown in figure 7.5. It is observed that the rate of climb profile during climb initially converge in similar profiles with increasing final altitude and then decrease. This transition happens between 6000 and 8000ft of final climb altitude. The main reason for this transition is due to the final SOC constraint at the end of the climb phase. Basically, for minimum time the rate of climb must be maximized and for that the HEPS components must be operating at there maximum power output. The maximum power output of the battery is constraint at 120 kW and if the final climb altitude increases above about 6000ft, the battery SOC constraint would be violated so the power of the battery must go down. Therefore, also the rate of climb for minimum time to climb goes down. The same is observed in the objective function value shown in figure 7.6 where the time to climb increases linearly until transitioning to a steeper increase between 6000 and 8000ft (1828 and 2438m).

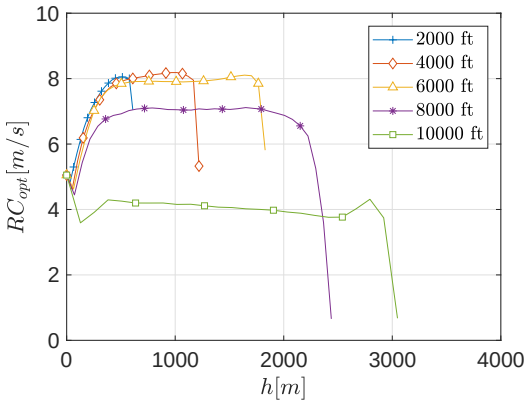

Figure 7.5: Optimum climb velocity profiles for minimum time objective for different final climb altitudes

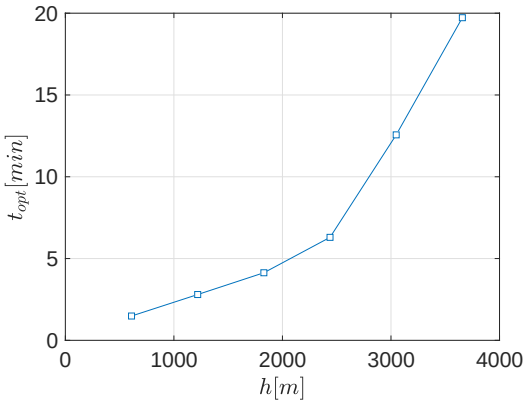

Figure 7.6: Optimum time to climb versus final climb altitude

For the minimum fuel of the climb optimization something else occurs. At first the velocity profiles increase with final altitude and again after 6000ft they decrease again, likely due to the same battery SOC constraint. The increase in velocity profiles in the first final altitudes is due to the extra energy in the acceleration term. Therefore, it is not fuel efficient to climb at a higher rate of climb when only climbing to a low altitude like 2000ft. In addition, the objective function value is shown in figure 7.8 and illustrates a quadratic increase in fuel mass burned for climb in the first final altitudes 8000ft (2438m) it increases linearly. Again a transition is observed due to the battery SOC constraint.

Next the strategy #2 cruise optimization is ran and the resulting velocity profiles for each cruise altitude are shown in figure 7.9. Again distinct regions are visible between the recharge and the ICE only mode. For the ICE only mode the optimizer converges to a rather constant velocity that increases as cruise altitude increases as well. For the velocity during recharging it increases as well with increasing altitude. The objective function value for the minimization of fuel burned during cruise increases with cruise altitude. This is quite contrary because it is expected that the airframe efficiency drives the optimum fuel burned during cruise down as altitude increases. However, theoretically the actual value of minimum drag force does not decrease with altitude for a constant CL-CD polar. Therefore, the minimum power required does increase with altitude resulting in

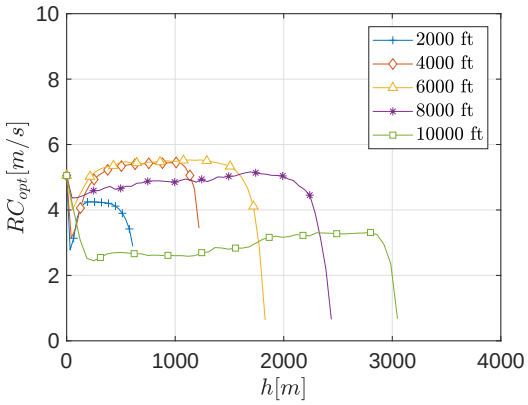

Figure 7.7: Optimum climb velocity profiles for minimum fuel objective for different final climb altitudes

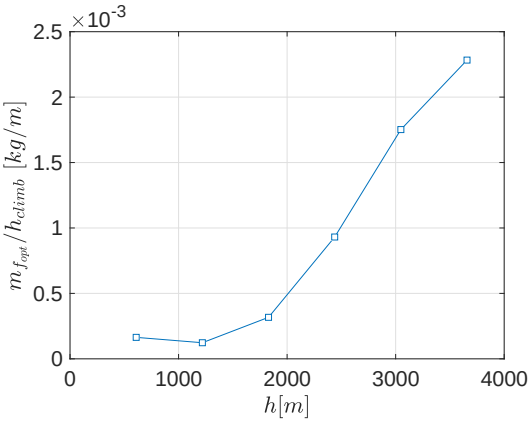

Figure 7.8: Optimum fuel to climb versus final climb altitude

a higher power required for horizontal symmetric flight which increases the power required from the ICE resulting in a higher fuel consumption.

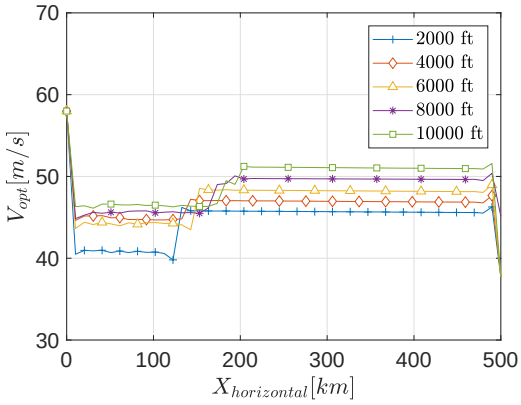

Figure 7.9: Optimum velocity profiles for different cruise altitudes with the minimum fuel objective

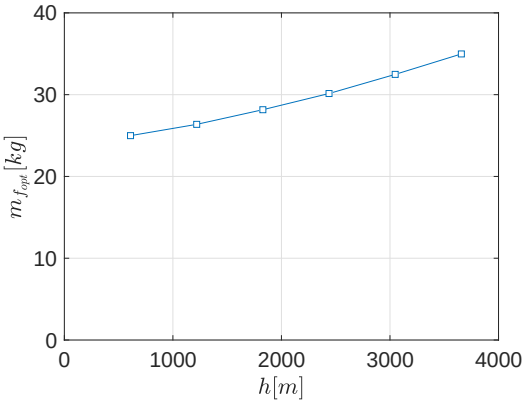

Figure 7.10: Optimum fuel to cruise versus cruise altitude

For the minimum time objective the velocity profiles are shown in figure 7.11. Here, again it is observed that the initial point, where the recharge mode switches to ICE only mode influences the optimum solution significantly. It is observed that the gradient based optimization algorithms is not able to sufficiently cope with the switching between modes when time is optimized for this discretization method. Looking at the objective value, the same is observed. The optimum time decreases with increasing cruise altitude but makes a jump between 6000 and 8000ft which can only be explained by the same phenomena.

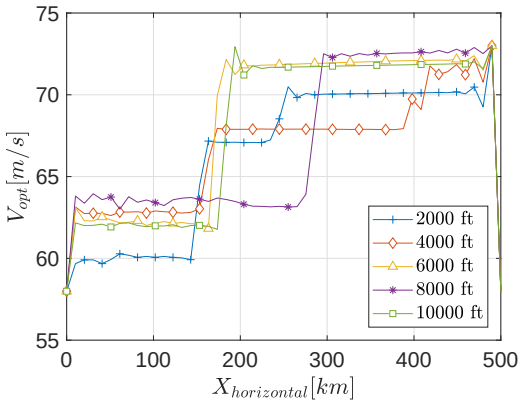

Figure 7.11: Optimum velocity profiles for different cruise altitudes with the minimum time objective

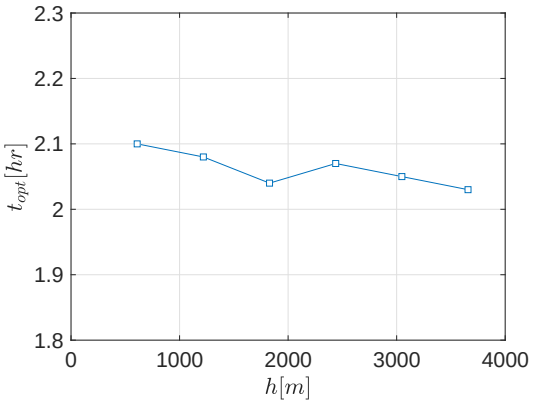

Figure 7.12: Optimum time to cruise versus cruise altitude

7.3 Range

The range has the most significant influence on the cruise performance and it is therefore investigated in this sensitivity analysis. The cruise altitude for these optimizations is set at the reference mission cruise altitude of 8000ft. The effect of range on the cruise is shown in figure 7.13 for the velocity profiles. Please note that the points in the lines are for illustrative purposes only and do not represent the actual points. The main observation that is made here is that the range for charging stay rather constant resulting in a fully recharging cruise at a range of 150 km with the lowest speed since it must recharge before ending the range. Figure 7.14 shows the mass of fuel that has been burned during cruise normalized to the range. It is observed that the cruise becomes more efficient at a larger range. This is mainly becomes for each the same amount of energy goes into the battery to recharge.

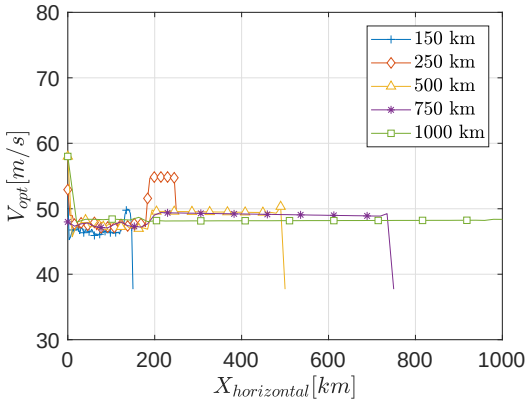

Figure 7.13: Optimum velocity profiles for different ranges with the minimum fuel objective

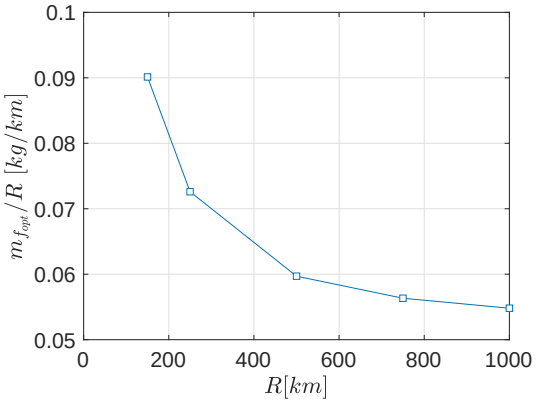

Figure 7.14: Optimum fuel to cruise versus range

7.4 Simplified battery model

Because the sophisticated battery model has proven to be the bottle neck in terms of computational time for the optimizations, the influence of a simplified battery model is investigated as well. If a simplified model results in similar optimum flight conditions and propulsion system settings, then there is no real benefit in using the more sophisticated and time consuming model. Since the climb optimization has proven to be to most susceptible to changes in battery properties, it is used to investigate this properly.

The simplified battery model takes the requested power, the initial SOC and the time for a charge/discharge session as an input just like the sophisticated model. Contrary, the voltage for the simplified model is considered constant at the battery nominal voltage (3.7 V). Similarly, the battery capacity is not a function of the C-rate anymore but is also kept constant at the nominal capacity (75 Ah). This means that the inherent battery properties are not modeled correctly for the simplified battery model because it gets rids of the exponential functions that the sophisticated model uses. In addition, the efficiency is not modeled correctly to all the inherent battery properties as well. Figure 7.15 shows the optimum rate of climb versus altitude for the three different objectives and for both the results with the sophisticated and simple battery model. Clearly, there is a difference in the optimum rate of climb profiles for the different battery models and the difference is quite substantial. The same can be observed in figure 7.16 which shown the output power from the battery versus the altitude. The lower SOC constraint of 0.3 is also active for the simple battery model optimum points, meaning the same ΔSOC is reached. It is therefore concluded that the sophisticated battery model is worth considering since the results differ by a lot. The inherent battery properties are important to include in the model since these influence the optimum conditions substantially.

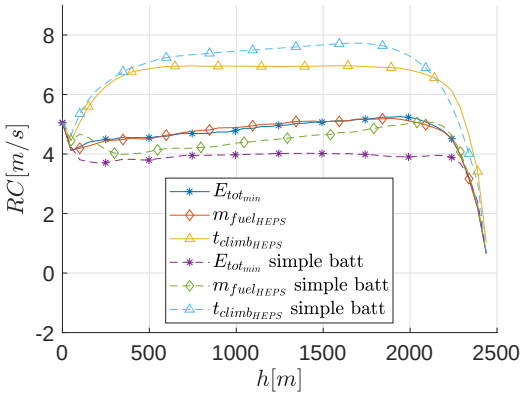

Figure 7.15: Rate of climb versus altitude for different objectives and with simple battery model

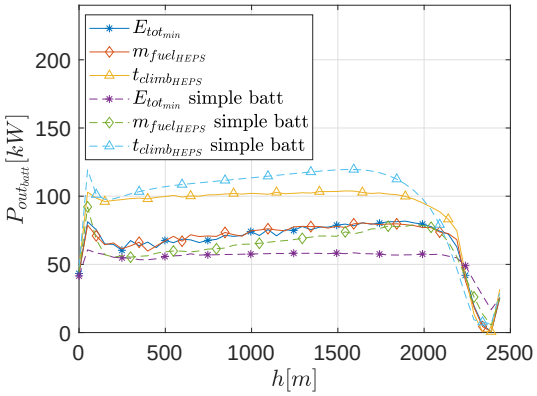

Figure 7.16: Power out of battery versus altitude for different objectives and with simple battery model

Chapter 8

Conclusions & Recommendations

The main goal of the research is to answer to questions that are set up in section **??**, where the main question is on the effectiveness of flight path optimization for a general aviation aircraft with a series HEPS. Additional sub questions are given in section **??** as well and in this final section a global answer is given for these questions in the form of conclusions. Thereafter, recommendations are given both for further research and for operating the HEPS general aviation reference aircraft together with some initial design choices.

8.1 Conclusions

The methodology that is developed uses a discretization of the flight path coupled with the aircraft performance. The performance parameter variables at each point are coupled to the Matlab optimizer *fmincon*. With the results presented in this paper it can be concluded that the method works sufficiently for a certain number of discretized segments. For a low number of segments the method cannot cope with the variables of the problem like changing altitude and the optimization results on an unrealistic and oscillating profile for most of the variables. However, with increasing the number of points the profiles becomes more smoother and more realistic. The biggest problem with using this method coupled to a gradient based optimization like *fmincon* is when the HEPS switches between different operating modes. This switch creates a discontinuity in the objective function value where the initial conditions seem to slightly influence the optimum condition. This seems to be a problem with the minimization of time but not for the minimization of fuel. This is because the time is directly coupled to the discretization of the flight path and you can observe oscillations in the convergence plot for the time optimizations only.

Assessing the basic performance of the HEPS aircraft, the maximum power output of the ICE seems to be quite limiting in comparison to the conventional case. The main problem that arises here is that the battery is almost completely discharged during climb for all optimizing objectives. This means that during cruise the ICE is responsible for

the generation of power, either in recharging mode or in ICE only mode. This lower maximum power output decreases the maximum power significantly resulting in a longer mission flight time compared to the conventional case for each objective.

In addition, the fixed taxi and take off performance for the HEPS has quite a significant influence on the initial battery SOC at the beginning of the climb. It has been found that the battery is discharged by 8% during these two phases. For the climb optimization it is concluded that the optimum fuel and optimum total energy occurs at an increasing velocity profile with increasing altitude. Therefore, the optimum power output from the propeller increases as well during climb. For the minimum time objective the main limiting factor is the battery capacity. For a climb to a significantly high cruise altitude the battery is not able to constantly supply the HEPS with maximum power output, resulting in a lower rate of climb than is theoretically possible. In addition, the difference between total energy and total fuel minimization for the climb is very minor and seem to converge to the same local minimum. Overall, it can be concluded that for the decoupled climb optimization the HEPS aircraft performs better in terms of fuel consumption for all objectives and only performs slightly less better in terms of time for the minimum energy objective, compared to the conventional aircraft.

For the cruise optimization, it is concluded that strategy #1, where the aircraft cycles between recharging mode and full electric mode is not advantageous in terms of fuel, energy and time. Due to more energy conversions with this strategy more energy is lost and lower flight velocities are achievable. Contrary both other strategies are advantageous for the minimization of fuel used during cruise compared to the conventional aircraft. However, the most fuel efficient cruise is the third strategy where the battery is not recharged during cruise. In terms of time all strategies for each objective result in less performance relative to the conventional aircraft where the minimization of fuel for strategy #2 results in the largest time to cruise.

Furthermore, coupling the climb and cruise and performing an optimization on the totality, it is observed that the optimum conditions are significantly different for the decoupled. This is mainly for the minimum fuel objective since with that the battery is not fully discharged to its constraint during climb. This results in less fuel required to recharge the battery. Therefore, a smaller battery capacity would most likely yield in a lower mass of fuel required for a mission with a cruise altitude of 8000 ft. Overall it can be concluded that the HEPS aircraft for the total mission only performs better in terms of fuel but not in terms of time.

By varying the range for the strategy #2 cruise, it is concluded that the cruise becomes more efficient in term of fuel burned per km. This is mainly due to the fact that a shorter cruise needs a quicker recharge. The influence of battery rated capacity seems to be the most influential performance parameter. With the reference battery capacity of 14.9 kWh is just to little to obtain the theoretically maximum rate of climb for a climb to 8000 ft. A battery with the capacity of double that amount is able to climb at the maximum rate of climb and reaches the cruise altitude with about 10% capacity left before reaching its lower constraint. This means that for a climb to 8000 ft a battery capacity between 14.9 and 30.5 is most optimum. Most likely, Pipistrel selected the battery for a lower cruise altitude mission. Therefore, the influence of cruise altitude shows this same behavior. With the fixed reference battery rated capacity a climb to 6000 ft is sufficient to allow the aircraft to fly at its maximum rate of climb mostly.

A comparison between a simple battery model and the previously used sophisticated and computationally time consuming battery model, has resulted in the conclusion that it is important to model the inherent battery properties accurately. The optimum conditions with the simplified battery model differ from that with the sophisticated battery model. Modeling the battery as a function of its inherent properties and including the exponential behavior has proven to be more accurate.

8.2 Recommendations

Like mentioned previously the recommendations are split into recommendations for further research and recommendations for operating the HEPS general aviation reference aircraft together with some initial design choice recommendations.

Recommendations for further research:

- To investigate the effectiveness of using the propeller in descent to recharge the battery. At the moment the fully electric Pipistrel Alpha aircraft uses this capability but it results in a very low power of 2-5 kW back into the battery. Considering how short the descent for the total mission, the effective recharge energy is most likely insignificant. However, this depends largely on how and when the descent will occur.
- To search for a different means of modeling a lithium based battery which would result in a less computational expensive model without compromising the accuracy of the model compared to the reference case.
- To investigate a means of coupling fuel minimization to time minimization by means of one single objective function which is based on an economic motivation.
- To investigate other means of using optimization for different operating modes during flight by either switching to a different and not gradient based optimization method or to search for other ways to smoothen the objective function value where the switching between modes occurs, especially for time based optimizations.

Recommendations for operation and design choices:

- When choosing a strategy on how to perform the mission it is recommended to charge the battery during cruise, if a quick turn around time is required or the airfield at the destination does not have charging facilities. Contrary, with charging capabilities present and the turn around time may exceed about 30 minutes, it is recommended to not charge the battery during flight but on the airfield of arrival.
- During cruise a constant velocity is recommended depending largely on the operating mode of the HEPS. In different modes different optimum velocities occur but stay rather constant.
- As mentioned in the conclusions it is recommended as a preliminary design choice to upscale the ICE slightly to match the cruise performance of the conventional aircraft better. Actually, as of current state Pipistrel changed it's initial ICE to a slightly larger ICE with a 100kW maximum power output.
- Another preliminary design choice is the choose the battery capacity carefully by keeping the cruise altitude of the selected mission in mind, especially when quick climb performance is required. Allowing the ability to swap a certain amount of battery capacity with payload capability might by interesting for varying missions.

Appendix A

Table overview HEPS aircraft

Project	Hybrid alatus	ECO-eagle	DA36 E-Star	DA36 E-Star 2	HEPA	Hypstair
Research institution	Cambridge University, flylight	Embry-riddle	Siemens, EADS, Diamond Aircraft	Siemens, EADS, Diamond Aircraft	Cambridge University	Pipistrel
Maiden flight	2010	2011	2011	2013	2014	-
Airframe	Alatus-M	Stemme S10	HK 36 DIMONA	HK 36 DIMONA	Gramex SOUL	Pipistrel Panthera
MTOW	235 kg	980 kg	770 kg	770 kg	235 kg	1315 kg
ICE-type	4-stroke	4-stroke	Wankel	Wankel	4-stroke	4-stroke
ICE power ($h = 0$)	2.8 kW	74.5 kW	30 kW	30 kW	8 kW	80 kW
EM power	12 kW	29.8 kW	70 kW	65 kW	12 kW	200 kW
Battery	LiPo, 40Ah	LiPo	Unknown	Unknown	LiPo	LiPo, 100Ah
Lay out	Parallel	Parallel	Series	Series	Parallel	Series
Recharge battery	No	No	Yes	Yes	Yes	Yes
Take-off	ICE + EM	ICE	ICE + GE + EM	ICE + GE + EM	ICE + EM	ICE + EM
Cruise	ICE + EM	EM	ICE + GE + EM	ICE + GE + EM	ICE + GE	ICE + EM
Climb	ICE + EM	ICE	ICE + GE + EM	ICE + GE + EM	ICE + EM	ICE + EM
Landing/Taxiing	Unknown	Unknown	Unknown	Unknown	Unknown	EM

Table A.1: Table representing some specific data for the existing HEPS aircraft [10] [2] [4]

Appendix B

Overview of connected models

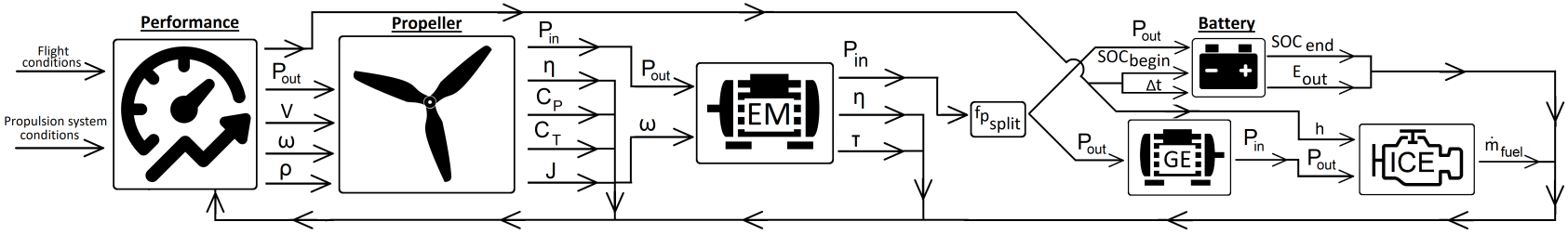

Figure B.1: Overview of all models connected together with the corresponding input and outputs

Appendix C

Battery model optimization results

In this appendix the optimization results of the battery model are given. The battery model is based on a manual read out of the reference data of the end of exponential zone voltage (V_{exp}) and end of nominal zone voltage (V_{nom}), used to model the battery as described in chapter 5. Figure C.1, C.3, C.5, C.7, C.9 and C.11 show the voltage versus the capacity for the Kokam battery cell for the reference data, the estimated calculated data and the optimized calculated data for each reference discharge rate. For the optimization the sum of the errors between the graphs is minimized. Therefore, the error versus the capacity between the calculated data that is estimated and the reference data, together with the calculated data that is optimized and the reference data is shown in figure C.2, C.4, C.6, C.8, C.10, C.12 for each discharge current.

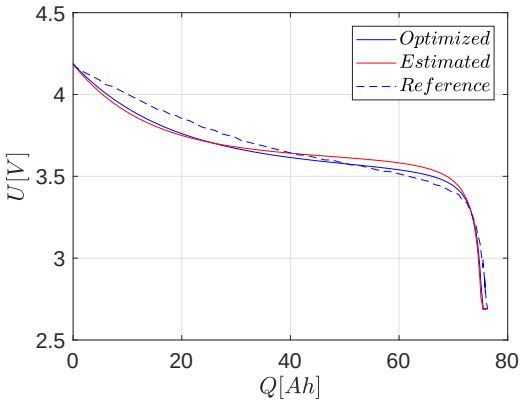

Figure C.1: Voltage versus battery cell capacity of reference data, calculated data from estimation and from optimization for discharge rate of 0.5C

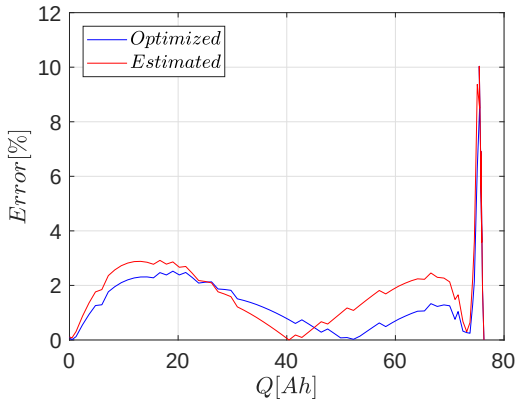

Figure C.2: Error between reference data and estimated data and optimum data versus capacity for discharge rate of 0.5C

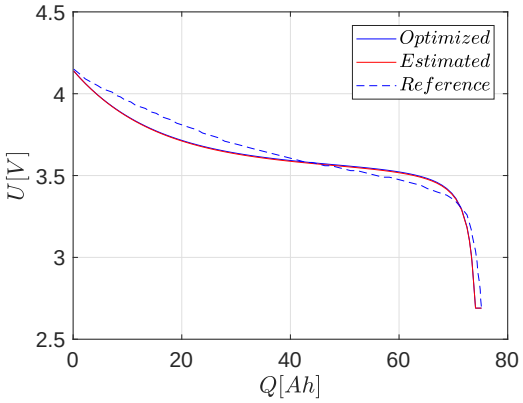

Figure C.3: Voltage versus battery cell capacity of reference data, calculated data from estimation and from optimization for discharge rate of 1C

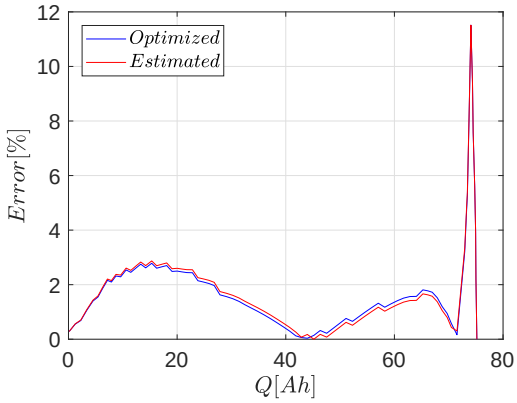

Figure C.4: Error between reference data and estimated data and optimum data versus capacity for discharge rate of 1C

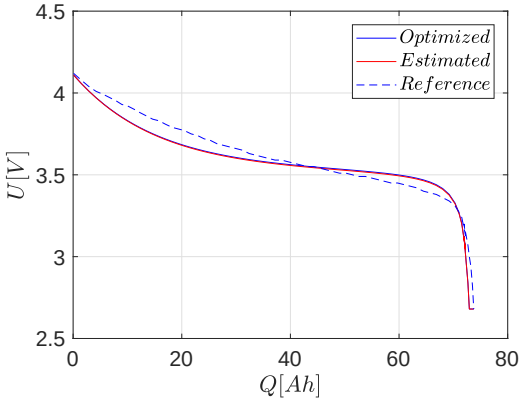

Figure C.5: Voltage versus battery cell capacity of reference data, calculated data from estimation and from optimization for discharge rate of 2C

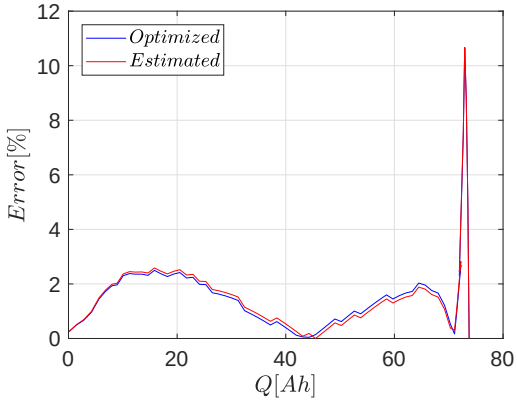

Figure C.6: Error between reference data and estimated data and optimum data versus capacity for discharge rate of 2C

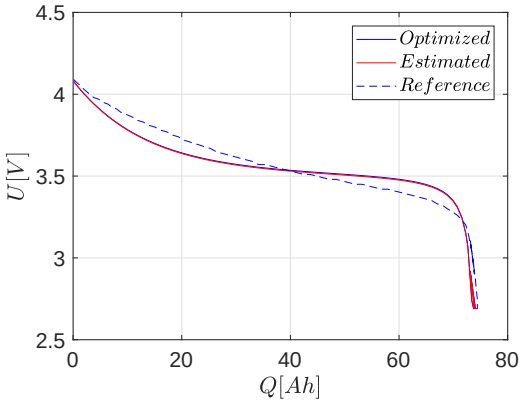

Figure C.7: Voltage versus battery cell capacity of reference data, calculated data from estimation and from optimization for discharge rate of 3C

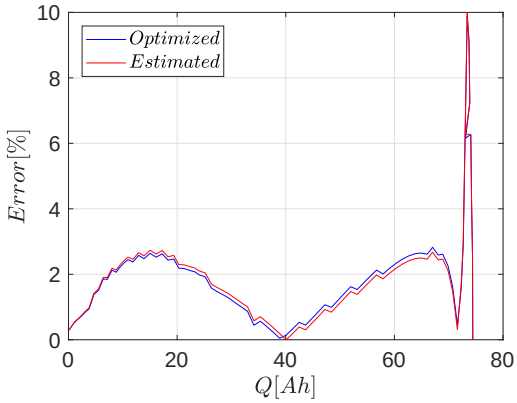

Figure C.8: Error between reference data and estimated data and optimum data versus capacity for discharge rate of 3C

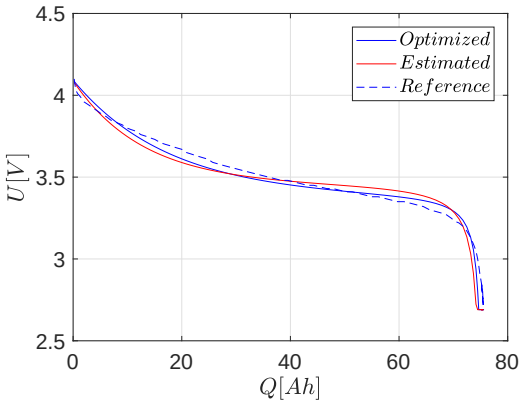

Figure C.9: Voltage versus battery cell capacity of reference data, calculated data from estimation and from optimization for discharge rate of 5C

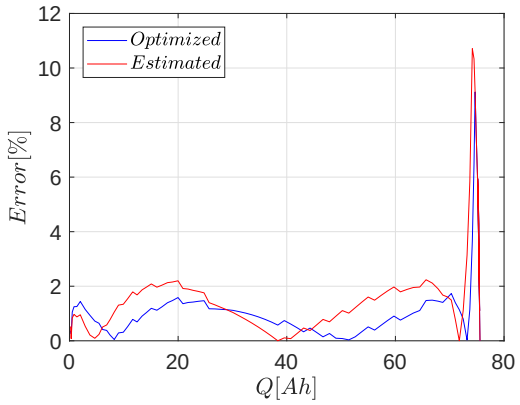

Figure C.10: Error between reference data and estimated data and optimum data versus capacity for discharge rate of 5C

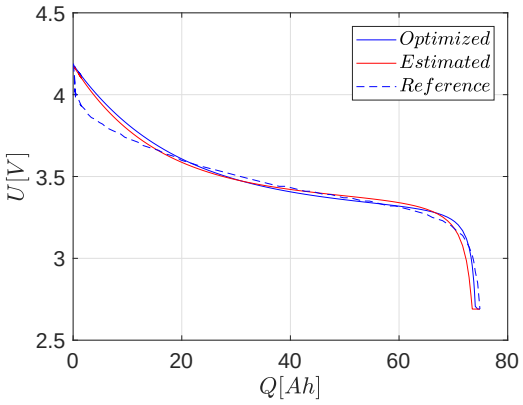

Figure C.11: Voltage versus battery cell capacity of reference data, calculated data from estimation and from optimization for discharge rate of 6C

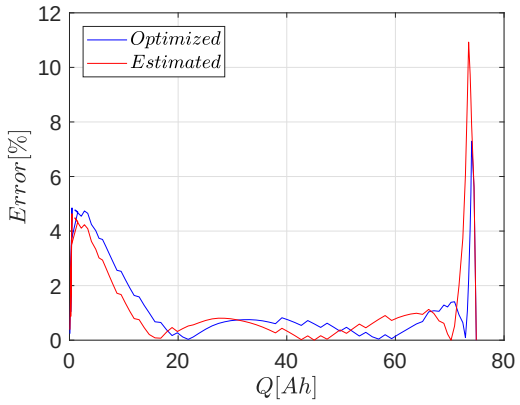

Figure C.12: Error between reference data and estimated data and optimum data versus capacity for discharge rate of 6C

Appendix D

Design Structure Matrix

In this appendix two Design Structure Matrices (DSM) are shown. Figure D.1 shows the overall DSM and figure D.2 shows a sub-DSM for the propulsion system part.

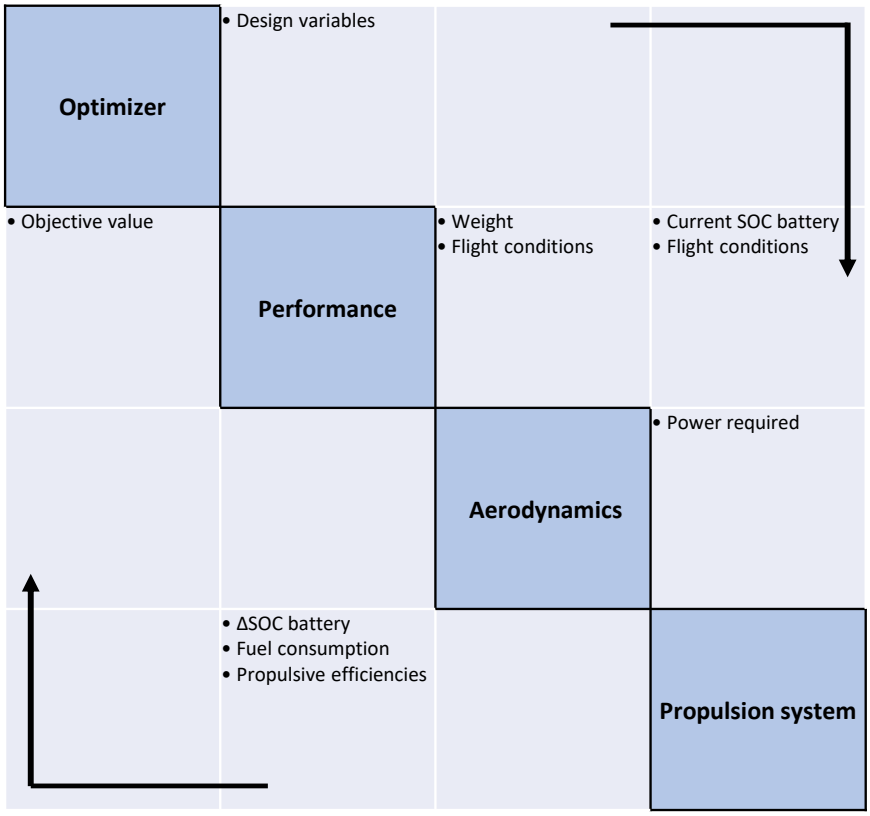

Figure D.1: Overall Design Structure Matrix

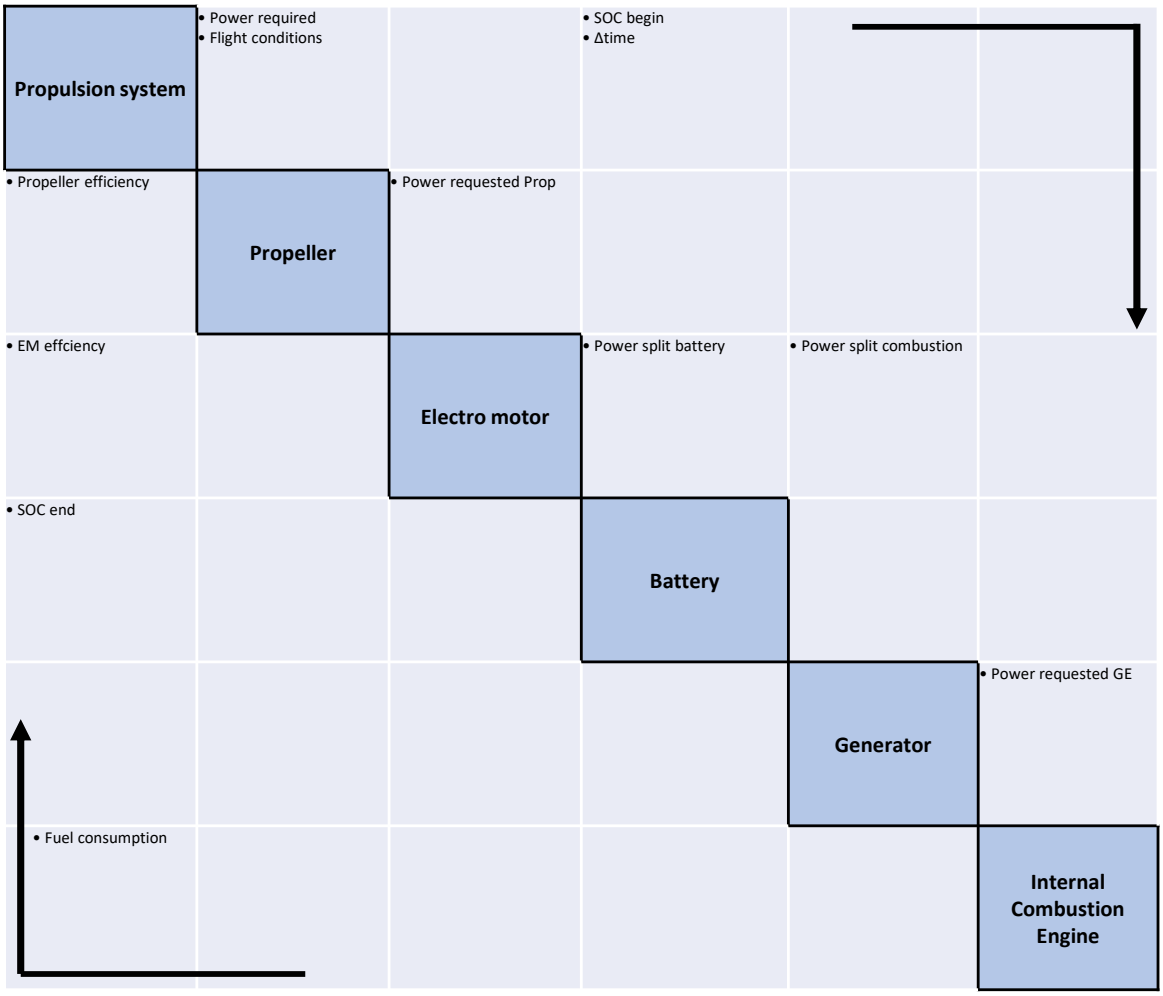

Figure D.2: Propulsion system Design Structure Matrix

Appendix E

Optimization convergence plots

E.1 Climb

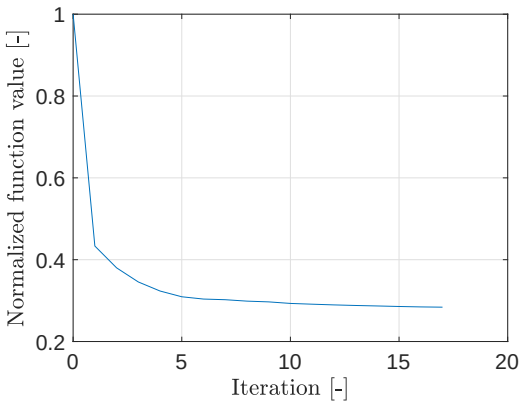

Figure E.1: Normalized function value versus iterations for climb phase optimization of energy

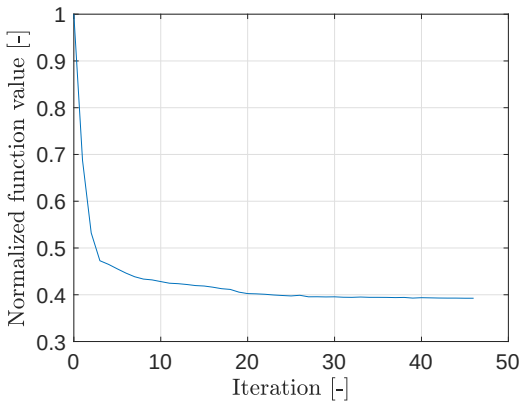

Figure E.2: Normalized function value versus iterations for climb phase optimization of fuel

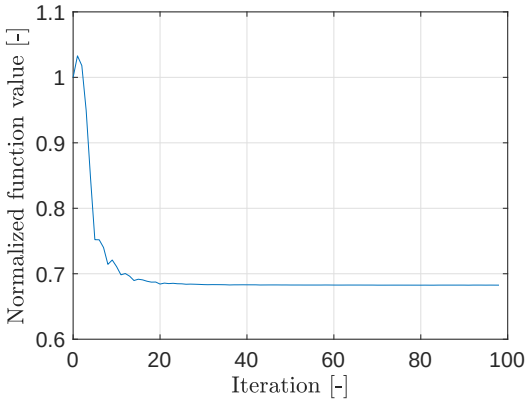

Figure E.3: Normalized function value versus iterations for climb phase optimization of time

E.2 Cruise

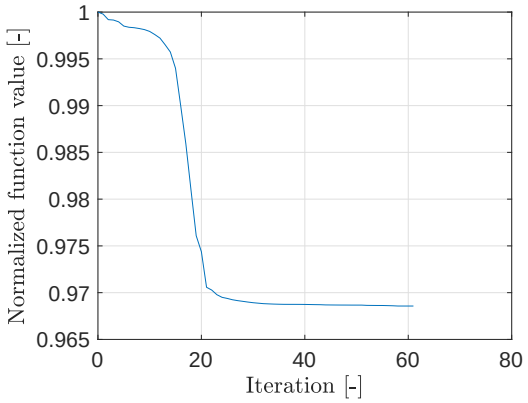

Figure E.4: Normalized function value versus iterations for cruise phase optimization of energy for strategy #1

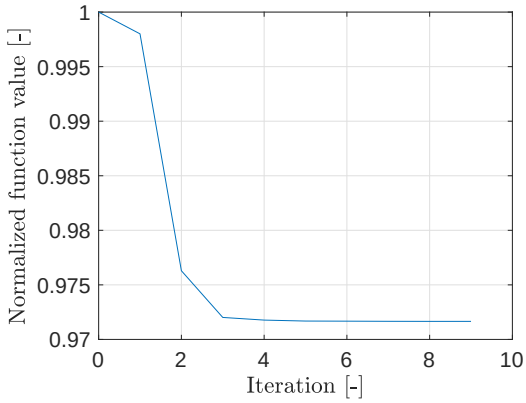

Figure E.5: Normalized function value versus iterations for cruise phase optimization of fuel for strategy #1

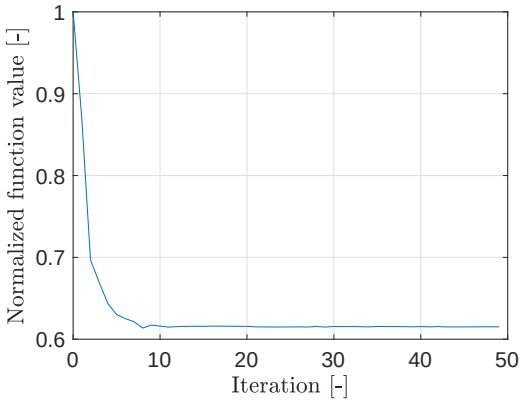

Figure E.6: Normalized function value versus iterations for cruise phase optimization of fuel for strategy #2

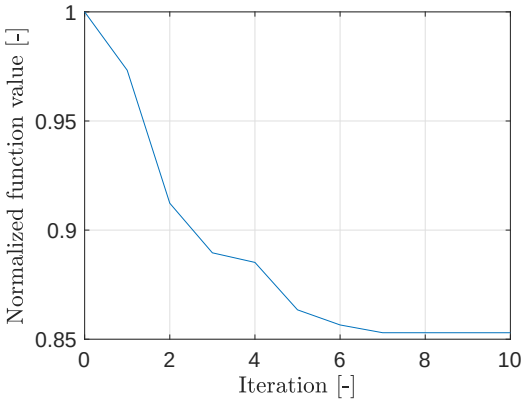

Figure E.7: Normalized function value versus iterations for cruise phase optimization of time for strategy #2

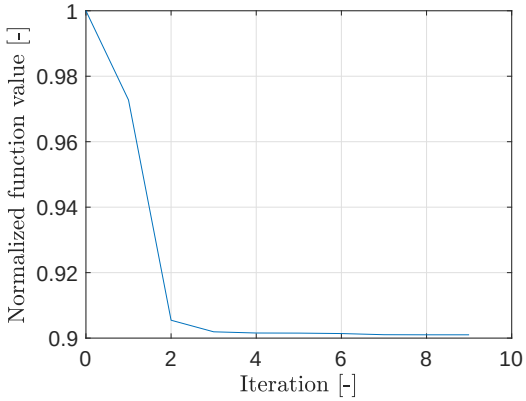

Figure E.8: Normalized function value versus iterations for cruise phase optimization of fuel for strategy #3

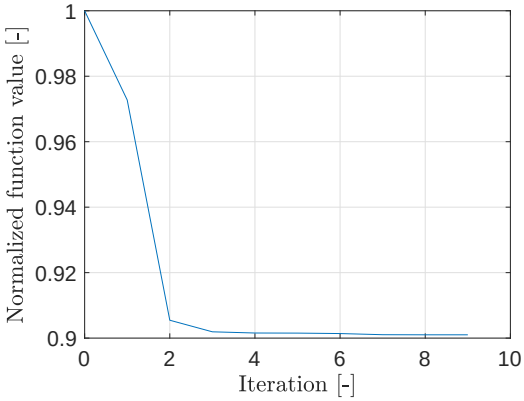

Figure E.9: Normalized function value versus iterations for cruise phase optimization of time for strategy #3

E.3 Mission

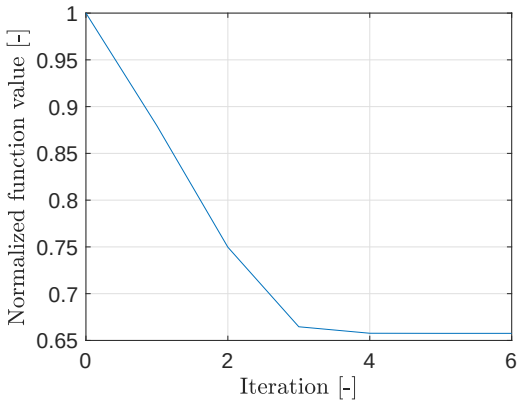

Figure E.10: Normalized function value versus iterations for mission optimization of fuel

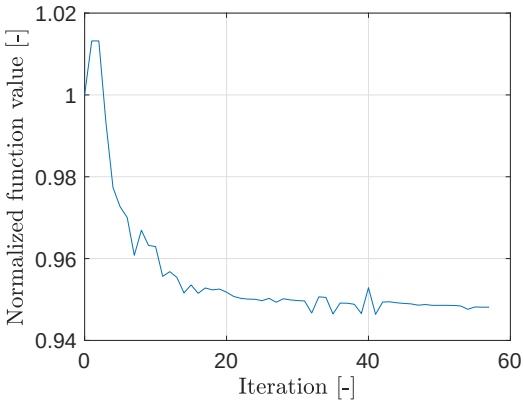

Figure E.11: Normalized function value versus iterations for mission optimization of time

References

[1] *Kokam SLPB (Superior Lithium Polymer Battery) Technical Specification.*

[2] Pipistrel. Website. Accessed: 2017-01-20.

[3] *Powersonic Sealed Lead-Acid Batteries Technical manual.*

[4] *ROTAX 912 operator's manual.*

[5] *SIEMENS 30HP Motor Specifications.*

[6] *Siemens Application Manual for NEMA Motors.*

[7] Shell avgas 100ll, 1999.

[8] *Lycoming O-540 Operators manual*, 4th edition, June 2006.

[9] Pierre T. Kabamba Andrew T. Klesh. Energy-optimal path planning for solar-powered aircraft in level flight. *AIAA Guidance, Navigation and Control conference and exhibit*, 2007.

[10] P. A. Robertson C. Friedrich. Hybrid-electric propulsion for automotive and aviation applications. *CEAS Aeronaut*, 2015.

[11] Paul A. Robertson C. Friedrich. Design of a hybrid-electric propulsion system for light aircraft. *AIAA Aviation Technology*, 2014.

[12] D. Mavris C. Perullo. A review of hybrid-electric energy management and its inclusion in vehicle sizing. *Aircraft Engineering and Aerodspace Technology: An International Journal*, 2014.

[13] Piers M. Forster Peter J. Newton Ron C.N. Wit Ling L. Lim Bethan Owen Robert Sausen David S. Lee, David W. Fahey. Aviation and global climate change in the 21st century. *Atmospheric Environment*, 2009.

[14] Rene Spee Dean Patterson. The design and development of an axial flux permanent magnet brushless dc motor for wheel drive in a solar powered vehicle. *IEEE TRANSACTIONS ON INDUSTRY APPLICATIONS*, 1995.

[15] European Aviation Safety Agency (EASA). *CS-23*, 2003.

[16] C. Friedrich and P.A. Robertson. Hybrid-electric propulsion for aircraft. *Journal of aircraft*, 2015.

[17] Gerald B.Kliman Hamid A.Toliyat. *Handbook of Electro Motors*. CRC Press, 2004.

[18] Frederick G. Harmon. Neural network control of a parallel hybrid-electric propulsion system for a small unmanned aerial vehicle. *Engineering and Computer Science Faculty Publications*, 2005.

[19] Austin Hughes. *Electric Motors and Drive*. Elsevier, 2006.

[20] Travis Don Husaboe. Effects of temperature on the performance of a small internal combustion engine at altitude. *AIR FORCE INSTITUTE OF TECHNOLOGY*, 2013.

[21] Mitchell Olszewski Don A. Casada Pedro J. Otaduy Leon M. Tolbert John S. Hsu, John D. Kueck. Comparison of induction motor field efficiency evaluation methods. *IEEE TRANSACTIONS ON INDUSTRY APPLICATIONS*, 1998.

[22] David J. Griggs David J. Dokken Mack McFarland Joyce E. Penner, David H. Lister. Aviation and the global atmosphere. *IPCC*, 1999.

[23] Ahmet Teke Kamil agatay Bayindir, Mehmet Ali Gzkk. A comprehensive overview of hybrid electric vehicle: Powertrain configurations, powertrain control techniques and electronic control units. *Elsevier: Energy Conversion and Management*, 2011.

[24] Mark I. Shoesmith Lars Ole Valen. The effect of phev and hev duty cycles on battery and battery pack performance. *Milj Innovasjon AS and E-One Moli Energy (Canada) Ltd.*, 2007.

[25] David S. Lee. Aviation's contribution to climate change. *ICAO Environmenal report*, 2010.

[26] Mark W. Lund. Powerstream. website. Accessed: 2016-12-19.

[27] Bill Fredericks Mark D. Moore. Misconceptions of electric propulsion aircraft and their emergent aviation markets. *American Institute of Aeronautics and Astronautics*.

[28] Florian Martini. Website, 2011. Accessed: 2017-01-23.

[29] Sebastien E. Gay Ali Emadi Mehrdad Ehsani, Yimin Gao. *Modern Electric, Hybrid Electric, and Fuel cell Vehicles*. CRC press, 2004.

[30] Vinh. X. Nguyen. *Optimal trajectories in atmospheric flight*. Elsevier, 1981.

[31] Louis-A Dessaint Olivier Tremblay. Experimental validation of a battery dynamic model for ev applications. *World electric vehicle journal*, 3:0289 – 0298, 2009.

[32] Arne Seitz Patrick C Vratny, Philipp Forsbach and Mirko Hornung. Investigation of universally electric propulsion for transport aircraft. *ICAS*, 2014.

[33] Hoolhorst A. Peeters P.M., Middel J. Fuel efficiency of commercial aircraft: An overview of historical and future trends. *National Aerospace Laboratory NLR*, 2005.

[34] Andrew Zettel Piotr Drozdz. Method and apparatus for adaptive hybrid vehicle control. Accessed: 2017-02-09.

[35] G. Pistoia. Batteries for portal devices. Technical report, Elsevier, 2005.

[36] David F. Rogers. Propeller efficiency rule of thumb. *American Bonanza Society*, 2010.

[37] Ger J. J. Ruijgrok. *Elements of airplane performance*. VSSD, 2009.

[38] A. Lecocq M. Petit V. Sauvant-Moynot F. Huet S. Abada, G. Marlair. Safety focused modeling of lithium-ion batteries: A review. *Elsevier*, 2016.

[39] Joachim Schmann. Hybrid-electric propulsion systems for small unmanned aircraft. Technical report, TECHNISCHE UNIVERSITT MNCHEN, 2013.

[40] Dimitri N. Mavris Taewoo Nam, Danielle S. Soban. Power based sizing method for aircraft consuming unconventional energy. *American Institute of Aeronautics and Astronautics*.

[41] David E. Parekh Thomas F. Fuller Dimitri N. Mavris Thomas H. Brandley, Blake A. Moffitt. Energy management for fuel cell powered hybrid-electric aircraft. *7th international energy conversion engineering conference*, 2009.

[42] Fabrizio Oliviero Vittorio Cipolla. Hypsim: A simulation tool for hybrid aircraft performance analysis. *Elsevier*, 2016.